

University of Louisville

ThinkIR: The University of Louisville's Institutional Repository

Electronic Theses and Dissertations

8-2023

Effects of environmental pollutants on liver disease: role of the gut-liver axis.

Ngozi Victoria Adiele
University of Louisville

Follow this and additional works at: <https://ir.library.louisville.edu/etd>



Part of the [Environmental Health Commons](#), [Polycyclic Compounds Commons](#), and the [Toxicology Commons](#)

Recommended Citation

Adiele, Ngozi Victoria, "Effects of environmental pollutants on liver disease: role of the gut-liver axis." (2023). *Electronic Theses and Dissertations*. Paper 4395.
Retrieved from <https://ir.library.louisville.edu/etd/4395>

This Master's Thesis is brought to you for free and open access by ThinkIR: The University of Louisville's Institutional Repository. It has been accepted for inclusion in Electronic Theses and Dissertations by an authorized administrator of ThinkIR: The University of Louisville's Institutional Repository. This title appears here courtesy of the author, who has retained all other copyrights. For more information, please contact thinkir@louisville.edu.

EFFECTS OF ENVIROMENTAL POLLUTANTS ON LIVER DISEASE: ROLE OF
THE GUT-LIVER AXIS

By

Ngozi Victoria Adiele
B.S., University of Toledo, 2020

A Thesis
Submitted to the Faculty of the
School of Medicine of the University of Louisville
In Partial Fulfillment of the Requirements
for the Degree of

Master of Science
In Pharmacology and Toxicology

Department of Pharmacology and Toxicology
University of Louisville
Louisville, KY

August 2023

Copyright 2023 by Ngozi Victoria Adiele
All rights reserved.

THE EFFECTS OF ENVIROMENTAL POLLUTANTS ON LIVER DISEASE:
ROLE OF THE GUT-LIVER AXIS

By

Ngozi Victoria Adiele
B.S., University of Toledo, 2020

Thesis Approved on

05/30/2023

By the following Thesis Committee:

Matthew C. Cave, M.D.

Banrida Wahlang, Ph.D.

J. Calvin Kouokam, Ph.D.

Barbara J. Clark, Ph.D.

Timothy O'Toole, Ph.D.

Mayukh Banerjee, Ph.D.

ACKNOWLEDGEMENTS

With a grateful heart, I would like to thank the Almighty God for His grace and mercy to achieve this milestone. I would also like to thank my mentors: Dr. Matthew C. Cave and Dr. Banrida Wahlang for providing the guidance and support to accomplish this milestone. I would like to thank the members of the environmental liver disease group: Tyler C. Gripshover, Oluwanifemi Esther Bolatimi, Dr. Jianzhu Luo, Dr. Frederick Ekuban, Dr. Walter Watson, Kimberly Z. Head and Dr. Loretta Jophlin for their encouraging support and our collaborators: Dr. Timothy O'Toole and Dr. Jingjing Zhao. I would like to thank my committee members: Dr. Matthew C. Cave, Dr. Banrida Wahlang, Dr. J. Calvin Kouokam, Dr. Barbara J. Clark, Dr. Timothy O'Toole, and Dr. Mayukh Banerjee for their counsel and advise to the betterment of my project. I would also like to appreciate the members of the genomics and bioinformatics core: Dr. Melissa Smith, Elizabeth Hudson, Sabine Waigel, Vennila Arumugam, Dr. Eric Rouchka, Dr. Richa Singhal, and Dr. Julia Chariker for their help and support with my project. I would like to thank the University of Louisville, School of Medicine, Pharmacology and Toxicology department and integrated programs in biomedical sciences (IPIBS) program for the opportunity to study and earn my master's at the University of Louisville. Lastly, I would like to thank my family (Daniel Adiele and Mrs. Chinyere Otaka) and friends for their love, support and prayers that have brought me this far. Thank you and I love you.

ABSTRACT

EFFECTS OF ENVIRONMENTAL POLLUTANTS ON LIVER DISEASE: ROLE OF THE GUT-LIVER AXIS

Ngozi Victoria Adiele

May 30, 2023

Polychlorinated biphenyls (PCBs) and polystyrene (PS) microplastics are environmental pollutants associated with various diseases including toxicant associated fatty liver disease (TAFLD). Previously, exposure to Aroclor 1260 (a PCB mixture) has been shown to exacerbate TAFLD, partly through Aroclor 1260 induced gut dysbiosis. Studies has also demonstrated that PS exposure alters gut microbiome composition and induced obesity. However, the effects of Aroclor 1260 on the gut and the effects of PS on the liver are still understudied. Therefore, we hypothesize that environmental pollutants will disrupt the gut-liver axis through changes in gut and its microbiome as well as changes in liver functions. Our findings indicated that chronic Aroclor 1260 exposure could increase microbial activity and compromise gut barrier functions. While our findings on PS indicated a size-dependent effect on hepatic metabolic gene expression as well as the enrichment of hepatic receptor such as FXR and LXR receptors, involved in the regulation of metabolic pathways within the gut-liver axis. In conclusion, our findings showed minor changes in the gut and the liver by

both Aroclor 1260 and PS, respectively. However, further studies are needed to understand the effects of these compounds on the gut-liver axis.

TABLE OF CONTENTS

ACKNOWLEDGEMENTS.....	iii
ABSTRACT	iv
LIST OF FIGURES.....	viii
CHAPTER I: INTRODUCTION.....	1
CHAPTER II: INVESTIGATING THE CHRONIC EFFECTS OF AROCLOR 1260 ON THE GUT AND GUT MICROBIOME	10
INTRODUCTION	10
METHODS.....	13
RESULTS	20
DISCUSSION.....	40
CHAPTER III: INVESTIGATING THE EFFECTS OF POLYSTYRENE EXPOSURE ON THE LIVER.....	45
INTRODUCTION	45
MATERIALS AND METHODS	49
RESULTS	57
DISCUSSION.....	81
CHAPTER IV: SUMMARY.....	87

REFERENCES.....	92
APPENDIX	106
CURRICULUM VITAE	116

LIST OF FIGURES

Figure 1: Effects of Aroclor 1260 on microbiome alpha diversity.....	21
Figure 2: Effects of Aroclor 1260 on microbiome beta diversity.....	23
Figure 3: Effects of Aroclor 1260 on microbiome phylum taxonomy.	25
Figure 4: Effects of Aroclor 1260 on microbiome alpha diversity based on low and high NAS score.....	27
Figure 5: Effects of Aroclor 1260 on microbiome beta diversity based on low and high NAS score.....	29
Figure 6: Effects of Aroclor 1260 on microbiome phylum taxonomy based on low and high NAS score.	31
Figure 7: Effects of Aroclor 1260 on ileal permeability gene expression....	33
Figure 8: Effects of Aroclor 1260 on ileal functional gene expression.....	35
Figure 9: Effects of Aroclor 1260 on ileal inflammatory gene expression. .	37
Figure 10: Effects of Aroclor 1260 on PXR and CAR target genes gene expression.....	39
Figure 11: PS effects on body composition.....	58
Figure 12: PS on H&E staining of liver tissue and foci count.....	61
Figure 13: PS effects on hepatic cholesterol and triglyceride levels.....	62
Figure 14: PS effects on plasma AST and ALT.....	63
Figure 15: PS effects on inflammation related genes gene expression.	67
Figure 16: PS effects on hepatic profibrotic gene expression.	68

Figure 17: PS effects on hepatic oxidative stress.	70
Figure 18: PS effects on genes involved in hepatic cholesterol metabolism.	73
Figure 19: PS effects on genes involved in hepatic lipid metabolism.	74
Figure 20: PS effects on genes involved in glucose metabolism and normal liver function.	75
Figure 21: Predicted differentially expressed genes (DEGs) with polystyrene microplastics exposure.	79
Figure 22: Enrichment analysis of DEGs identified in different sizes of polystyrene exposure.	80
Figure 23: Summary of Aroclor 1260 findings.	90
Figure 24: Summary of Polystyrene exposure findings.	91

CHAPTER I: INTRODUCTION

Toxicant associated fatty liver disease (TAFLD) and toxicant associated steatohepatitis (TASH)

Despite significant advancements in technology and economic growth since the industrial revolution/era, there have been negative impacts on the ecosystem. For example: harm to wildlife, reduction in biodiversity, and harmful effects on human health due to the introduction of various chemicals. Without a thorough understanding/knowledge of their detrimental effects, the production and use of chemicals for industrial activities such as manufacturing, mining, metal working and agriculture resulted in the release of various pollutants into the air, water, and soil. For example, the incidence of vinyl chloride exposure in Rubbertown, Louisville, KY has been linked to various kinds of cancers including hepatic angiosarcoma, a rare form of liver cancer [1, 2]. This among other incidences, have provided evidence of the harmful chemical effects on human health. Over time, adverse health effects from these chemical exposures became more apparent, and regulations have been put in place to limit their use and release into the environment. However, many of these chemicals remain persistent in the environment and have been referred to as "forever chemicals" because they do not break down easily and can remain in the environment for decades [3].

One of the organs largely affected by environmental pollutants is the liver. The liver is the largest internal organ in the body, responsible for the detoxification of xenobiotics and the metabolism of macromolecules (carbohydrates, lipids, nucleic acids, and proteins) to produce energy. Both energy production and xenobiotic metabolism in the liver are mainly regulated by the activation of hepatic receptors such as aryl hydrocarbon receptor (AhR), constitutive androstane receptor (CAR), estrogen receptor (ER), glucocorticoid receptor (GR), farnesoid X receptor (FXR), liver X receptor (LXR), peroxisome proliferator-activated receptor (PPAR), pregnane X receptor (PXR), and retinoic acid receptor (RXR). The activation of these receptors by environmental pollutants have been shown to play a role in a myriad of health outcomes such as cardiovascular disease, cancer, and metabolic syndrome manifestation [4, 5].

According to Cobbina & Akhlaghi (2017), metabolic syndrome is defined by the presence of at least three of the following health conditions occurring together: abdominal obesity, increased triglycerides levels, reduced high-density lipoprotein (HDL) cholesterol, increased blood pressure, and hyperglycemia increases the risk for: type 2 diabetes, cardiovascular diseases, liver diseases, inflammation and immune disorders in the body [6]. In the liver, the manifestation of the metabolic syndrome is characterized by the development of fatty liver disease [7].

Fatty liver disease is a pathological spectrum of diseases ranging from simple steatosis (accumulation of lipids in hepatocytes) to steatohepatitis (development of inflammation with steatosis). Steatohepatitis can eventually lead

to fibrosis with or without progression to cirrhosis, and possibly to hepatocellular carcinoma (HCC) [5]. Over the years, the term fatty liver disease was largely associated with alcohol consumption, also known as Alcohol-associated liver disease and steatohepatitis (ALD/ASH). The term “nonalcoholic fatty liver disease and nonalcoholic steatohepatitis (NAFLD/NASH)” describes the occurrence of fatty liver disease in non-alcohol drinkers who were mildly obese, differentiating the occurrence of fatty liver due to alcohol consumption and other factors such as a high caloric diet [8]. This term was further adjusted to encompass other etiologies of fatty liver disease such as toxicant associated fatty liver disease/ toxicant associated steatohepatitis (TAFLD/TASH) and chemotherapy associated steatohepatitis (CASH) [5].

The term TAFLD/TASH was initially coined by our research group to describe the presence of non-alcoholic steatohepatitis (NASH) which was characterized by insulin resistance, decreased antioxidants, and increased pro-inflammatory cytokines in non-alcohol drinkers who did not present obesity [1, 9]. Eventually, it was used to describe fatty liver disease development from exposure to both industrial/ occupational and/or environmental toxicants [9, 10]. Some of these toxicants include organochlorine pesticides, vinyl chloride, carbon tetrachloride, polychlorinated biphenyls (PCBs), polychlorinated dibenzo-p-dioxins (dioxins), particulate matter, metals, volatile organic chemicals (VOCs), pesticides and others [11]. Most of these chemicals are now further identified as endocrine disrupting chemicals, metabolism disrupting chemical and/or signaling

disrupting chemicals due to their ability to disrupt essential physiological processes in the body [12].

Mechanisms contributing to TAFLD/TASH

Environmental pollutants are often categorized by the systematic effects they produce. For example, endocrine disrupting chemicals affect the endocrine system, while metabolism disrupting chemicals impact metabolism of endogenous and xenobiotic molecules, and signaling disrupting chemicals interfere with the signaling pathways of receptors in the body such as epidermal growth factor receptor (EGFR) signaling. Furthermore, disruption of normal physiological processes in other functionally linked organs such as the gut can contribute to hepatotoxicity effects [12]. For the purposes of this thesis, we will focus on metabolic disrupting chemicals (MDCs), also known as metabolic disruptors, their effects on the liver and how the effects of environmental pollutants on gut and its microbiota contribute to hepatotoxicity.

MDCs are chemicals that increase the susceptibility of animals including humans to diabetes, obesity and other metabolic disorders [13]. The liver is the main organ responsible for the metabolism of endogenous and xenobiotic molecules. However, an interesting theory, which has emerged in recent years is the role of the gut and its microbiome in hepatotoxicity [12, 14]. Recent studies have shown that the alteration of the gut and its microbiome contributes both directly and indirectly to hepatotoxicity through the activation of nuclear receptors [5, 15-17]. Alterations to the gut and its microbiome can lead to the leaking of intestinal content including harmful bacteria into systemic circulation and the liver

resulting in increased hepatic susceptibility to inflammation and metabolic disruption [17]. In addition to xenobiotic metabolism, activation of xenobiotic nuclear receptors PXR and CAR can also regulate energy metabolism, gut microbiome function and bile acid homeostasis [5, 15]. Activation of these receptors have been demonstrated to contribute to the modulation of steatosis, obesity, insulin resistance and inflammation [15]. Recent studies by Wahlang et al. demonstrated that the activation of PXR and CAR by Aroclor 1260 in the gut contributed to the exacerbation of hepatic steatosis in diet-induced obese mice [15].

An indirect pathway by which the gut and its microbiota can contribute to metabolic disruption in the body, specifically in the liver, is through enterohepatic circulation which facilitates the gut-liver interaction [18]. The alteration of gut microbiome can influence the composition of secondary bile acids reabsorbed into the liver and consequent activation of nuclear receptors such as FXR [16] while also altering cholesterol regulation by LXR.

Primary bile acids [Cholic acid, chenodeoxycholic acid and α - and β -muricholic acid (found in mice)] are synthesized from cholesterol. Primary bile acids are then conjugated by the addition of glycine and taurine to make them more soluble [16]. Bile acids are stored in the gallbladder, where they are ejected into the small bowel for the emulsification of dietary fat and the absorption of lipids and lipid soluble vitamins. Approximately 90% of bile acids are reabsorbed into the liver through the portal vein and is regulated by transporters found in the enterocytes and hepatocytes. This process of bile acid excretion into the gut and

reabsorption into the liver is known as enterohepatic circulation. Although 5% of the daily released bile acid are excreted out in feces, 1-2% of the released bile acid are transformed/ deconjugated into secondary bile acids by gut microbiome in the terminal ileum. Transformed/ deconjugated bile acids are then reabsorbed into the liver through systematic circulation [16]. Bile acid composition through its antimicrobial properties regulate gut microbiome composition. Gut microbiome also regulates bile acid composition by modulating their deconjugation. This regulatory effect is mediated by FXR signaling through various mechanisms. Bile acids are ligands of FXR and regulate bile acids, lipids, and glucose metabolism as well as inflammation and fibrosis through FXR activation. FXR is localized in the liver and in the gut and the activation of FXR in the gut and/or liver results in lipid and glucose regulation via the binding of bile acids. FXR signaling can reduce hepatic triglyceride through Ppara activation and sterol-regulatory element-binding protein-1c (SREBP-1c) inhibition via induced expression of atypical nuclear receptors small heterodimer partner (SHP). Additionally, hepatic function is also regulated via ileal FXR activation which suppresses bile acid synthesis by the activation of FGFR4 via Fgf15 binding [16, 19].

Environmental pollutants such as PCBs has also been demonstrated to undergo enterohepatic circulation and are known to alter gut microbiome composition [11, 20]. As mentioned earlier, gut microbiome composition regulates the diversity of bile acids and the antimicrobial properties of bile acids. For example, rats on cholic acid diet showed a 0-37% decrease in the *Bacteroidetes* bacterial phylum but a 54%-95% increase in the *Firmicutes*

bacterial phylum. Notably, the relative abundance for dehydroxylating bacterial species *Clostridium* and the *Ruminococcus* genus belonging to the phylum *Firmicutes* were increased in these rats. This resulted in the increased conversion of cholic acid to deoxycholic acid, a better antimicrobial agent than cholic acid [21]. Therefore, if environmental pollutants altered gut microbiome composition, the subsequently deconjugated primary bile acids can either activate or inhibit FXR signaling in a context dependent manner.

Significance of the study

The liver is the largest internal organ in the body, weighing approximately 3lbs in a human adult. As previously mentioned, the liver is a vital organ in the body, as it is responsible for critical functions such as metabolism and detoxification of both endobiotic and xenobiotics molecules. The liver functions to detoxify environmental toxicants which may cause injury and induction of disease. Various environmental chemicals such as dioxins, PCBs, pesticides, metals, microplastics, and others have been associated with TAFLD [10, 12, 22]. However, the similar pathology between NAFLD and TAFLD, prevents the proper etiological distinction between the two diseases clinically. Furthermore, the study of TAFLD is still relatively new and therefore, there are no clinical effective ways to distinguish between NAFLD and TAFLD. Hence, the importance of studying the effects of environmental toxicants on the liver and how they contribute to the induction/ exacerbation of TAFLD/TASH [23].

There is a worldwide increase in the prevalence of NAFLD [24]. The global prevalence for NAFLD is estimated to be 25.5% and the prevalence for NAFLD in

North America is estimated to be 24.1%, based on previously reported findings in adults aged 18 and older as well as published peer-reviewed journals from 1989 to 2015 [25]. In addition, NAFLD projection studies revealed the global prevalence of NAFLD will increase to 33.5% by 2030 with approximately a hundred million adults in the United States living with NAFLD [26]. These estimations prompt the investigation of the factors that contribute to NAFLD including environmental toxicant and gut barrier dysfunction.

The importance of studying the effects of environmental chemicals on the liver also extends to understanding extra-hepatic effects. These chemicals have been associated with negative effects on other organs and tissues such as cardiovascular and reproductive diseases. However, organ-organ interactions and the effects of these chemicals are largely understudied, for example, the effects on the gut-liver axis. Recent studies have shown that changes to the gut and its microbiome can lead to a leaky gut. Subsequently, leaky gut has been shown to induce or exacerbate liver disease [17]. Therefore, it is important to investigate the roles of these chemicals in the induction of liver disease as well as their role in the gut and ultimately the gut-liver axis.

Overall objective

The objective of the current study was to evaluate two groups of toxicants, namely: microplastics (MPs) and polychlorinated biphenyls (PCBs) on their role in dysregulating the gut-liver axis and/or impacting the integrity of gut permeability.

Growing evidence suggests that microplastics exposure induces obesity and diabetes as well as alter gut microbiome composition in rodent and marine models [27]. This finding suggests that MP exposure could potentially cause TAFLD and/or TASH. Additionally, findings by Deng et al. suggest that MP exposure leads to increased inflammation and lipid droplet deposition in H&E-stained liver tissues [22]. These findings show that microplastics alter the gut-liver axis. However, the investigation of the liver with the possible induction of TAFLD/TASH by MP exposure and the contribution of the gut and its microbiome is still unstudied. Furthermore, multiple studies including studies from our group have shown the effects of polychlorinated biphenyls on the liver. We have demonstrated that a PCB mixture (Aroclor 1260) can promote steatohepatitis in part through the activation of nuclear receptors [5, 15, 28]. Some of the effects of Aroclor 1260 on the liver were shown to be contributing effects from gut barrier dysbiosis and gut microbiome composition alteration [15]. However, the chronic effects of PCBs on the gut barrier function and integrity as well as the gut microbiome composition has not been studied.

Hypothesis

Therefore, we hypothesize that environmental pollutants will disrupt the gut-liver axis by altering gut microbiome composition resulting in increased intestinal permeability and decreased intestinal function and this subsequently impacts liver morphology and function.

CHAPTER II: INVESTIGATING THE CHRONIC EFFECTS OF AROCLOR 1260 ON THE GUT AND GUT MICROBIOME

INTRODUCTION

Polychlorinated biphenyls (PCBs) are polyhalogenated aromatic hydrocarbons containing up to 10 chlorine atoms on a biphenyl ring [28]. Based on the positioning of these chlorine atoms, it was theorized that there are 209 possible PCB congeners and 130 of these congeners were produced until they were banned in 2001 worldwide [28]. PCB congeners have been grouped into two distinct identifications: coplanar and non-coplanar. Coplanar PCBs are also referred to as dioxin-like PCBs because they are similar to dioxins and can bind and activate aryl hydrocarbon receptors (AhR). Non-coplanar PCBs, are also known as non-dioxin-like PCBs or phenobarbital-like PCBs, referring to their activation of pregnane xenobiotic receptors (PXR) and constitutive androstane receptors (CAR) [11, 12].

PCBs were produced in North America by the Monsanto manufacturing plant located in Anniston, Alabama until production was discontinued in 1970's by the US congress. PCBs were produced for use as dielectric fluids (coolants) in transformers, capacitors, and other electric equipment. Monsanto commercially sold PCBs as mixtures of congeners, under the trade name "Aroclor". The subsequent numbers after Aroclor signify the number of carbon atoms consisting of the phenyl rings and the percentage of chlorine atom by mass of mixture. For

example, Aroclor 1260 is a mixture of mostly non-coplanar PCBs. The 12 indicates the number of carbon atoms on the phenyl rings and while 60 refers to the 60% chlorination by weight of mixture [29]. The chemical and physical properties of some of the PCB congeners contribute to their distribution in the environment as well as their degradation. For example, lower chlorinated and smaller molecular weights PCB congeners make them more volatile and airborne prone compared to highly chlorinated PCB congeners. A high percentage of chlorination, however, make certain PCB congeners more resistant to biodegradation [30]. These higher molecular weight PCB congeners tend to bioaccumulate in fatty tissues in the body due to their increased lipophilicity compared to the lower molecular weight PCB congeners [31]. Although PCBs manufacturing has been banned for over 30 years, they are still present in the environment and subsequently amplify across trophic levels of the food chain [30, 32]. Humans are exposed to PCBs through the air, water, and soil [33]. These exposures cause a myriad of health effects including cardiovascular disease, insulin resistance, obesity, reproductive defects, cancer, and hepatotoxicity such as toxicant associated fatty liver disease (TAFLD) [34, 35].

A previous study by our group utilizing a diet-induced obesity model with Aroclor 1260 exposure for 12 weeks demonstrated that in addition to activation of hepatic CAR and PXR, Aroclor 1260 can induce TAFLD/TASH through extrahepatic effects. An extrahepatic effect previously shown to contribute to the effects of Aroclor 1260 on the liver is the gut and its microbiome [36]. CAR and PXR are known for their roles in the detoxification of xenobiotics molecules

including environmental pollutant, however, recent studies has demonstrated that CAR and PXR regulate of energy metabolism as well as intestinal homeostasis and gut microbiome composition [15, 37]. The gut and the gut microbiome are involved in energy metabolism and the metabolism of xenobiotics. Studies have shown that the gut microbiome plays a role in intestinal homeostasis as well as in energy and endobiotic (such as bile acids) metabolism, which can influence liver health [16, 17].

A study by our group showed that 12-week Aroclor 1260 exposure in diet-induced obese mice altered bacteria composition and decreased the gene expression for tight junction marker in the ileum and intestinal functional markers. These findings were shown to contribute to the exacerbation of steatohepatitis in the exposed mice, indicating the importance of the study of the gut-liver axis and environmental pollutants [15].

However, chronic studies on the effects of Aroclor 1260 on the gut is still largely unknown. We aimed to investigate the chronic effects of Aroclor 1260 exposure on gut microbiome composition and ileal gene expression in the absence of a high fat diet. **Therefore, we postulate that chronic Aroclor 1260 exposure will disrupt gut microbiome composition resulting in a decrease in tight junction and mucosal barrier integrity genes and an increase in pro-inflammatory markers in the intestine.**

METHODS

Animal experiments, diets and chemicals use

The University of Louisville Institutional Animal Care and Use Committee (IACUC) approved the animal use, protocol, and care. Forty 8-week-old male C57BL/6J mice were purchased from Jackson Laboratory (Strain#: 000664; Bar Harbor, Maine). We chose male mice for this study to establish a baseline for future studies investigating sex-dependent effects. The mice were divided into two groups: Control (10 mice) and Aroclor 1260 exposure (30 mice). The study design was based on a previous study using mice exposed to Aroclor 1260 and were fed either high-fat diet or a low-fat diet [38]. Five mice per cage were housed in a pathogen-free, temperature regulated (23.9 °C) room with a twelve-hour light-dark cycle that is accredited by the Association for Assessment and Accreditation of Laboratory Animal Care (AAALAC). Mice were allowed to acclimatize to the animal facility for one week. The mice were fed an autoclaved low-fat diet containing 10.2% kcal from fat (from Harlan Teklad, TD.06416) from the first week and had *ad libitum* access to food and water. Mice were given either a single dose of corn oil for unexposed control mice or a single dose of Aroclor 1260 (catalog: C-260N-1G; AccuStandard, New Haven, CT) at 20 mg/kg via oral gavage on week 3. Dosing was designed to mimic the highest PCB levels observed in Anniston cohort as previously reported [39, 40]. Additionally, a single dose was administered for this study because the half-life for highly chlorinated PCBs such as Aroclor 1260 are estimated to be between 33 -34 months [41], therefore, we postulated that administering a single dose will be

sufficient for the duration of the study. Mice were allowed to age to 33 weeks and were euthanized by the intraperitoneally (I.P.) administration of 120/16 mg/kg body weight of ketamine/xylazine mixture for anesthesia and euthanasia was performed by portal vein exsanguination. Ileum scrapings and cecum samples were collected at the time of euthanasia.

16S Metagenomics sequencing library preparation and sequencing

Cecum samples were snap frozen during mice euthanasia and tissue collection. Using the Illumina MiSeq technology, cecal microbiome composition was analyzed targeting the 16S library ribosomal RNA variables V3 and V4 regions. Firstly, microbial genomic DNA was isolated from the cecal samples using the DNeasy Powersoil pro isolation Kit (catalog: 47014, Qiagen, Germantown, MD, USA) keeping in line with the manufacturer's instructions. DNA was quantified using the Nanodrop™ One^C Microvolume UV-Vis Spectrometer from Thermo Scientific (catalog: 701-058112; Madison, MI) and followed by a further quantitation of microbial genomic DNA using the Qubit Broad Range (BR) assay (Thermo Fisher Scientific, Waltham, MA) in a Qubit 2.0 fluorometer. V3 and V4 regions on the resulting DNA were amplified using forward (5' TCGTCGGCAGCGTCAGATGTGTATAAGAGACAGCCTACGGGNGGCWGCAG) and reverse (5' GTCTCGTGGGCTCGGAGATGTGTATAAGAGACAGGACTACHVGGGTATCTAATCC) primers complementary to the region of interest with overhang adapters (Forward overhang: 5' TCGTCGGCAGCGTCAGATGTGTATAAGAGACAG-

[locus specific sequence]; Reverse overhang: 5'

GTCTCGTGGGCTCGGAGATGTGTATAAGAGACAG- [locus specific

sequence]) according to the Illumina's 16S amplicon PCR guide (Illumina, San Diego, CA, USA). Next, the V3 and V4 amplicons were purified using AMPure XP beads (catalog: A63881, Beckman coulter genomics, Indianapolis, IN, USA) and then the libraries were prepared by index PCR according to the Illumina's 16S library preparing guide. Briefly, Index PCR was carried out using the Nextera XT Kit (catalog: FC-121-1012, Illumina, San Diego, CA, USA) to attach dual indices and Illumina sequencing adapters. A pooled library was made by mixing aliquots of the libraries and the concentration of the pooled library was determined using a bioanalyzer. The pooled libraries were denatured and PhIX control (Illumina, San Diego, CA, USA) library was mixed into the pooled library. To confirm sample concentration, sequencing was performed on a Nano-300 cycle test chip (MS-103-1001). Lastly, the sequencing was followed by the Illumina MiSeq reagents kit v3 (600 cycles (MS-102-3003) at 9pM and 30% PhIX. This method has been previously published by our group [15].

Sequencing data analysis

Before statistical analysis, raw sequenced data's quality was checked using FastQC (<https://www.bioinformatics.barraham.ac.uk/projects/fastqc/> version 0.10.1). Several assessments were carried out using multiple algorithms to encompass all information from the sequenced data. First, the sequence data was cut and analyzed using QIIME 2 software [42-45]. The sequenced reads were demultiplexed and then the demultiplexed sequence reads were denoised

into amplicon sequence variants or into clusters of operational taxonomic units (OTU) using Divisive Amplicon Denoising Algorithm (DADA2) [43, 45, 46]. Alpha and beta diversity analyses of the feature table were performed, and a phylogenetic tree was generated using representative sequences. Various algorithms (Shannon index, observed features and faith_Pd) were used in the assessment of alpha diversity. The differences in bacteria richness/ abundance in each sample were assessed using the Shannon index algorithm [47, 48]. Observed features/ species algorithm also known as OTUs was used to measure the number of unique/ different bacteria present in each sample [49]. The faith_ phylogeny distance (Faith_pd) algorithm was used to measure the biodiversity of each sample based on phylogeny or based on their relatedness [50]. The faith_pd simply measures the evolutionary relationship between bacteria species. The *Emperor* tool was employed to assess for sample metadata (distance between sample or Beta diversity) on a principal covariant analysis plot using both UniFrac (weighted and Unweighted) and Jaccard algorithms. UniFrac and Jaccard algorithm was used to assess the beta diversity between the two groups. The unweighted variants (measures the absence and presence of species between groups) [51] and the weighted (measures the abundances of individual species between each group while taking into account the absences or the presence of each species) [52] of the UniFrac (measures the phylogenetic distance between samples) beta diversity [51, 53] was envisaged displayed as a three principal coordinates plot using principal covariant analysis on the *Emperor tool*. The Jaccard (measures the similarity between the groups) [54] algorithm

was also displayed as a three principal coordinates plot. Phylum taxonomy analysis was performed using pre-trained classifiers which have sequences assigned to certain OTUs at a 99% similarity to the Greengenes database (<http://greengenes.lbl.gov/> v13.8) [55] from the V3V4 regions of sequences. Taxa results from QIIME 2 was analyzed on the Galaxy platform [56] and generated results were bar graphs represented as relative abundance (frequency of the taxa relative to the frequency of other taxa) with significance set at $\alpha \leq 0.05$ obtained using a Mann-Whitney U test. NAFLD activity score (NAS), a score calculated using the sum of steatosis (0-3), lobular inflammation (0-3) and hepatocyte ballooning (0-2) in each liver section, was used to further evaluate the alpha, beta and phylum taxonomy into low and high NAS score compared to the control [57].

Real-time qPCR of ileal scrapings

Ileal scraping samples were collected by cutting the ileum open to expose the epithelial lining. Ileal epithelial lining was scraped out and placed in a tube with RNA-STAT60 (Tel-Test, Inc., Friendswood, TX, USA) and 0.5 mm silica beads (Biospec Products, Bartlesville, OK, USA). Tissues were then homogenized using a Mini-Beadbeater 16 bead mill homogenizer (Biospec Products, Bartlesville, OK, USA). Total RNA was extracted using RNA-STAT 60 chloroform and phenol manufacturer's protocol (Tel-Test, Inc., Friendswood, TX, USA) from the homogenized tissue. Resulting RNA was eluted in nuclease free water and quantified using NanoDrop™ One^C Microvolume UV-Vis Spectrometer from Thermo Scientific (catalog: 701-058112; Madison, MI). cDNA was prepared

from RNA samples by reverse transcription using single step cDNA synthesis reagent, QScript (catalog: 95048-500; Quantabio; Beverly, MA). RT-qPCR was performed using the iTaq universal probe super mix from Bio-Rad (catalog: 1725134; Hercules, CA) on the CXX384™. Expression for genes of interest were investigated employing commercially available predesigned TaqMan Gene Expression Assays (Applied Biosystems, Foster City, CA, USA): Tight-junction protein -1 (*Tjp1*); (Mm01320638_m1), Occludin (*Ocln*); (Mm00500910_m1), Mucin 2 (*Muc2*); (Mm01276676_m1), Regenerating family member 3 gamma (*Reg3g*); (Mm00441127_m1), Claudin-1 (*Cldn*); (Mm00516701_m1), Claudin-2 (*Cldn2*); (Mm00516703_s1), Interferon gamma (*Ifng*); (Mm01168134_m1), Trefoil factor 3 (*Tff3*); (Mm00495590_m1), Interleukin-6 (*Il-6*); (Mm00446190_m1), Cadherin-5 (*Cdh5*); (Mm00486938_m1), Fibroblast growth factor 15 (*Fgf15*); (Mm00433278_m1), Interleukin-1 beta (*Il-1β*); (Mm00434228_m1), Claudin-3 (*Cldn3*); (Mm00515499_s1), Cathelicidin antimicrobial peptide (*Camp*); (Mm00438285_m1), Interleukin-10 (*Il-10*); (Mm01288386_m1), tumor necrosis factor (*Tnfa*); (Mm00443258_m1), Transforming growth factor beta (*Tgfb*); (Mm01178820_m1), Intercellular adhesion molecule (*Icam*); (Mm00516023_m1), cytochrome P450, family 1, subfamily a, polypeptide 1 (*Cyp1a1*); (Mm00487218_m1), cytochrome P450, family 2, subfamily b, polypeptide 10 (*Cyp2b10*); (Mm01972453_s1), cytochrome P450, family 3, subfamily a, polypeptide 11 (*Cyp3a11*); (Mm00731567_m1), cytochrome P450, family 2, subfamily c, polypeptide 29 (*Cyp2c29*); (Mm07306461_m1). 18S rRNA (18s) (catalog: 4319413E; Applied biosystems; Waltham, MA) was used as the

housekeeping gene and relative mRNA expressions was calculated using the 2- $\Delta\Delta C_t$ method. Mean expression of each gene in the control mice (corn oil fed) were normalized to 1. Data for all other animals were as fold induction compared to mean control.

Statistical analyses

Data were analyzed using a Mann Whitney U test or a Kruskal-Wallis test (for Aroclor 1260 exposed mice divided based on low and high NAS score) on GraphPad Prism (version 9.5.1) for windows (GraphPad Software Inc., La Jolla, CA, USA), by comparing the control and the Aroclor 1260 exposed mice. Graphs were expressed as mean \pm SD and statistical significance was set at $p \leq 0.05$.

RESULTS

Previous studies [15] have indicated that Aroclor 1260 exposure altered expression of genes encoding proteins for gut permeability and function as well as inflammatory markers. The aim was to assess the effects of Aroclor 1260 on gut function (intestine and intestinal microbiome maintenance and repair), permeability, and inflammation, and correlate to the effect observed in the 16S analyses of ileal gene expression. Although the intestine comprises the duodenum, the jejunum and the ileum, the ileum was used for this study because it is more immunologically active compared to the other parts of the gut [58]. Importantly, the ileum is often used in the assessment of leaky gut (gut barrier dysfunction) because the ileum is most susceptible to alterations in gut permeability [15, 58]. Gut dysbiosis is characterized by disruption to gut barrier, gut microbiome alterations and an increase in inflammation resulting in a leaky gut. The intestinal barrier comprises of structural and functional genes that encode proteins involved in cell adhesion (*Tjp1* and *Cldn2*), maintenance/ repair (*Tff3*), and physical defense (*Muc1*) such as the mucosal layer [59, 60].

Effects of Aroclor 1260 on alpha diversity

Alpha diversity measures the diversity in bacterial composition present within each sample. The Shannon index showed no change between the Aroclor 1260 exposed mice compared to the control (Fig 1A). The observed features (Fig 1B) and the Faith_pd (Fig 1C) also showed no change between the Aroclor 1260 exposed mice compared to the control.

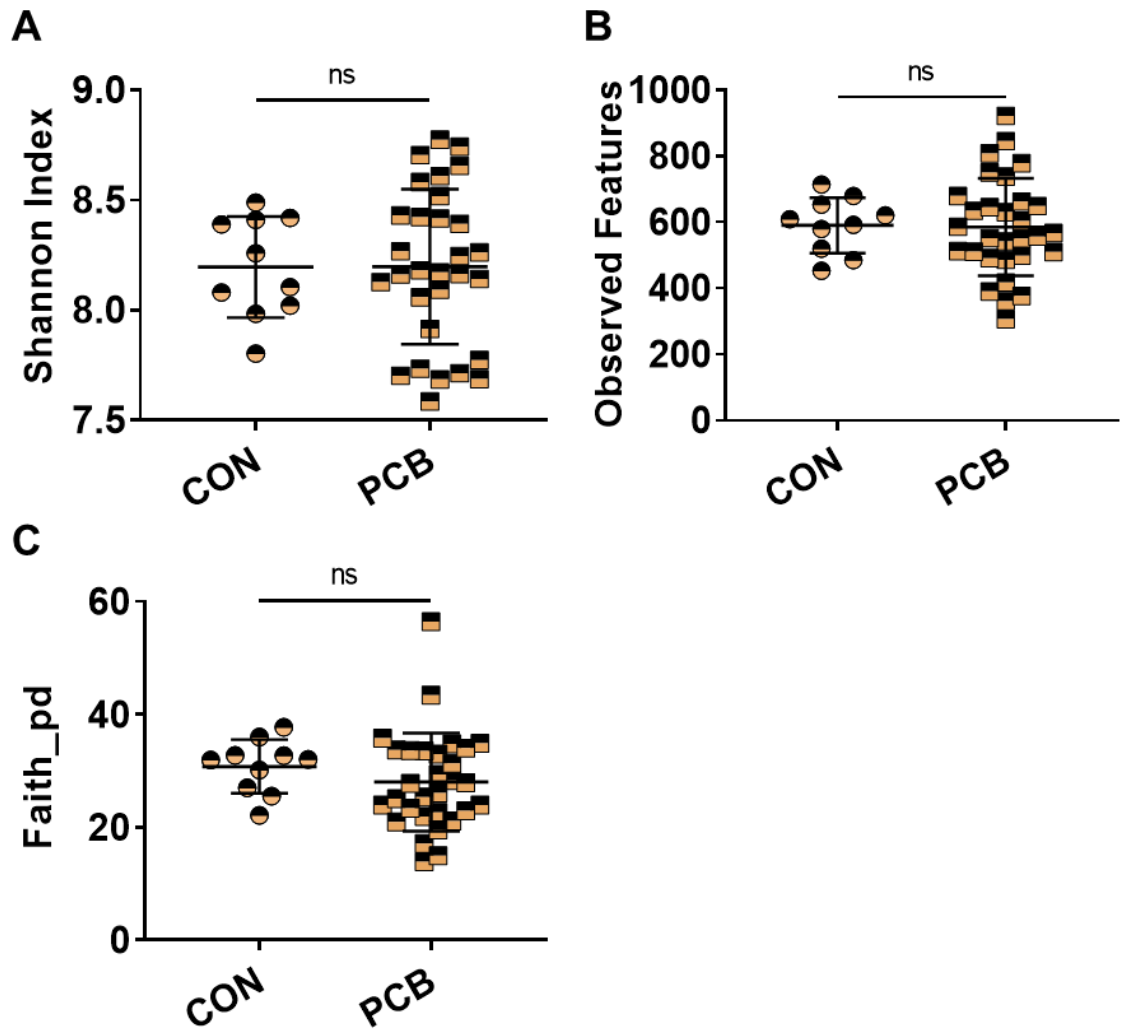


Figure 1: Effects of Aroclor 1260 on microbiome alpha diversity.

Microbiome alpha diversity was measured using three QIIME algorithm namely: Shannon index (measures the number of different bacteria present in a sample) **(A)**, Observed features/species (measures the bacteria richness of the sample) **(B)** and Faith_pd (measures biodiversity based on phylogeny) **(C)**. Values are represented as mean \pm SD with significance defined as $p \leq 0.05$. p -values were determined using the Mann-Whitney-U statistical test.

Effects of Aroclor 1260 on beta diversity

Beta diversity is used to assess gut microbiome composition between two groups by considering the distance between samples on a principal components analysis (PCA) plot. The UniFrac and the Jaccard algorithms (Fig 2A, B & C) showed no changes between the control and the Aroclor 1260 exposed mice. However, the Jaccard algorithm showed two distinct separate groups on the three axis principal coordinates plots.

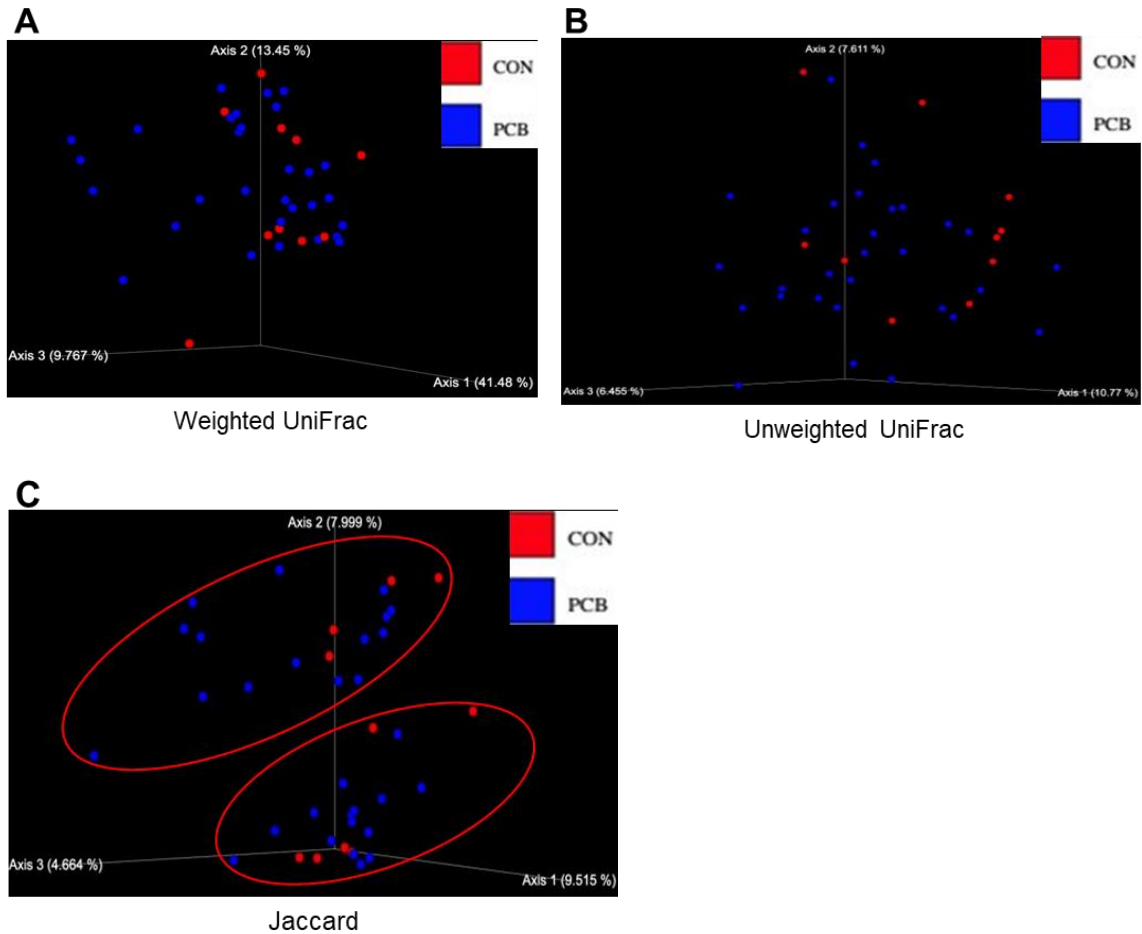


Figure 2: Effects of Aroclor 1260 on microbiome beta diversity.

Microbiome beta diversity was determined using UniFrac (unweighted and weighted variants) and Jaccard. Weighted and Unweighted UniFrac (**A and B**) and Jaccard (**C**) for beta diversity. Measurements were envisaged with principal covariant analysis. q -values < 0.05 depicts significance between control group and Aroclor 1260 group using PERMANOVA.

Effects of Aroclor 1260 on microbiome phylum taxonomy

When assessing microbiome phylum taxonomy, the following microbiome phylum were assessed: *Firmicutes*, *Bacteroidetes* and *Proteobacteria*. The *Firmicutes* and *Bacteroidetes* (F/B) ratio is often used in the assessment of obesity and inflammatory bowel disease (IBD). A high F/B ratio is associated with obesity while a low F/B ratio is associated with IBD [61]. Additionally, *Proteobacteria* is associated with inflammation [62]. There was no change in the relative abundance of *Firmicutes* or *Bacteroidetes* phylum (Fig 3A & B) between the control and the Aroclor 1260 exposed mice. There was no change to the F/B ratio (Fig 3C) between the control and the Aroclor 1260 exposed mice. However, the relative abundance of the *Proteobacteria* phylum (Fig 3D) showed a trending increase ($p = 0.06$) in the Aroclor 1260 exposed mice.

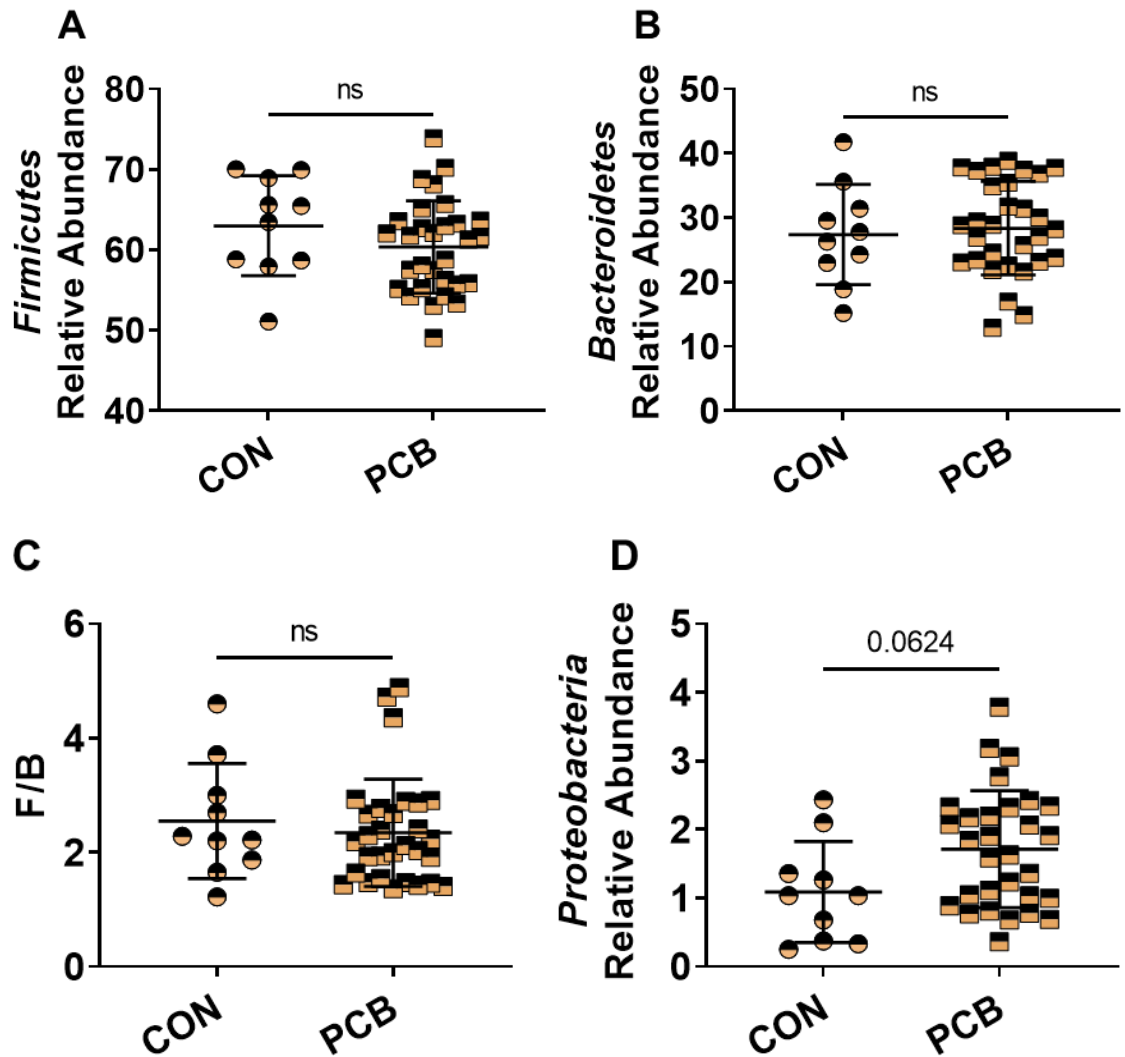


Figure 3: Effects of Aroclor 1260 on microbiome phylum taxonomy.

Relative abundance of bacteria at the phyla level in each sample was analyzed using a Mann Whitney U test. Bacteria namely: *Firmicutes* (A), *Bacteroidetes* (B) and *Proteobacteria* (D). A *Firmicutes/ Bacteroidetes* ratio (C) was calculated. Values are represented as mean \pm SD with significance defined as $p \leq 0.05$.

Analysis of alpha and beta diversity and phylum taxonomy based on NAFLD activity score (NAS)

The Jaccard algorithm showed two distinct group in the PCA plot. Previous finding have associated worsening of NAFLD with a decrease in gut microbiome [63]. We postulate that the two distinct groups observed in the Jaccard PCA plot could be low and high NAS score. To understand the distinct groups, the alpha and beta diversity as well as phylum was assessed based on the NAFLD activity score (NAS) which is a score calculated using the sum of steatosis (0-3), lobular inflammation (0-3) and hepatocyte ballooning (0-2). A total score of 1-4 was classified as simple steatosis/ low NAS score and a total score of 5-8 was classified as steatohepatitis (NASH) / high NAS score. The quantification for the NAS score was based according to previous reports [57].

Effects of Aroclor 1260 on alpha diversity based on low and high NAS score.

Aroclor 1260 exposed group was reevaluated based on low and high NAS score from liver samples. Microbiome alpha diversity using the Shannon index, Observed features and Faith_pd (Fig 4A, B & C), showed no changes in alpha diversity between the control mice and the Aroclor 1260 exposed mice expressed as low and high NAS score.

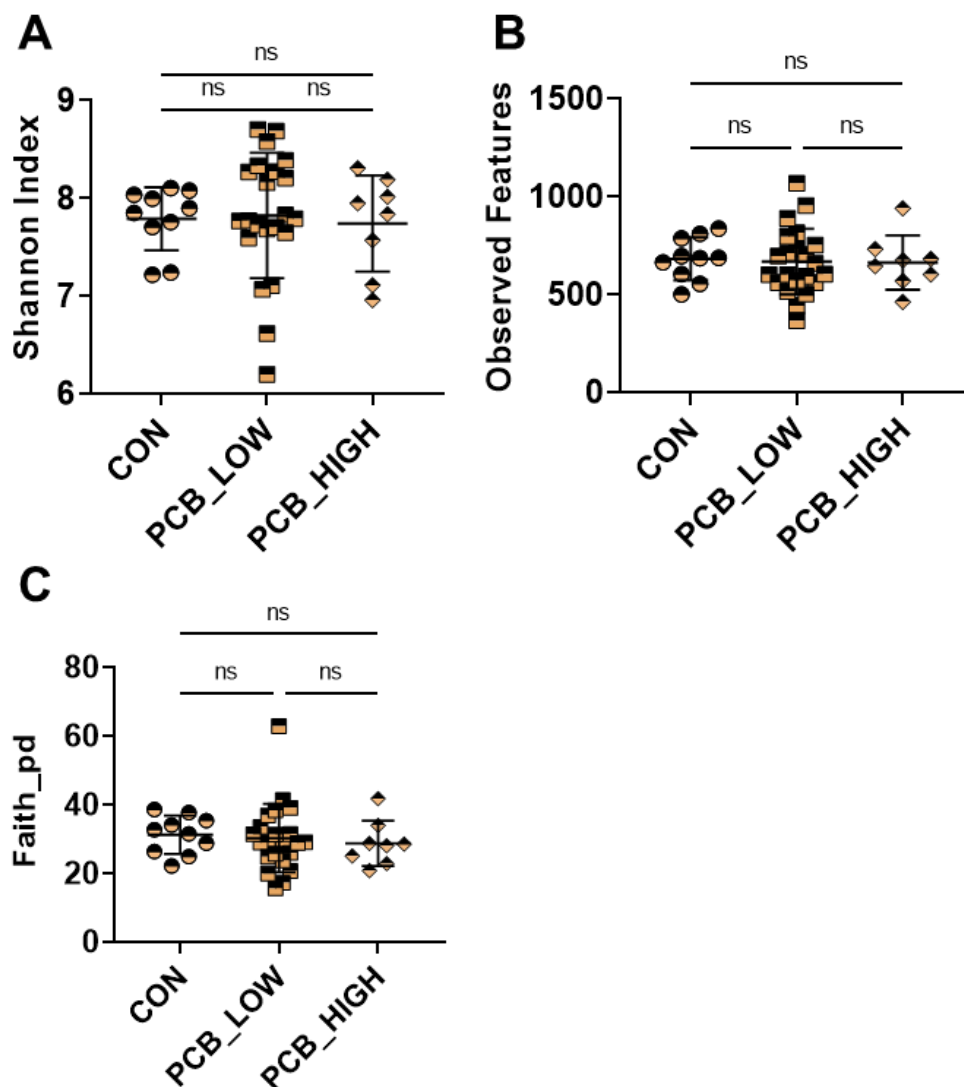


Figure 4: Effects of Aroclor 1260 on microbiome alpha diversity based on low and high NAS score.

Alpha diversity was measured using three QIIME algorithm namely: Shannon index (measures the number of different bacteria present in a sample) **(A)**, Observed features/species (measures the bacteria richness of the sample) **(B)** and Faith_pd (measures biodiversity based on phylogeny) **(C)**. Aroclor 1260 exposure group was divided into two groups based on low and high NAS score. Values are represented as mean \pm SD with significance defined as $p \leq 0.05$. p -values were determined using a Kruskal -Wallis statistical test.

Effects of Aroclor 1260 on beta diversity low and high NAS score

Aroclor 1260 exposed mice was reevaluated based on low and high NAS score from liver samples. Microbiome beta diversity using weighted and unweighted UniFrac and Jaccard algorithms (Fig 5A, B & C), showed no changes in beta diversity between the control and the Aroclor 1260 exposed mice expressed as low and high NAS score.

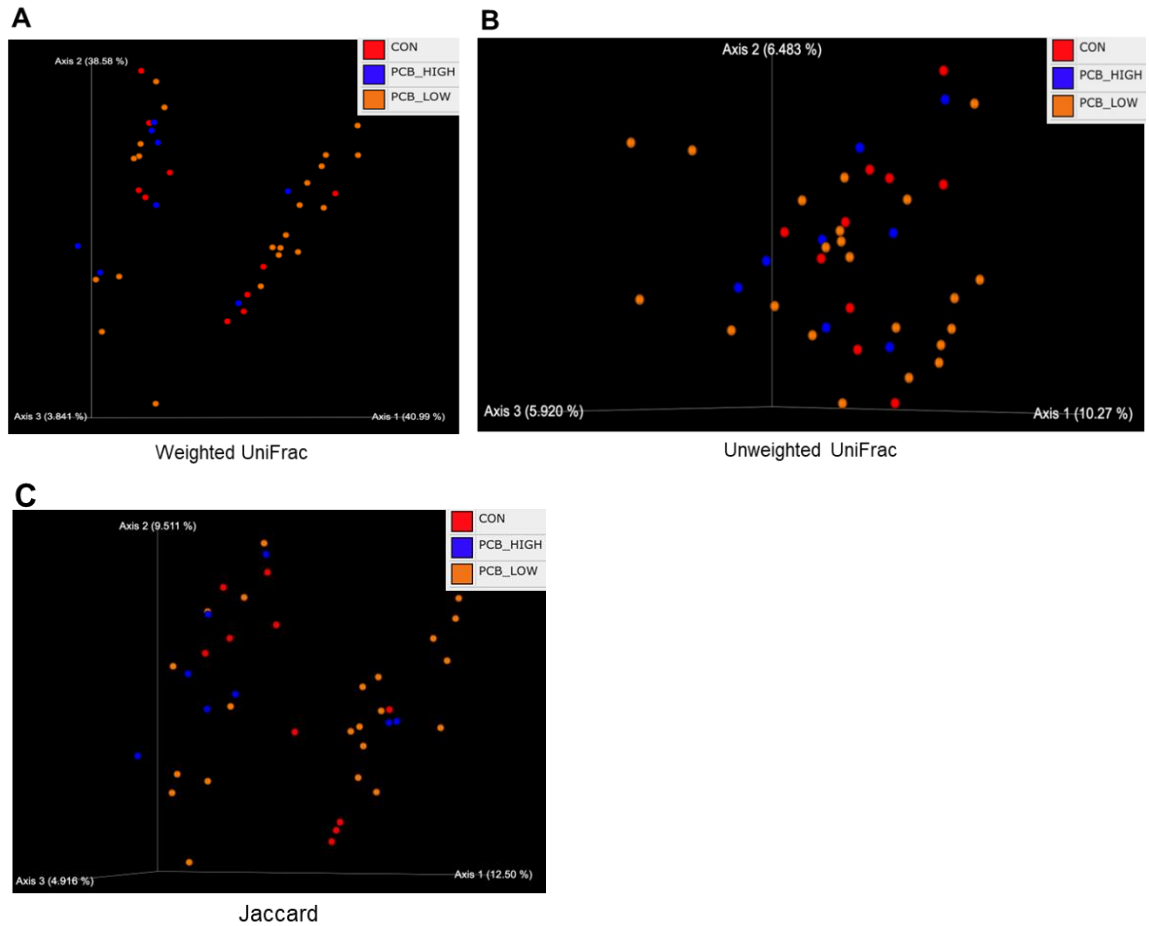


Figure 5: Effects of Aroclor 1260 on microbiome beta diversity based on low and high NAS score.

Microbiome beta diversity was determined using UniFrac (unweighted and weighted variants) and Jaccard. Weighted and Unweighted UniFrac (**A and B**) and Jaccard (**C**) for beta diversity. Measurements were envisaged with principal covariant analysis. q-values depicts significance between control mice and Aroclor 1260 exposed mice expressed as low and high NAS score using PERMANOVA.

Effects of Aroclor 1260 on microbiome phylum taxonomy low and high NAS score

Microbiome phylum distribution in Aroclor 1260 exposed mice was reevaluated based on low and high NAS score from liver samples. The following microbiome phylum were assessed: *Firmicutes*, *Bacteroidetes* and *Proteobacteria*. There were no changes in the relative abundance of *Firmicutes*, *Bacteroidetes* and *Proteobacteria* phylum (Fig 6A, B &D) between the control and the Aroclor 1260 exposed mice expressed as low and high NAS score. There were no changes to the F/B ratio (Fig 6C) between the control and the Aroclor 1260 exposed mice expressed as low and high NAS score.

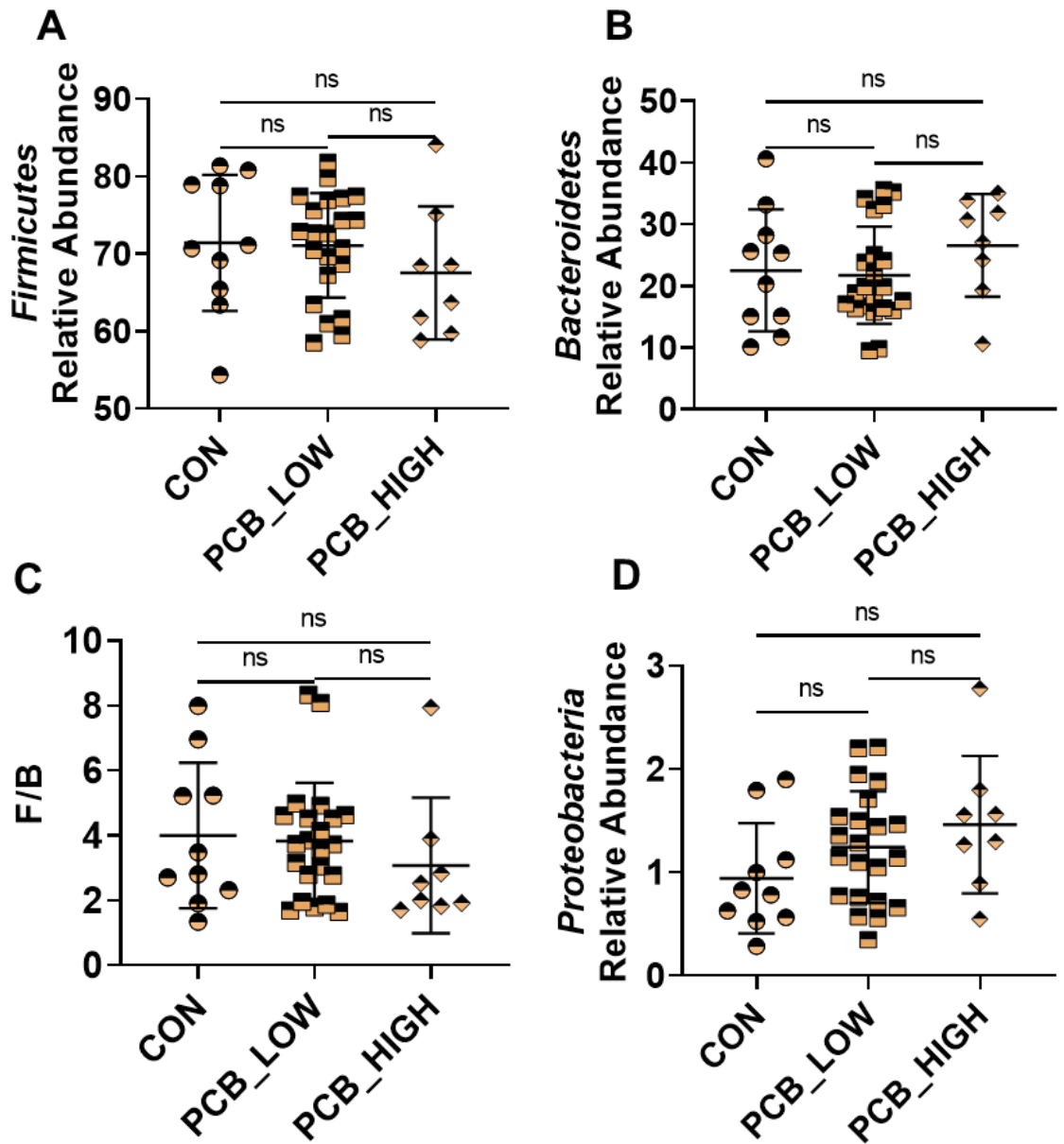


Figure 6: Effects of Aroclor 1260 on microbiome phylum taxonomy based on low and high NAS score.

Relative abundance of bacteria at the phyla level in each sample was analyzed using a Kruskal-Wallis test based on low and high NAS score. Bacteria phyla namely: *Firmicutes* (A), *Bacteroidetes* (B) and *Proteobacteria* (D). A *Firmicutes/Bacteroidetes* ratio (C) was calculated. Values are represented as mean \pm SD with significance defined as $p \leq 0.05$.

Effects of Aroclor 1260 on ileal permeability genes

To assess the effect of Aroclor 1260 on ileal permeability, ileal mRNA level for genes that encode for protein involved in epithelial cell adhesion were measured. Occludin (*Ocln*), and claudins 1, 2 and 3 (*Cldn 1, 2 & 3*) are transmembrane protein that are linked to the actin cytoskeleton by tight junction scaffolding protein such as zonula occludens -1 which is encoded by the gene tight junction protein 1 (*Tjp1*). Vascular endothelial (VE) -Cadherin 5 is an adhesion molecule between cells encoded by the gene cadherin 5 (*Cdh5*). Comparing the effects of Aroclor 1260 on gene expression of various tight junction and adhesion junction genes to the control, it was observed that Aroclor 1260 did not alter the gene expression of *Ocln*, *Cldn 1, 2 & 3* or *Tjp1* (Fig 7A, B and Appx. Table 1). However, *Cdh5* (Fig 7C) was significantly decreased in the Aroclor 1260 exposed mice. It could be inferred that Aroclor 1260 disrupts certain cell adhesion molecules such as cadherin 5 resulting in increased permeability in the gut.

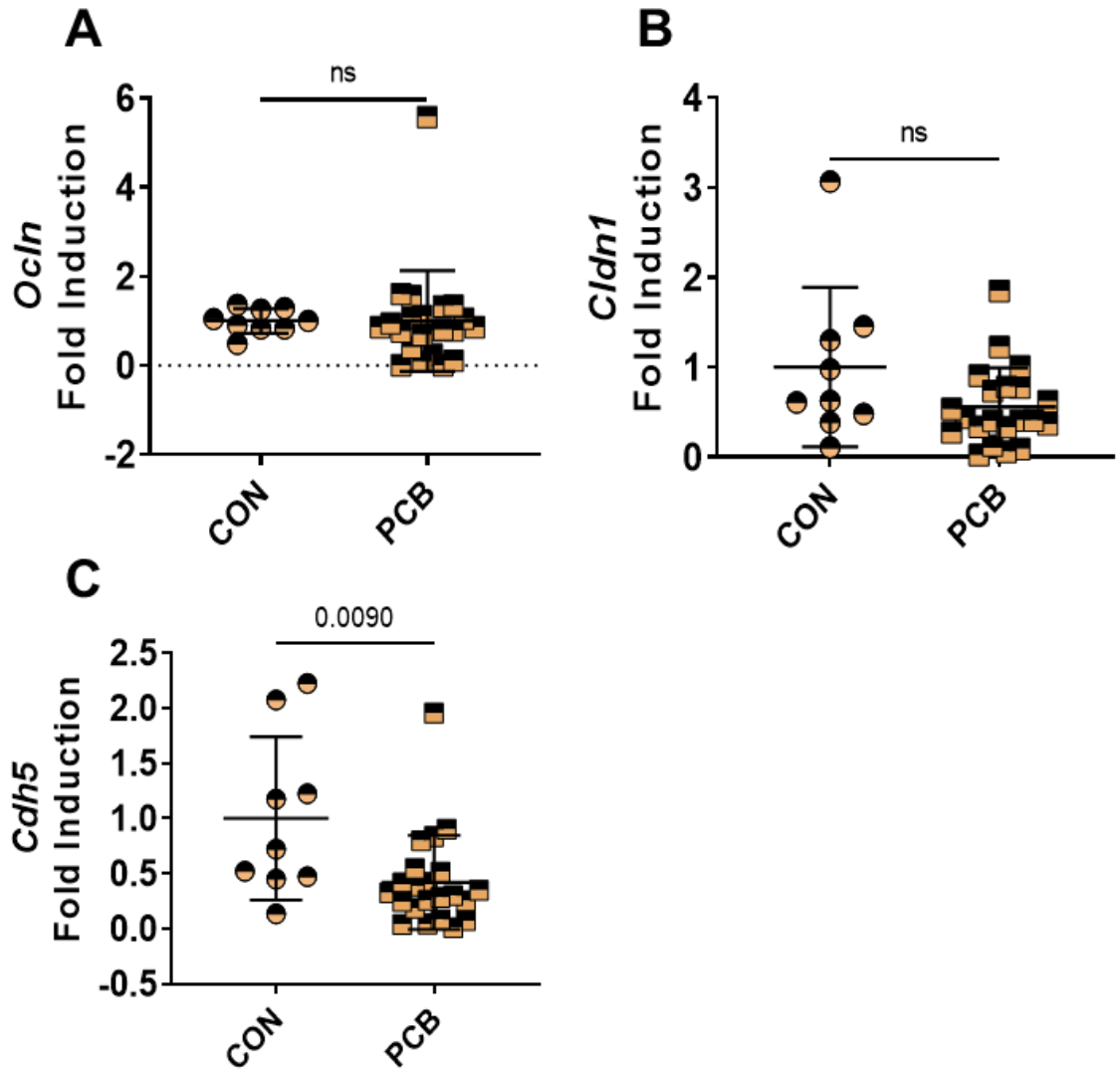


Figure 7: Effects of Aroclor 1260 on ileal permeability gene expression.

RT-qPCR was used to assess ileal permeability by measuring the mRNA levels of Occludin (*Ocln*) (A), Claudin-1 (*Cldn-1*) (B) and Cadherin-5 (*Cdh5*) (C). Values are represented as mean \pm SD with significance defined as $p \leq 0.05$. p -values were determined using the Mann-Whitney-U statistical test.

Effects of Aroclor 1260 on ileal function genes

To further examine the effect of Aroclor 1260 on ileal mRNA levels, ileal functional genes was assessed. Ileal function gene which encodes for the mucus gel forming protein such as mucin 2 (*Muc2*), proteins involved in the maintenance/ repair/ regulation of the mucosal layer and tight junction such as trefoil factor 3 (*Tff3*) and bile acid homeostasis regulatory and liver repair protein such as fibroblast growth factor 15 (*Fgf15*) were assessed. *Muc-2* and *Fgf15* mRNA level were not changed due to Aroclor 1260 exposed (Fig 8A & B). However, *Tff3* expression was increased in the Aroclor 1260 exposed mice (Fig 8C), suggesting that the intestine was responding to the disruption of the cell adhesion molecules.

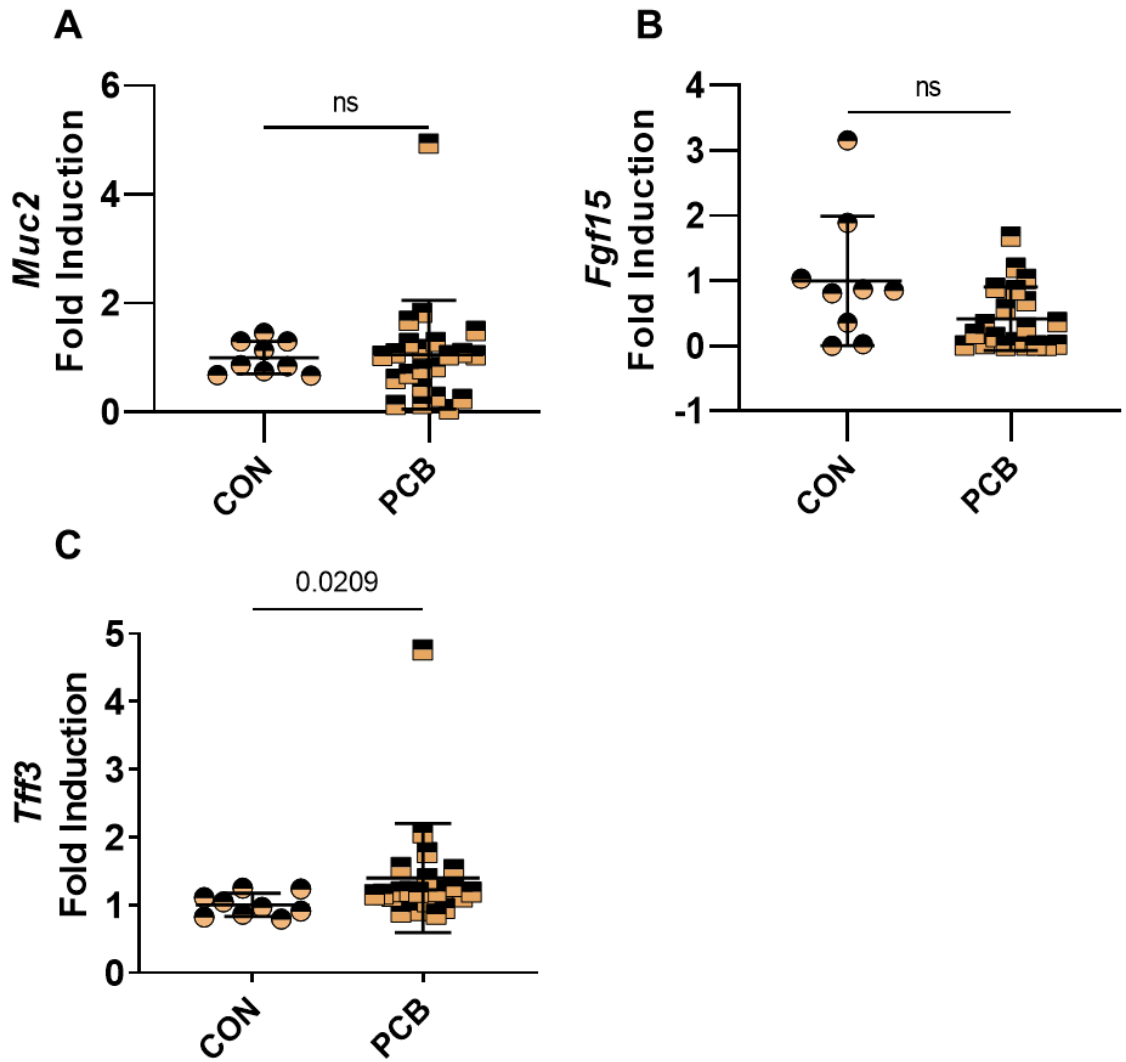


Figure 8: Effects of Aroclor 1260 on ileal functional gene expression.

RT-qPCR was used to assess ileal function by measuring the mRNA levels ileal functional markers such as: Mucin-2 (*Muc2*) (A), Fibroblast growth factor-15 (*Fgf15*) (B), and Trefoil factor-3 (*Tff3*) (C). Values are represented as mean \pm SD with significance defined as $p \leq 0.05$. p -values were determined using the Mann-Whitney-U statistical test.

Effects of Aroclor 1260 on ileal inflammatory genes

Another important set of genes to investigate are genes involved in inflammatory and the maintenance of a healthy ileum. Tumor necrosis factor alpha (*Tnfa*) genes encodes proteins involved in the release of immune cells and regenerating islet-derived protein 3 gamma (*Reg3g*) gene encodes proteins involved in antimicrobial functions in the intestines. The mRNA levels of *Tnfa* and *Reg3g* (Fig 9A & B) were not changed due to Aroclor 1260 exposure. Other inflammatory markers such as pro inflammatory genes: interleukin 6 (*Il-6*), interleukin 1 beta (*Il-1b*), and intercellular adhesion molecule (*Icam*) (Appx. Table 1) and anti-inflammatory genes: interleukin 10 (*Il-10*) (Appx. Table 1) were assessed and no changes were observed. However, the mRNA level for cathelicidin anti-microbial peptide (*Camp*) (Fig 9C), that encodes for a preproprotein which is secreted by macrophages and neutrophils when it becomes a matured protein, showed a trending decrease ($p = 0.055$) in the Aroclor 1260 exposed mice.

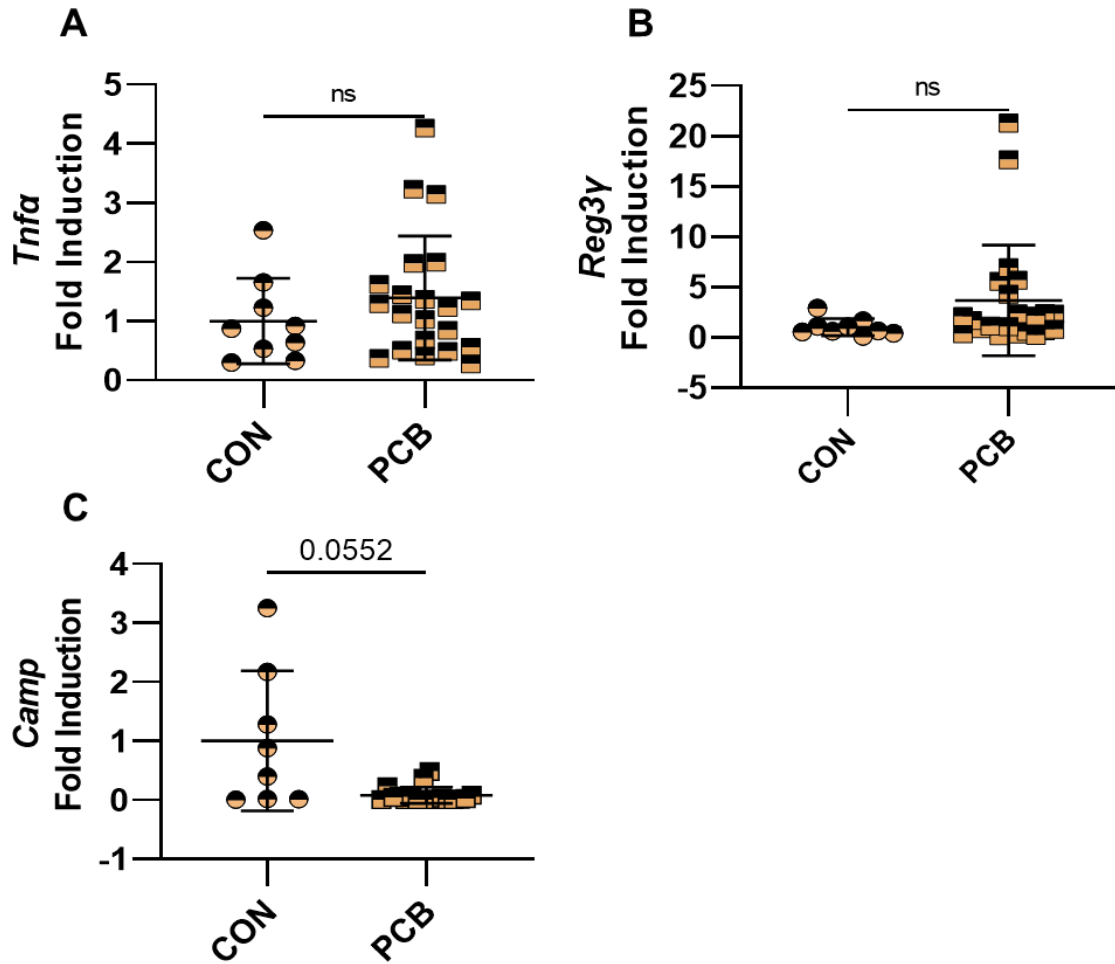


Figure 9: Effects of Aroclor 1260 on ileal inflammatory gene expression.

RT-qPCR was used to assess ileal inflammation by measuring the mRNA levels inflammatory genes such as: Tumor necrosis factor (*Tnfa*) (**A**), Regenerating Family member 3 gamma (*Reg3y*) (**B**) and Cathelicidin antimicrobial peptide (*Camp*) (**C**). Values are represented as mean \pm SD with significance defined as $p \leq 0.05$. p -values were determined using the Mann-Whitney-U statistical test.

Effects of Aroclor 1260 on nuclear receptors target genes

Previous studies have indicated that Aroclor 1260 affects nuclear receptor specifically xenobiotic nuclear receptor such as PXR and CAR [15, 36]. To observe if these receptors were activated, nuclear receptor target gene mRNA were assessed. The following genes were analyzed: cytochrome P450, family 3, subfamily a, polypeptide 11 (*Cyp3a11*), cytochrome P450, family 2, subfamily b, polypeptide 10 (*Cyp2b10*), and cytochrome P450, family 2, subfamily c, polypeptide 29 (*Cyp2c29*) (Fig 10A-C). The mRNA levels of these genes were not changed due to Aroclor 1260 exposure.

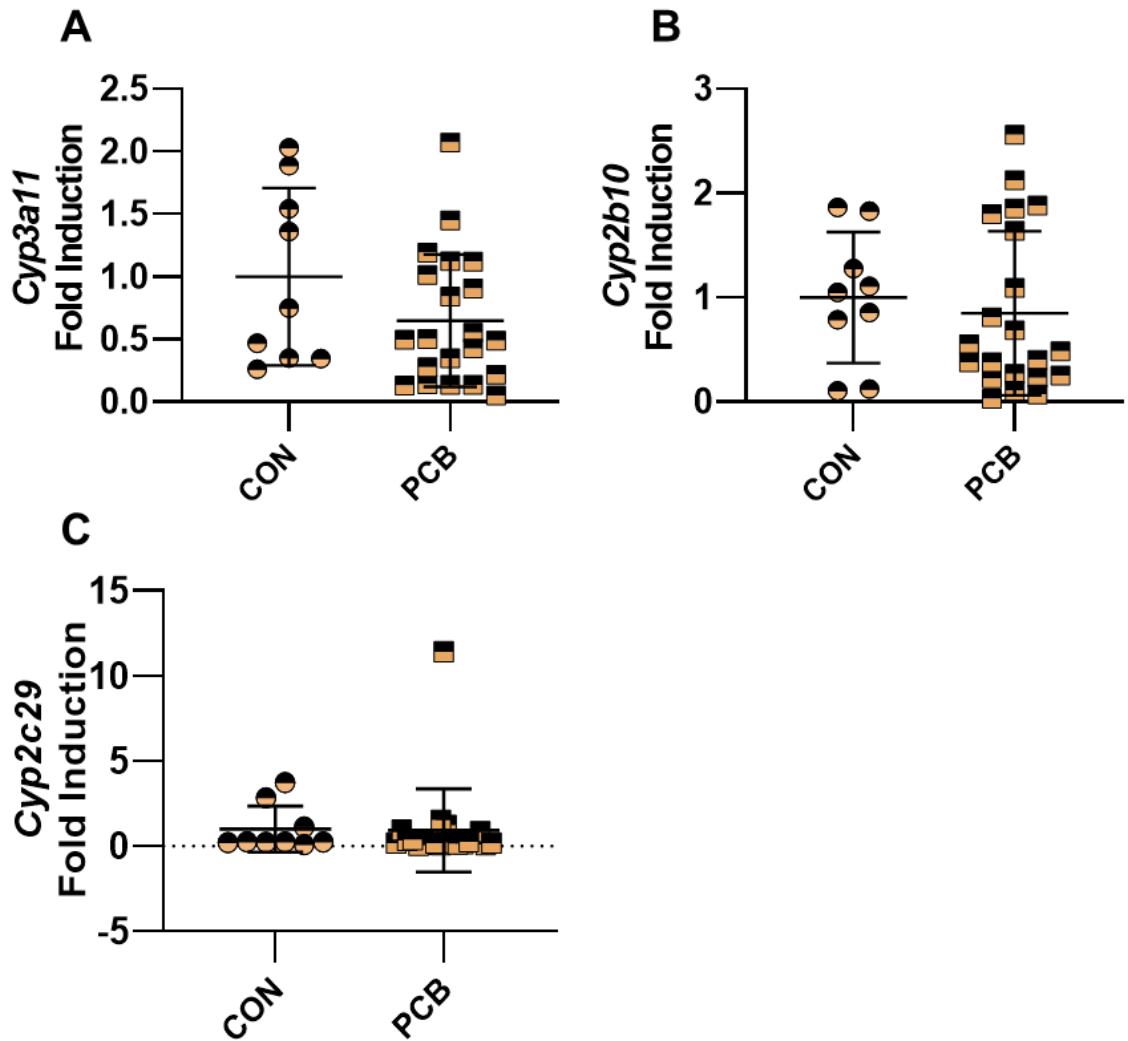


Figure 10: Effects of Aroclor 1260 on PXR and CAR target genes gene expression.

RT-qPCR was used to assess the activation of nuclear receptors in ileal by measuring the mRNA levels of nuclear receptor target genes: Cytochrome P450, family 3, subfamily a, polypeptide 11 (*Cyp3a11*) (A), Cytochrome P450, family 2, subfamily b, polypeptide 10 (*Cyp2b10*) (B), and Cytochrome P450, family 2, subfamily c, polypeptide 29 (*Cyp2c29*) (C). Values are represented as mean ± SD with significance defined as $p \leq 0.05$. p -values were determined using the Mann-Whitney-U statistical test.

DISCUSSION

Aroclor 1260 is a mixture of PCBs which are popularly referred to as “forever chemical” due to their resistance to degradation and persistence in the ecosystem. Aroclor 1260 is composed largely of PCB congeners that are heavily chlorinated and have the tendency to bioaccumulate, and thus mimics PCB bioaccumulation patterns observed in the human population [28, 64]. Although studies have shown the effects of PCBs and PCB mixtures including Aroclor 1260 in acute and sub-chronic studies, chronic studies evaluating the effects of PCB mixtures on the body especially the gut and its microbiome, have not been investigated.

Sub-chronic exposure to Aroclor 1260 has previously been shown to exacerbate steatohepatitis in diet-induced obese mice in part through the activation of nuclear receptor PXR and CAR [36]. Furthermore, extrahepatic PXR and CAR activation in the gut was shown to contribute to the effects observed in the liver [15]. The study findings showed that gut microbiome composition was altered by Aroclor 1260 which concurrently decreased intestinal integrity. These findings showed the effects of Aroclor 1260 on the gut and implicated the gut-liver axis as a mechanistic arm of environmental pollutants’ contribution to NAFLD. For this study we aimed to investigate the chronic effects of Aroclor 1260 exposure on the gut microbiome composition as well as intestinal permeability and inflammation endpoint in the absence of diet-induced obesity. To investigate the effects of Aroclor 1260 on the gut and its microbiome, we assessed the following endpoints for the gut dysbiosis: gut microbiome

composition (alpha diversity, beta diversity and phylum taxonomy) and intestinal integrity and functions (intestinal permeability, function, inflammation, and nuclear receptor activation). Our result showed that gut microbiome associated with intestinal inflammation was not directly altered by Aroclor 1260 exposure. In addition, minor decrease in adhesion molecules gene expression as well as a minor increase in intestinal maintenance and repair gene expression indicates signs of a possible compensatory mechanism in place for injury.

To assess the effect of Aroclor 1260 on the gut, we examined the effects on the gut microbiome composition post-exposure. Contrary to what we expected, we observed no change in alpha diversity, a parameter often used to assess the overall wellness and richness of the gut microbiome. Similarly, beta diversity, which is an assessment of the differences in the total species composition was not altered by Aroclor 1260 exposure. This suggests that chronic Aroclor 1260 exposure did not alter gut microbiome composition nor bacteria richness/ wellness, which is partly consistent to previously reported findings which suggests that Aroclor 1260 did not alter alpha diversity although bacterial composition (beta diversity) was altered. This could be explained by the added effects of a high fat diet, previously reported to have contributed to the alteration of beta diversity [15]. Furthermore, we suspected that the exposure to a single dose of Aroclor 1260 was not sufficient to induce gut microbiome changes with such chronic studies. A deeper look into the effects of Aroclor 1260 on bacterial phylum showed no significant changes in the relative abundance of *Firmicutes*, *Bacteroidetes* and the ratio of *Firmicutes* and *Bacteroidetes*. These

phyla of bacteria are not only the dominant bacterial phyla community in the human gut but the ratio of these two phyla has been correlated with obesity [65]. Nonetheless, mice exposed to Aroclor 1260 showed a non-significant trend for increased abundance of *proteobacteria* which have been correlated with various inflammatory diseases including but not limited to NAFLD [62].

The reevaluation of the alpha, beta and phylum diversity based on low and high NAFLD activity score (NAS) score also showed no changes between the low and high NAS score group and the control. This suggests the degree of NAFLD progression did not alter the alpha, beta diversities and phylum taxonomy. This is contrary to previous report stating that the gut microbiome of NAFLD patients become less diverse with NAFLD progression especially with worsening fibrosis [63]. The study also showed different bacterial phylum abundance at different stages of NAFLD. Our findings on the effect of Aroclor 1260 on the gut microbiome were not in concordance with previous findings and what we expected to observe. One plausible explanation for this could be age-related gut microbiome changes that were not accounted for in this chronic study, and potential changes in gut microbiome either with initial exposure or even during the mid-study period that were not captured.

Based on these findings, we plan to collect fecal samples intermittently throughout the study period to evaluate the effects of aging on gut microbiota and microbiome changes over time. Furthermore, another explanation for the absence of gut microbiota changes in this chronic study could be that the single oral gavage of Aroclor 1260 may not have been sufficient or ideal for such

chronic studies, or Aroclor 1260 may have partitioned to other organ systems such as the adipose tissue, with time. The latter explanation is partially confirmed by the lack of xenobiotic receptor target gene induction in the ileum as assessed by RT-PCR for the CYP P450 enzymes. To account for the partitioning of Aroclor 1260 to other organs, we plan to collect the adipose tissue and test for changes in the adipokine gene expression and their respectively protein expression levels.

Assessments on the effect of Aroclor 1260 on ileal gene expression suggests that Aroclor 1260 could have induced a leaky gut in the ileum. We observed a decrease in the gene encoding the cadherin protein, CDH5, in the Aroclor 1260 exposed mice, suggesting an increase in permeability between epithelial cells. However, the increase in *Tff3* gene expression suggests a possible compensatory protective mechanism of the Aroclor 1260 induced injury to the intestine. Consistent with our findings on the trend for increased *Proteobacteria* abundance, we observed a trend for decreased gene expression of *Camp*, an antimicrobial peptide encoding gene, suggesting possible increased microbial activity. While our findings suggest the existence of an Aroclor 1260 induced intestinal injury which is trying to heal, the decrease in inflammatory gene expression suggests a possible increase in microbial activity as observed with increased *Proteobacteria* abundance. Although our findings suggested no changes on gut microbiota composition with chronic exposure to Aroclor 1260, which could be a result of aging, ileal changes at the transcript levels suggest possible protective mechanisms being initiated (Increased *Tff3*) to ileal injury induced by Aroclor 1260 exposure (decrease of *Camp*).

While this pilot project is one of the first studies to investigate the chronic effects of Aroclor 1260 on the gut and its microbiome, it is not without limitations. As discussed earlier, one vital limitation was the lack of frequent monitoring of fecal changes over time. As this was a chronic study, monitoring of fecal change over time would provide more information on how the gut microbiome change during the course of exposure. Observations on microbiome changes overtime would also provide more information on the impact of aging on the effects we observed. Importantly, we also did not mimic the exposure pattern of continuous exposure observed in humans. Humans are exposure to PCBs continuously based on food consumption patterns, among other factors. Therefore, it is important to design a continuous PCB exposure similar to human population exposures. Lastly, we did not account for sex differences. While the liver is a sexually dimorphic organ, sex differences in PCB activation of xenobiotics receptors and target gene induction has also been reported [57, 66]. However, in the current study, only male mice were used. Therefore, in future studies, we aim to: investigate the role of aging on gut microbiome with Aroclor 1260 exposure by monitoring fecal change over the course of the study; include a continuous dosing regimen; and investigate sex differences in a chronic Aroclor 1260 exposure. Future directions for this study include: performing western blot experiments to measure ileal protein levels and measuring bacterial metabolite levels (possibly over time) to better correlate gut microbiota profile with liver function.

CHAPTER III: INVESTIGATING THE EFFECTS OF POLYSTYRENE EXPOSURE ON THE LIVER

INTRODUCTION

Plastics, which are synthetic organic polymers have become a daily necessity in modern human life; however, they have also become a threat to human health and the environment. The versatility of plastics resulting from their physical and chemical properties has led to increased production and use of plastics for commercial and industrial purposes [67, 68]. Globally, the production of plastics has increased from 1.5 million metric tons in the 1950s to 390.7 million metric tons in 2021 [69]. This steady yet exponential increase in the production of plastics is estimated to triple by 2050 [70]. However, a major problem with these versatile products is that, despite the efforts to eliminate/ recycle them, majority of these products end up as environmental (both terrestrial and aquatic ecosystem) waste. According to the Organization for Economic Co-operation and Development (OECD), only 9% of the world's plastic is recycled. The remaining 91% are either in a landfill (50%), incinerated (19%) or mismanaged and uncollected as litter [71]. The presence of plastic waste in the environment has become a major environmental research focus, as it was identified that marine plastic debris majorly impacts aquatic life in the 1980s [72, 73]. However, a more growing concern is the equally increasing presence of microplastics in the environment and in human tissues [73, 74].

Microplastics was a term coined by Thompson et.al in 2004 to describe the tiny size of plastics found in the environment [73]. Microplastics is now generally defined as plastic fragments <5000µm (microns) in diameter. The lower size limit for microplastics is inconsistent, however, it is assumed that the lower size limit is the starting size for nanoplastics which is 100nm [72]. Microplastics can be classified based on their origin (polystyrene (PS), polyacrylate (PA), Polyester (PES), polyethylene (PE)), and their structure or form such as fibers, fragments, and spherical beads [72, 74, 75]. By and large though, they are classified based on their source. There are two sources of microplastics: primary and secondary microplastics. Primary microplastic describes the plastics produced at the <5000µm sizes. These were designed to be used at this size for commercial and industrial purposes and until 2015, microplastics were used in cosmetics and personal hygiene products [72]. In 2015, the U.S Congress amended the Federal Food, Drug and Cosmetic Act (FD&C Act) by passing the Microbead-free water act, which prohibited “the manufacturing, packaging, and distribution of rinse-off cosmetics containing plastic microbead as well as non-prescription drugs such as toothpaste). Secondary microplastics are derived from the physical and/or chemical (wind shear and thermo-oxidative process) degradation of large plastic debris. In addition, microplastics also include fiber shed of synthetic fabrics during laundry/ drying and fibers from abrasion of tires [76-78].

Regardless of the source, microplastics have been measured in human stool samples, blood samples, placenta, and breastmilk [67, 79-81].

Unsurprisingly, this observation shows that the accumulation of microplastics is not just in marine and terrestrial life but also in humans. The route of exposure includes ingestion of food and water contaminated with microplastics, and inhalation and dermal exposures via products containing microplastics [67, 82]. However, the main routes of exposure are ingestion and inhalation [67]. The health consequences of microplastics exposure are still largely unclear. The health effects of microplastics can vary based on various factors such as the size, physical and chemical compositions, the exposure levels, and extent of bioaccumulation in various cells and tissue type depending on the organism or species [22, 83]. Furthermore, it has also been shown that various environmental chemicals such as Polycyclic Aromatic Hydrocarbons (PAHs), PCBs [77, 84] and microorganism [85] can bind to microplastics which can be released during leaching, adding to the numerous adverse health effects of microplastics on the body. This could also mean that secondary microplastics are more toxic than primary microplastics as identified by Xia et al. [86]. The biological responses due to the exposure of microplastics have been shown to be due to triggering immune responses leading to the generation of reactive oxygen species (ROS). The resulting inflammation can lead to increased permeability of epithelial barriers allowing for the translocation of microplastics to various tissues such as the gut, liver, spleen, and other organs [22, 87]. Microplastics have also been shown to decrease energy metabolism as ATP concentration was low and lactate dehydrogenase activity was high resulting in decreased liver weight [22]. Deng et al. also observed a decrease in liver weight, total cholesterol, and triglycerides. It

has also been shown that microplastic exposures alters gut microbiome composition [22, 27, 88].

Previous studies have shown that, in both aquatic organisms as well as rodents, microplastics can cause inflammation, metabolic disorders and alterations in gut-microbiome composition [87]. A prior publication [27] showed polystyrene (PS) microplastics acted as a dose- and size- dependent obesogen. This study also showed that PS exposure led to an increase in *Firmicutes*/*Bacteroidetes* ratio, which has been positively associated with obesity (a known risk factor for NAFLD) [89, 90]. In addition, these findings have shown that microplastics accumulate in liver tissues [22]. Based on these findings, we aimed to investigate the effects of PS exposure on the liver using the two sizes (0.5 μm and 5 μm) which have previous being shown to induce obesity and diabetes in C57BL/6J mice [27]. **Therefore, we postulate that PS exposure will induce hepatic transcriptional reprogramming through gut-liver crosstalk, possibly as a consequence of alteration in gut microbiome, and in gut-derived signaling molecules such as bile acid.**

MATERIALS AND METHODS

Animals, diets, and chemical use

Animal protocols, procedures and care were done according to the University of Louisville Institutional Animal Care and Use Committee (IACUC). For this study, Thirty, 12 weeks old male C57BL/6J male mice were purchased from Jackson Laboratories (Bar Harbor, ME. USA). Five mice per cage were housed in an AALAC -and USDA- accredited facility at the University of Louisville. Mice were allowed to acclimatize for a week and mice were randomly selected to cages (5 mice per cage and 2 cages per exposure group). Mice were given either normal (filtered, autoclaved water) or normal water containing PS beads at a 1.0µg/ml concentration. Two PS bead stock solutions were purchased from Creative Diagnostics (Shirley, NY. USA) at sizes 5 µm beads (range= 4.5-4.9µm; 5.0% w/v dispersed in DI water (8.28×10^8 particles/ml)) and 0.5 µm beads (range= 0.4-0.6µm; 5.0% w/v dispersed in DI water (1.4×10^{12} particles/ml)). To prevent aggregation, freshly water solutions were prepared every other day using sonicated stock beads (prepared 30mins before dilution). On days fresh solutions were not supplied, previously supplied water bottles were perturbed to prevent potential settling of the PS beads. Water supplies and normal chow diet were accessible to the mice at *ad libitum*. These conditions were maintained for 12 week and the mice were then euthanized by sodium pentobarbital (150mg/Kg body weight) injection. Liver samples were collected and weighed at the time of euthanasia. Initial and final body weight were recorded at the beginning and end of study respectively while body mass

analysis was obtained by Lunar (Chicago, IL, USA) PIXImus Dual Energy X-ray Absorptiometer (DEXA) scanning after 9 weeks of PS exposure.

Histopathological analysis: Hematoxylin-eosin staining

The middle section of the right and left lobes of the liver tissue for each sample were fixed in 10% neutral buffered formalin for at least 48 hours. Tissues were then dehydrated in 75% ethanol until processing and paraffin embedding. After paraffin embedding, tissues were sectioned at 5 μm with Leica Biosystem's Histoscore Autocut Automated Rotary Microtome (Leica Biosystem; Deer Park, IL). Tissue sections were stained with Modified Mayers hematoxylin (catalog: 22-110-639; Eprelia 72804; Kalamazoo, MI) and Eosin-Y w/ Phloxine (catalog: 22-050-197; Eprelia 71304; Kalamazoo, MI) (H&E) to assess hepatic morphology. Images were captured using an Aperio GT 450 – Automated, high-capacity pathology slide scanner (Leica Biosystems; Deer Park, IL). H&E images were captured on Aperio Image Scope software at 10 and 20X magnification, respectively (v12.4.6.5003) (Leica Biosystems Pathology Imaging; Deer Park, IL). H&E foci scoring was performed using Aperio image scope application. On the application, the area of the right and the left lobe was measured and presence of foci (three or more granulocyte cells clusters) on each of the lobes were counted [91]. Foci counts were divided by the area of either the right or left lobes and then multiplied by 10^7 to transform the data to whole numbers. The relative foci count for each sample was determined by the sum of the resulting (foci count/area) x Fig 107) number from the right and left lobe.

Blood chemistry analysis

Blood samples were obtained at the time of euthanasia, by cardiac puncture using 0.2M EDTA as an anticoagulant. Plasma was isolated by centrifugation and aliquots were used to measure liver enzymes: (alanine transaminase (ALT), aspartate transaminase (AST)) and plasma lipids: total cholesterol, triglyceride, high density lipoprotein (HDL) and low-density lipoprotein (LDL) using an Axcel Clinical Chemistry Analyzer (West Caldwell, NJ, USA).

Hepatic triglyceride and cholesterol measurement

Liver tissues were bead homogenized in 50 mM sodium chloride solution. Homogenates were extracted using chloroform and methanol (2:1 v/v) solution according to the modified Bligh and Dyer method [92, 93]. Hepatic lipids were extracted from the lower chloroform layer and then evaporated to dryness. Hepatic triglyceride and cholesterol were colorimetrically quantified using each lipid's respective infinity reagents to generate standards (catalog: T7531-STD, C7509-STD, Thermo Fisher Scientific, Inc., Middletown, VA, USA). Standards and duplicated samples absorbance were read using a microplate absorbance reader at 500 nm (BioTek Gen 5, Winooski, VT). Hepatic triglyceride and cholesterol values were calculated from the standard curve based on the clinical standard from Pointe Scientific (Horiba Medical, Japan). Result triglyceride and cholesterol values obtained as mg/dL were mathematically restructured as mg triglyceride or cholesterol per gram of liver tissue.

GSH and GSSG measurement using HPLC

To ascertain oxidative stress in this study, glutathione (GSH) and glutathione disulfide (GSSG) levels were measured by HPLC [94]. Liver tissues were sonicated in 5% perchloric acid and 0.2 M boric acid using 10 μ M γ -glutamyl glutamate as an internal standard for ~5 seconds on ice to form a homogenate. Homogenized liver tissues were centrifuged for 5 minutes at 16000x g, and the resulting deproteinized supernatant was derivatized with iodoacetate and dansyl chloride to produce S-carboxymethyl and N-dansyl derivatives, while the resulting pellet was reconstituted in 0.1 M sodium hydroxide for protein quantification using BioRad DC protein assay. S-carboxymethyl and N-dansyl derivatives were analyzed on an Arc HPLC equipped with a Spherisorb NH2 analytical column (4.6 x 150mm) and W2475 fluorescence detector (Waters Corporation, Milliford, MA, USA). Concentrations of cysteine (Cys), cystine (CySS), GSH and GSSG were determined by comparison to the internal standard and normalized to total protein. Redox potentials were calculated from the Nernst equation ($E_h = E_0 + 30 \cdot \log([\text{oxidized}] / [\text{reduced}]^2)$), where $E_0 = -250$ mV for Cys/CySS and -264 mV for GSH/GSSG).

Real-time qPCR of liver samples

Liver samples were homogenized in RNA-STAT60 and 0.5 mm silica beads (Biospec Products, Bartlesville, OK, USA), and total RNA was extracted using the RNA-STAT 60 manufacturer's protocol (Tel-Test, Inc., Friendswood, TX, USA). RNA quantity and purity was assessed with a NanoDropTM One^C Microvolume UV-Vis Spectrometer from Thermo Scientific (catalog: 701-058112; Madison, MI). cDNA was reverse transcribed using single step cDNA synthesis

reagent, QScript (catalog: 95048-500; Quantabio; Beverly, MA). Polymerase chain reaction (PCR) was performed on the CFX384™ Real-Time System (Bio-Rad; Hercules, CA) using the iTaq universal probe super mix from Bio-Rad (catalog: 1725134; Hercules, CA) during RT-qPCR set-up. Expression for genes of interest were investigated employing commercially available predesigned TaqMan Gene Expression Assays (Applied Biosystems, Foster City, CA): glutamate-cysteine ligase, catalytic subunit (*Gclc*); (Mm00802658_m1), glutamate-cysteine ligase, modifier subunit (*Gclm*); (Mm01324400_m1), interleukin six (*Il-6*); (Mm00446190_m1), macrophage inflammatory protein 2 alpha (*MIP2α*); (Mm00436450-m1) monocyte chemo attractant protein 1 (*MCP1*); (Mm00441242-m1), Serine protease inhibitor protein (*Serpine 1*); (Mm00435858_m1), tumor necrosis factor alpha (*TNFα*); (Mm00443258-m1), transforming growth factor-beta 1 (*TGFβ1*); (Mm01178820_m1), tissue inhibitor of metalloproteinases-1 (*TIMP-1*); (Mm00441818_m1). Glyceraldehyde-3-phosphate Dehydrogenase (GADPH) (catalog: 4352339E; Applied biosystems; Waltham, MA) was used as the housekeeping gene and relative mRNA expressions was calculated using the $2^{-\Delta\Delta C_t}$ method. Mean expression of each gene in the control (given H₂O) were normalized to 1. Data for all other animals were expressed as fold induction compared to mean control.

Statistical Analysis

Statistical analyses were performed using GraphPad Prism version 9.5.1 for Windows (GraphPad Software Inc., La Jolla, CA, USA). Data were initially

assessed for normality using the D'Agostino & Pearson test as well as homoskedasticity using Barlett's test. Based on result of these test, comparison of central tendencies was performed employing One Way ANOVA followed by a Tukey's post-hoc test (for parametric and homoscedastic data) or Kruskal-Wallis test followed by Dunn's Multiple Comparison Test (for nonparametric and homoscedastic data), or Brown-Forsythe and Welch ANOVA test followed by Dunnett post-hoc test (for parametric but heteroskedastic data). Graphs are visually expressed as mean \pm SD and a p -value ≤ 0.05 was considered statistically significant for all tests.

RNA sequencing extraction, library preparation and sequencing run

Total RNA was isolated from snap frozen liver tissues using the RNeasy plus mini kit (catalog: 74134; Qiagen; Germantown, MD) following to the manufacturer's instructions. RNA was assessed for purity using the NanoDrop™ 2000 Spectrophotometer (catalog: 701-058112); Thermo Scientific; Madison, MI) and quantified by Qubit fluorometer using the Qubit RNA HS Assay Kit (catalog: Q32855; Thermo Fisher; Waltham, MA). RNA integrity was assessed using the Agilent 2100 bioanalyzer with RNA Nano 6000 kit (catalog: 5067-1511; Agilent; Santa Clara, CA). mRNA strand libraries were prepared with Illumina stranded mRNA prep ligation (96 samples) (catalog: 20040534; Illumina; San Diego, CA) following the manufacturer's protocol (document: 1000000124518 v03; Illumina; San Diego, CA). In brief, poly(A) mRNA was purified from 200ng total RNA using oligo dT beads and then the first and second strands were reverse transcribed to form cDNA. Amplification of cDNA was done according to protocol with a total of

13 cycles and barcoded indexes (IDT for Illumina RNA UD Indexes Set A, Ligation (Catalog: 20040553; Illumina; San Diego, CA) were simultaneously added. Quantity control for the libraries were performed by Qubit Fluorometer using Qubit 1X dsDNA HS assay kit (catalog: Q33231; Thermo Fisher; Waltham, MA) and average library size analysis was performed by Agilent 4159 TapeStation System on a D5000 screen tape (catalog: 5067-5588; Agilent; Santa Clara, CA) and FA. Individual samples were normalized to 10nM prior to pooling and then re-quantified using the Qubit quantification assay. According to the NextSeq 2000 system guide (document: 1000000109376 v06; Illumina; San Diego, CA), the 2nM pooled libraries and PhiX control were diluted, and libraries were loaded at 750pM with 2% PhiX spiked in. Libraries were further diluted and denatured on-instrument according to manufacturer's protocol (Illumina; San Diego, CA). Sequencing was performed on the Illumina NextSeq 2000 platform using a P3 100 cycle reagent kit with a P3 flow cell. Libraries were sequenced with a single 101 cycle read length with 2 index reads of 10bp each. FASTQ files were generated for analysis by BaseSpace DRAGEN analysis Version 1.2.1 [95].

Sequencing data analysis

The quality of the raw sequences was assessed using the Fastqc software (V 0.10.1) [96], the sequences were of good quality and no trimming was necessary. The sequences were aligned to the *Mus musculus* reference genome assembly (GRCm39.fa) using STAR (v 2.6) [97] to generate alignment files in bam format. HTseq (v 0.10.) [98] was used to obtain the raw read counts from the STAR aligned bam format files. Normalized raw counts obtained using the

Relative Log Expression (RLE) method were filtered to exclude genes with fewer than 10 counts across samples. DESeq2 [99] analysis which employs Benjamini-Hochberg for FDR calculations was used to assess differential expressed genes (DEGs). Enriched gene ontology biological processes and KEGG pathways were identified using R package ClusterProfiler [100] from the differential expressed genes. Core Pathway analysis was performed using Ingenuity Pathway Analysis (IPA) software (Qiagen, Germantown, MD) to determine overrepresented pathways based on differentially expressed genes for each comparison. Significance for up-regulated and down-regulated genes as well as overrepresented, activated or suppressed core pathways were set at a q-value < 0.05 with a log₂ fold change = 0.

RESULTS

Effects of polystyrene on body composition

To investigate the effects of PS on body composition and metabolic disruption, we calculated the percentage (%) body weight increase, liver weight (% of body weight) and % fat. Using the final body weight at the end of the study period, and the initial body weight of the mice in each group, % body weight increase (Fig 11A) was calculated. The resulting data showed no changes in body weight between the control and exposed groups (0.5 μm and 5 μm). Analysis of % organ weight to body weight showed a significant decrease in % liver to body weight (Fig 11B) in 0.5 μm PS exposed mice compared to the unexposed mice. Similarly, there was a decrease in % liver to body weight in 5 μm PS exposed mice compared to the unexposed mice. However, % fat assessment showed no change between the exposed groups (0.5 μm and 5 μm) and the control group (Fig 11C).

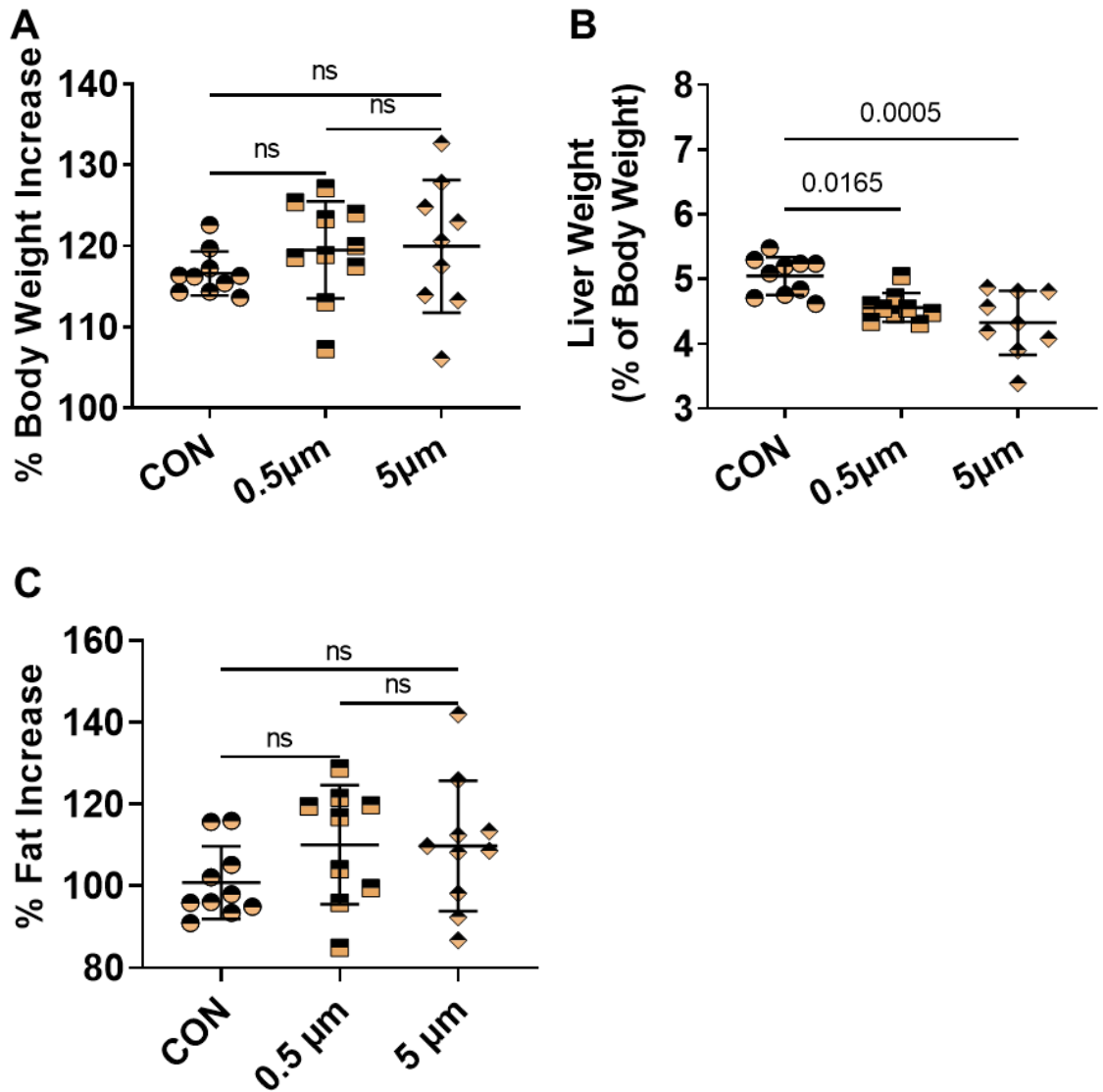


Figure 11: PS effects on body composition.

% Body weight increase (**A**) and liver weight (% of body weight) (**B**) were calculated using the initial and final body weight. % Fat increase was calculated using initial and final DEXA body mass (**C**). Values are expressed as mean \pm SD with significance defined as $p \leq 0.05$. p -values were determined using either a Brown-Forsythe and Welch ANOVA test with a Dunnett's post hoc (% body weight increase) or a one-way ANOVA test with a Tukey's post hoc (Liver weight and % fat) after normality and homoskedasticity were determined.

Effects of Polystyrene on hepatic steatosis and liver injury

To determine the effects of PS exposure effect on the liver and its function, H&E-stained liver sections were analyzed for the fatty droplet deposition and inflammatory foci were counted. Hepatic triglyceride and cholesterol levels were analyzed to assess lipid accumulation in the liver. Aspartate transferase (AST) and alanine transferase (ALT) plasma level, indicative of liver injury, were assessed. The H&E-stained liver sections (Fig 12A) showed no steatosis or histological changes between the control and the PS exposure groups. In addition, inflammatory foci count showed no difference between the control and PS exposure groups (Fig 12B). Analysis of hepatic lipids (Fig 13A & B) showed significant changes in the increase of liver cholesterol (Fig 13A) in both 0.5 μm and 5 μm exposed mice compared to control mice. However, there was no significant difference in hepatic cholesterol between the 0.5 μm and 5 μm exposed mice. Like the comparison between the exposure group for hepatic cholesterol, there was no significant change in hepatic triglyceride levels (Fig 13B) between the control and exposure groups as well as between the exposure groups, suggesting a possible disruption in the cholesterol pathway by PS microplastics exposure. Interestingly, plasma cholesterol showed a significant decreased in total cholesterol level in the 5 μm exposed mice compared to control mice (Table 1) while plasma triglyceride (Table 1) showed no changes between the exposure groups and the control group or between the exposure groups. However, Plasma HDL and LDL were significantly decreased in the 5 μm exposed mice compared to the control (Table 1). There was no change in AST

and ALT levels (Fig 14A &B) observed between the exposure groups and the control group as well as between the exposure groups (Fig 14A &B), suggesting that there was no liver injury.

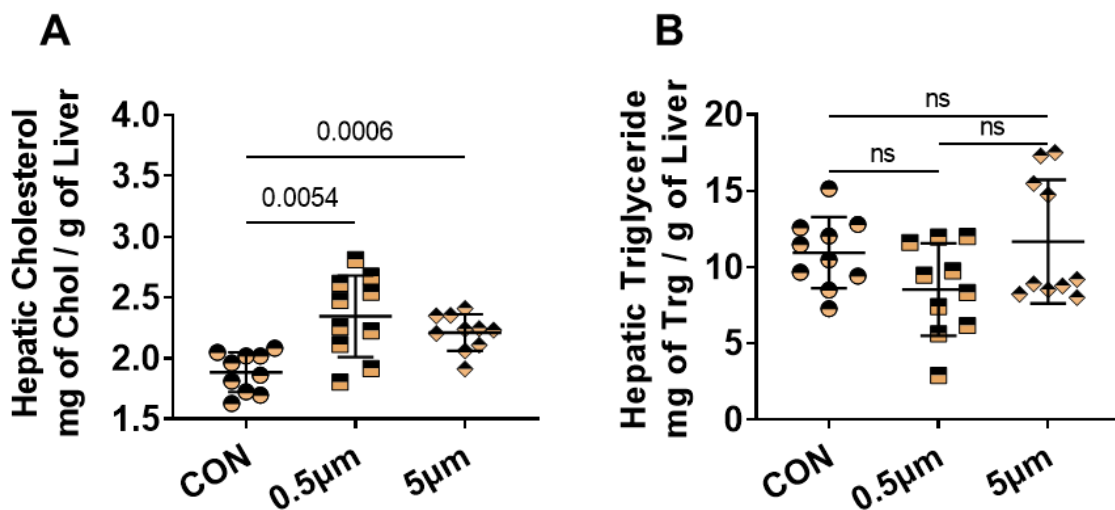


Figure 13: PS effects on hepatic cholesterol and triglyceride levels.

Hepatic cholesterol (**A**) and hepatic triglyceride (**B**) were quantified from liver samples using a colorimetric assay. Values are expressed as mean \pm SD with significance defined as $p \leq 0.05$. p -values were determined using either a Brown-Forsythe and Welch ANOVA test with a Dunnett's post hoc (cholesterol) or a one-way ANOVA test with a Tukey's post hoc (triglyceride) after normality and homoskedasticity were determined.

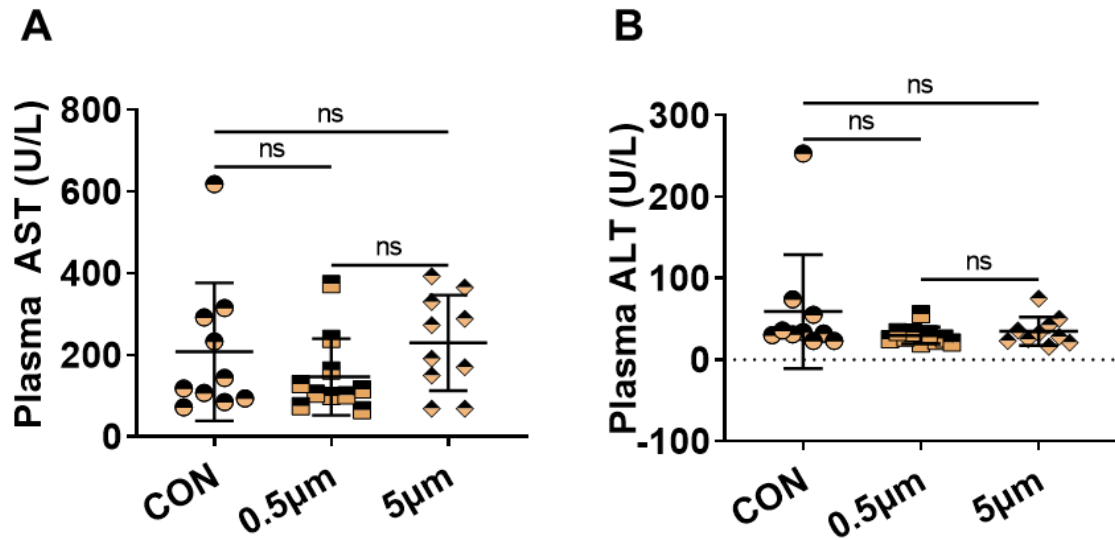


Figure 14: PS effects on plasma AST and ALT.

Plasma AST (A) and ALT levels (B) were measured using an Axcel Clinical Chemistry Analyzer. Values are expressed as mean \pm SD with significance defined as $p \leq 0.05$. p-values were determined using Kruskal-Wallis followed by Dunn's post hoc test (AST & ALT) after normality and homoskedasticity were determined.

Table 1: PS effects on total cholesterol, triglyceride, high-density lipoproteins and low -density lipoproteins.

	Con	0.5 μ m	5 μ m
Cholesterol (mg/dL)	83.60 \pm 6.48	92.2 \pm 14.01	61.70 \pm 8.29 ^{*‡}
Triglyceride (mg/dL)	74.80 \pm 14.37	68.40 \pm 22.31	76.80 \pm 33.52
HDL (mg/dL)	49.40 \pm 4.06	53.20 \pm 8.18	34.20 \pm 5.83 ^{*‡}
LDL (mg/dL)	19.24 \pm 3.05	25.32 \pm 8.63	12.14 \pm 7.46 ^{*‡}

Plasma lipid levels were measured using an Axcel Clinical Chemistry Analyzer. Values are expressed as mean \pm SD with significance defined as $p \leq 0.05$. p -values were determined by using either a one-way ANOVA test with a Tukey's post hoc (Plasma cholesterol, triglyceride and HDL) or a brown-Forsythe and welch ANOVA test with a Dunnett's post hoc (LDL), after normality and homoskedasticity was determined. * $p \leq 0.05$ between 5 μ m to control and ‡ $p \leq 0.05$ between 0.5 μ m and 5 μ m.

Effects of polystyrene on hepatic inflammation and fibrosis

Hepatic inflammation and fibrosis are indicators of advanced fatty liver disease. In previous studies, microplastics had been shown to induce inflammation [87]. To analyze the effects of PS on hepatic inflammatory and fibrotic markers, RT-qPCR was performed. The mRNA levels of genes encoding inflammatory markers: monocyte chemoattractant protein-1 (*Mcp-1*) and interleukin-6 (*Il-6*) were analyzed. There was an increase in *Mcp-1* gene expression in the 0.5 μm exposed mice compared to the control mice. Also, there was a significant increase in the 0.5 μm exposed mice compared to the 5 μm exposed mice (Fig 15A). There was a trend for decreased *Il-6* gene expression was in the 5 μm group compared to the control (Fig 15B). However, there was no change in the *Il-6* gene expression between the control and the 0.5 μm exposed mice nor between the two exposed groups. Additionally, other inflammatory markers namely, tumor necrosis factor alpha (*Tnfa*), and macrophage inflammatory protein-2 alpha (*Mip-2 α*) mRNA levels were not altered in the 0.5 μm and 5 μm exposures compared to the control (Appx. Table 2). Transforming growth factor beta 1 (*Tgf β -1*) and plasminogen activator inhibitor 1 (*Serpine1/Pai-1*) gene expressions were assessed for the presence of fibrosis. *Tgf β -1* mRNA level (Fig 16A) was significantly increased in the 5 μm exposed mice compared to the control mice. There were no changes in the steady state mRNA levels between 0.5 μm and the control mice or between the exposed mice. *Pai-1* mRNA levels (Fig 16B) were not altered between the control and exposed mice. However, there was a significant difference in the *Pai-1* mRNA levels between

the 0.5 μm and 5 μm exposed mice. Similarly, the gene expression for the fibrotic marker, tissue inhibitor of metalloproteinases (*Timp*) was not altered by PS exposure between the control and the exposed mice and the between the two exposed groups. Overall, the gene expression data on inflammatory and fibrotic markers suggest that there were few significant effects of PS on hepatic inflammation and fibrosis at the mRNA levels.

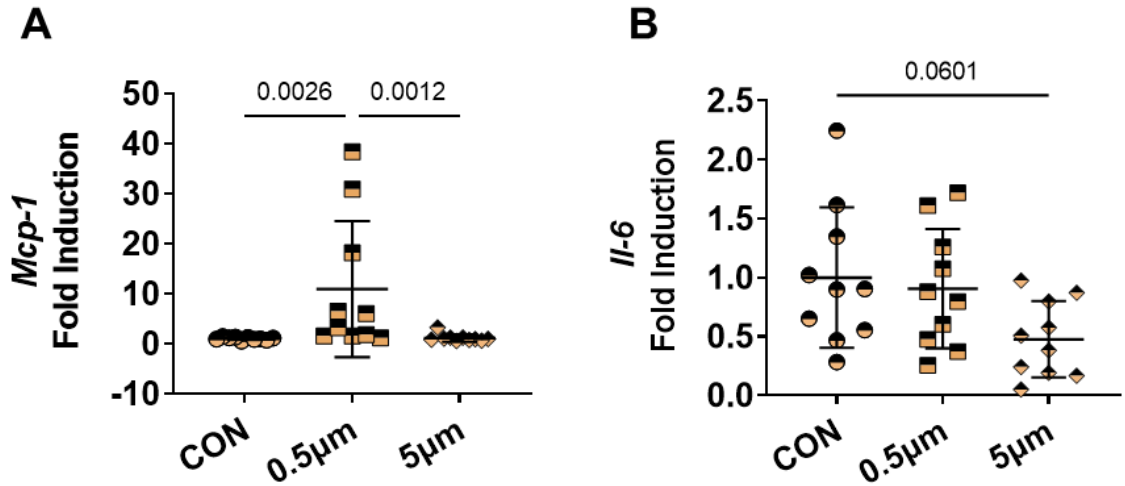


Figure 15: PS effects on inflammation related genes gene expression.

qRT-PCR was used to assess mRNA levels of hepatic Monocyte chemoattractant protein-1 (*Mcp-1*) (**A**), and Interleukin-6 (*Il-6*) (**B**). Values are presented as mean \pm SD with significance defined as $p \leq 0.05$. p -values were determined by either the Kruskal-Wallis test followed by a Dunn's post hoc test (*Mcp-1*), or one-way ANOVA followed by a Tukey's post hoc test (*Il-6*), after normality and homoskedasticity were determined.

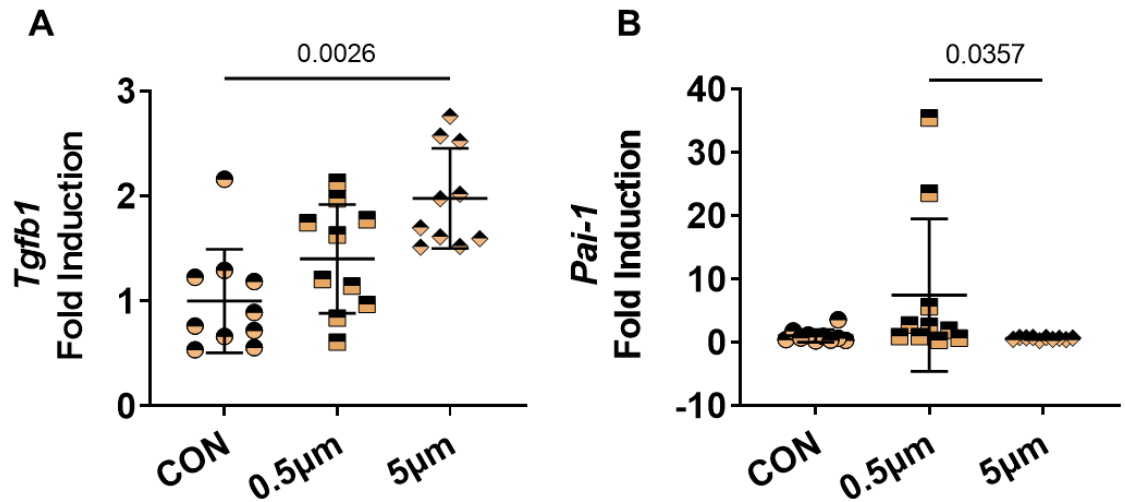


Figure 16: PS effects on hepatic profibrotic gene expression.

qRT-PCR was used to assess mRNA levels of the profibrotic marker Transforming growth factor beta 1 (*Tgfβ-1*) (A) and Plasminogen activator inhibitor-1 (*Pai-1*) (B). Values are presented as mean ± SD with significance defined as $p \leq 0.05$. p -values were determined by a Kruskal-Wallis test followed by a Dunn's post hoc test, after normality and homoskedasticity were determined.

Effects of polystyrene on oxidative stress

Microplastics has been shown to induce oxidative stress in other studies [22]. To ascertain if PS induced oxidative stress in our exposures, hepatic glutathione (GSH) and glutathione disulfide (GSSG) levels were measured and normalized to total protein. Hepatic GSH (Fig 17A) and GSSG (Fig 17B) levels were not changed in the PS-exposed mice compared to the control mice and between the exposed mice. Additionally, the GSH/ GSSG ratio (Fig 17C) which is an indicator for increased oxidative stress showed no difference between the control and PS-exposed groups as well as between the two PS-exposed groups. This suggested that PS exposure does not induce oxidative stress in the liver at the concentration and time point used. However, the total protein levels (Fig 17D) used to normalize the GSH and GSSG levels showed a significant increase in the 5 μm exposed mice compared to the control mice, suggesting that PS may have impacted protein metabolism. Furthermore, supplemental data showed the RT-qPCR analysis of genes involved in GSH synthesis namely, *Gclc* and *Gclm* were not altered due to PS exposure (Appx. Table 2).

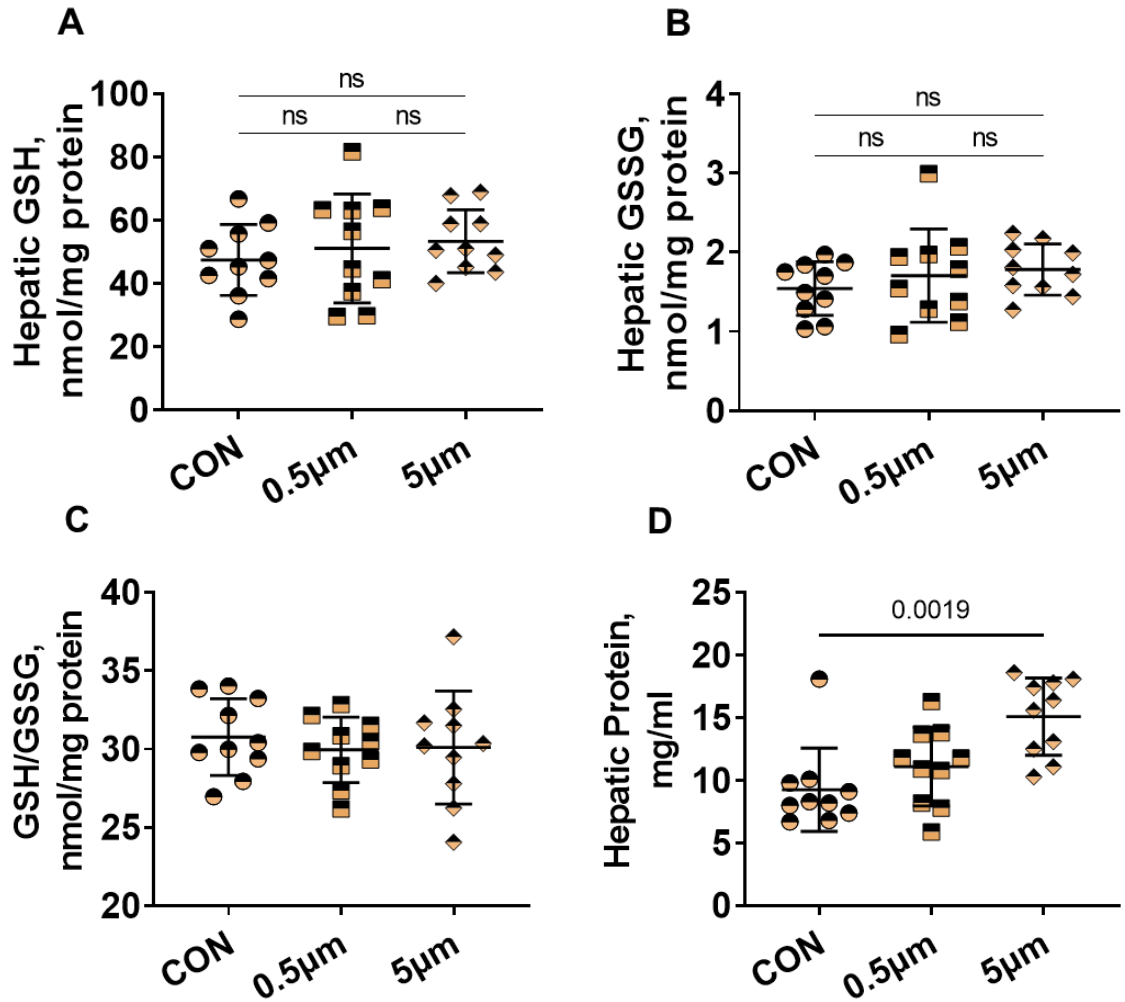


Figure 17: PS effects on hepatic oxidative stress.

Oxidative stress was assessed by measuring glutathione (GSH), glutathione disulfide (GSSG) and hepatic total protein levels. GSH (**A**) and GSSG (**B**) were measured using HPLC and resulting concentrations were used to calculate GSH/GSSG ratio (**C**). Hepatic total protein levels were measured using protein assay (**D**). Values are presented as mean \pm SD with significance defined as $p \leq 0.05$. p -values were determined using either a one-way ANOVA followed by a Tukey's post hoc test (GSH, GSSG & GSH/GSSG ratio) or Kruskal-Wallis for followed by a Dunn's post hoc test (Hepatic protein), after normality and homoskedasticity were determined.

Effects of polystyrene on genes involved in hepatic energy metabolism

The liver's main function is the metabolism and storage of macromolecules such as lipids, glucose, and proteins. To assess the effects of PS on liver physiological function, it is important to examine the effects of PS on energy metabolism. Cholesterol metabolism is one of the functions of the liver, Liver-X-receptor (*Lxr*) and its target gene cytochrome P450, family 7, subfamily a, polypeptide 1 (*Cyp7a1*) are genes involved in cholesterol and bile acid metabolism. There was no increase in *Lxr* mRNA levels in the PS exposed group compared to the control group. However, there was a significant decrease in the 5 μm exposed group compared to the 0.5 μm group (Fig 18A). In contrast, *Cyp7a1* (Fig 18B) showed a trend for increased gene expression in the 5 μm exposed group compared to the control group ($p = 0.0668$). Fatty acid binding protein-1 (*Fabp1*), carnitine palmitoyltransferase-1 alpha (*Cpt1a*), and carnitine palmitoyltransferase-2 (*Cpt2*) mRNA levels were used to examine the effects of PS exposure on lipid metabolism. There was a significant decrease in *Fabp1* gene expression in the 0.5 μm exposed group compared to the control group (Fig 19A). *Cpt1a* and *Cpt2* showed opposite effects in the 5 μm group. *Cpt1a* was significantly increased in the 5 μm exposed group compared to control group (Fig 19B) while *Cpt2* was significantly decreased between the two groups (Fig 19C). *Cpt2* was also significantly decreased in the 0.5 μm exposed group compared to the control group (Fig 19C). Genes which encode protein involved in glucose metabolism, namely, phosphoenolpyruvate carboxykinase-1 (*Pck1*) and glucose-6-phosphatase catalytic subunit-1 (*G6pc1*) were analyzed, and the

mRNA levels of these genes showed no difference between the PS exposed group and the control group as well as between the two exposed groups (Fig 20A&B). Lastly, the gene hepatocyte nuclear factor-4 alpha (*Hnf4α*) which encodes for the protein HNF4α and is involved in lipid and glucose homeostasis [101], was assessed. There was no difference in *Hnf4α* gene expression between any of the groups (Fig 20C). The findings suggest that PS exposure altered lipid metabolism, to an extent but had no effect on glucose metabolism. Furthermore, the overall homeostasis of the liver can be inferred to be normal based on the lack of alteration in *Hnf4α* gene expression. Information regarding additional metabolic genes assessed are provided in Appx. Table 2.

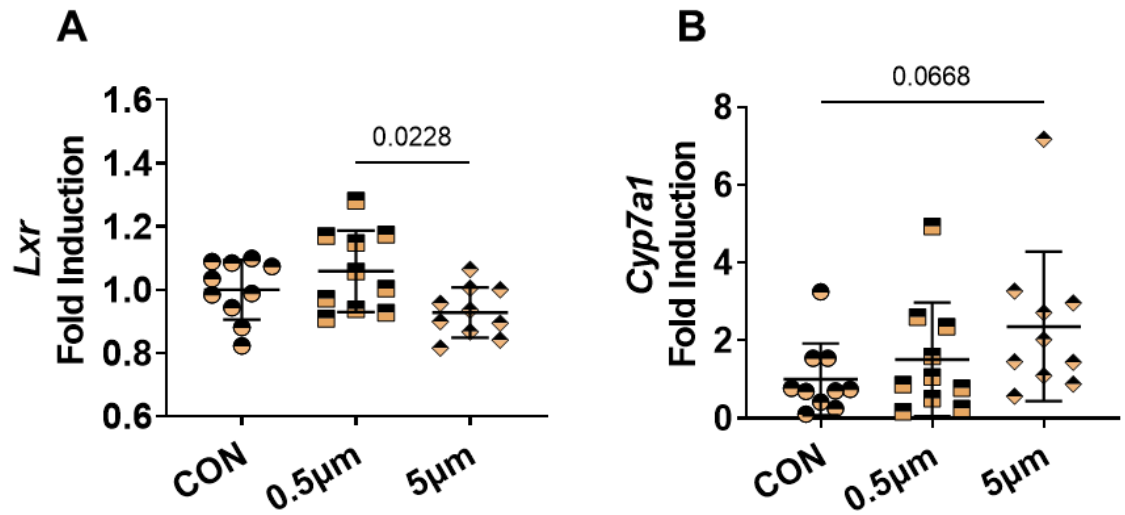


Figure 18: PS effects on genes involved in hepatic cholesterol metabolism.

qRT-PCR was used to assess mRNA levels of cholesterol and bile acids metabolism: Liver-X-receptors (*Lxr*) (**A**) and Cytochrome P450, family 7, subfamily a, polypeptide 1 (*Cyp7a1*) (**B**). Values are presented as mean \pm SD with significance defined as $p \leq 0.05$. p -values were determined by a one-way ANOVA followed by a Tukey's post hoc test (*Lxr*) and Kruskal-Wallis followed by a Dunn's post hoc test (*Cyp7a1*), after normality and homoskedasticity were determined.

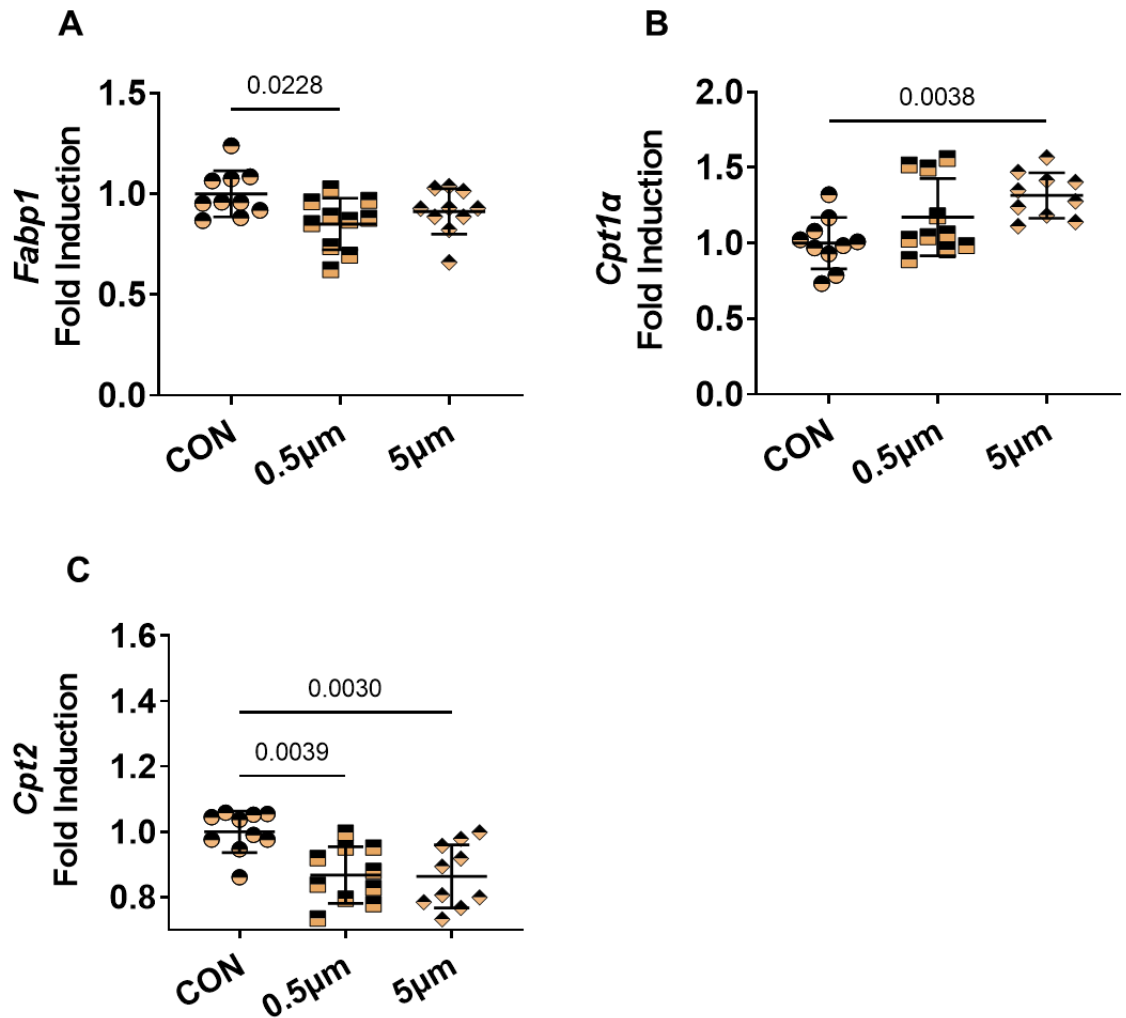


Figure 19: PS effects on genes involved in hepatic lipid metabolism.

qRT-PCR was used to assess mRNA levels of fatty acid metabolism marker: Fatty acid binding protein-1 (*Fabp1*) (A), Carnitine palmitoyltransferase-1 alpha (*Cpt1α*) (B), and Carnitine palmitoyltransferase-2 (*Cpt2*) (C). Values are presented as mean ± SD with significance defined as $p \leq 0.05$. p -values were determined by one-way ANOVA followed by a Tukey's post hoc test (*Fabp1*, *Cpt1α* & *Cpt2*), after normality and homoskedasticity were determined.

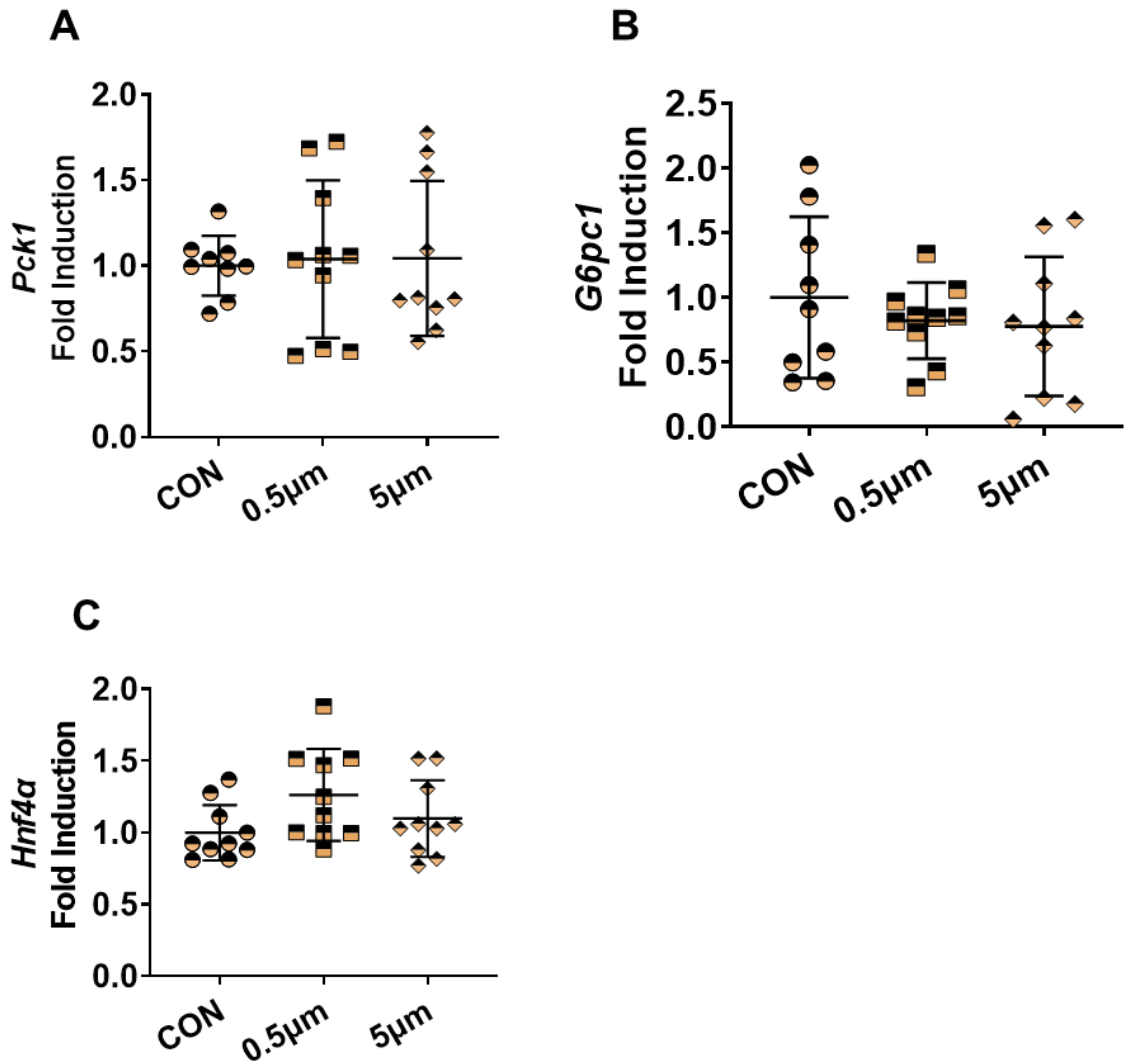


Figure 20: PS effects on genes involved in glucose metabolism and normal liver function.

qRT-PCR was used to assess mRNA levels of glucose metabolism marker: Phosphoenolpyruvate carboxykinase-1 (*Pck1*) (**A**), Glucose-6-phosphatase catalytic subunit-1 (*G6pc1*) (**B**), and Hepatocyte nuclear factor-4 alpha (*Hnf4α*) (**C**). Values are represented as mean ± SD with significance defined as $p \leq 0.05$. p -values were determined by one-way ANOVA followed by a Tukey's post hoc test (*Pck1*, *G6pc1* & *Hnf4α*), after normality and homoskedasticity were determined.

RNA sequencing analysis suggests polystyrene altered hepatic lipid gene expression

Differentially expressed genes were defined as those with q-value < 0.05 with no fold change cut off. RNA sequencing analysis demonstrated that 283 genes were differentially expressed in the 0.5 μm vs control comparison group while only 49 genes were differentially expressed in the 5 μm vs control comparison groups (Table 2). When we compared the 0.5 μm vs control group, 203 genes were predicted to be induced and 80 genes were predicted to be suppressed in the 0.5 μm vs control group (Table 2). Among the most induced genes were *Steap4*, *Tnfrsf3*, and *Ccl2* while among the most suppressed genes were *Tpm2*, *Trib3*, and *Pcp4l* (Fig 21 A&B). When we compared the 5 μm and control groups, 41 genes were predicted to be induced and 8 genes were predicted to be suppressed (Table 2). Among the most induced were *Firre*, *Fam193b*, and *Mug-ps1*, and among the most suppressed were, *Slpi*, *Ctgf*, and *Sgk1* (Fig 21A&B). There was very little overlap in the differentially expressed genes in the two comparisons (0.5 μm vs control and 5 μm vs control) as depicted in (Fig 21A). However, 5 genes were differentially expressed in both the 0.5 μm vs control and 5 μm vs control comparison groups, namely, *Rev1*, *Brpf1*, *Cnnt2*, *Cavin2*, and *Pea15a* (Fig 21A). Ingenuity pathway analysis (IPA) assessment predicted gene ontology (GO) processes enriched by 0.5 μm and 5 μm PS exposure. Importantly, FXR/RXR activation and LXR/RXR activation were enriched in 0.5 μm and 5 μm exposure groups compared to the control (Fig 22). In addition to FXR and LXR activation, IPA analysis also predicted the

enrichment of receptors involved in various processes in the gut-liver axis in the 0.5 μ m vs control comparison group. For example: LPS/IL-1 mediated inhibition of RXR function, aryl hydrocarbon receptor signaling, toll-like receptor signaling and xenobiotic metabolism AHR signaling pathways (Fig 22 and Appx. Table 7). Additional RNA seq processes and DEGs can be found in Appx. Table 3 -7.

Table 2: Differentially expressed genes (DEGs) from RNA seq of C57BL/6Jmouse liver samples exposed to polystyrene.

Exposure groups	Total DEG	No. of upregulated gene	No. of downregulated gene
0.5 μ m vs Control	283	203	80
5 μ m vs. Control	49	41	8

The number of DEGs in each PS exposure groups was compared to control (CON). Statistical significance determined by DESeq2 analysis: $p \leq 0.05$; $q \leq 0.05$; $\log_2FC \geq 0$, FPKM ≥ 1 in ≥ 3 sample; AVG FPKM ≥ 1 .

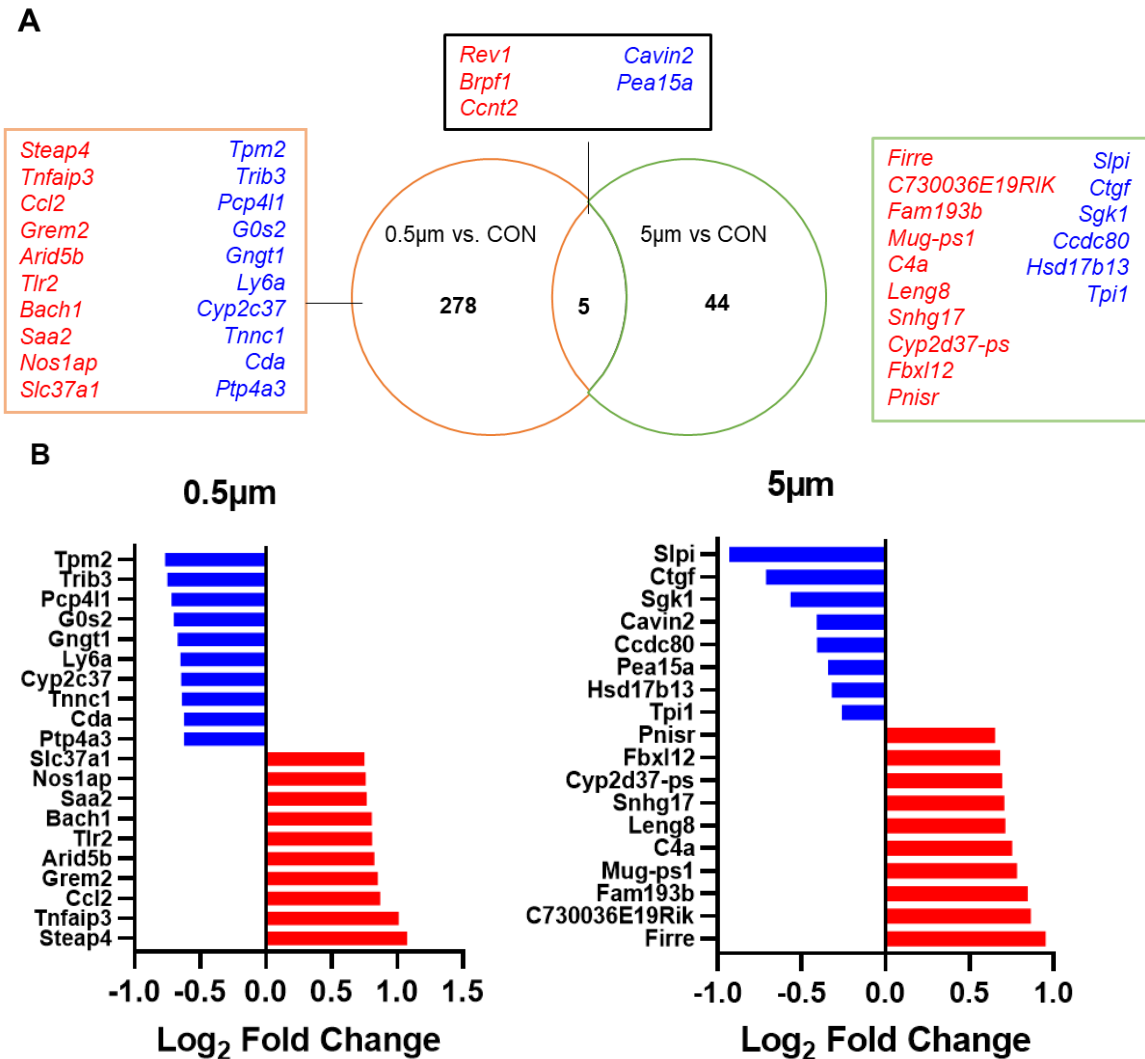


Figure 21: Predicted differentially expressed genes (DEGs) with polystyrene microplastics exposure.

Venn diagram showing the overlap and difference DEGs in 0.5 μm vs control and 5 μm vs control comparison groups **(A)**. Breakout boxes indicate the top 10 uniquely induced (red colored genes) and suppressed (blue colored genes) DEGs in the exposed group. Cut-off values are log₂ fold change of 0 and a q-value < 0.05. **(B)** The log₂ fold change values of the top 10 induced and suppressed DEGs in the 0.5 μm and 5 μm PS exposure groups. Additional DEGs for each PS exposure group in Appendix tables 3 –6.

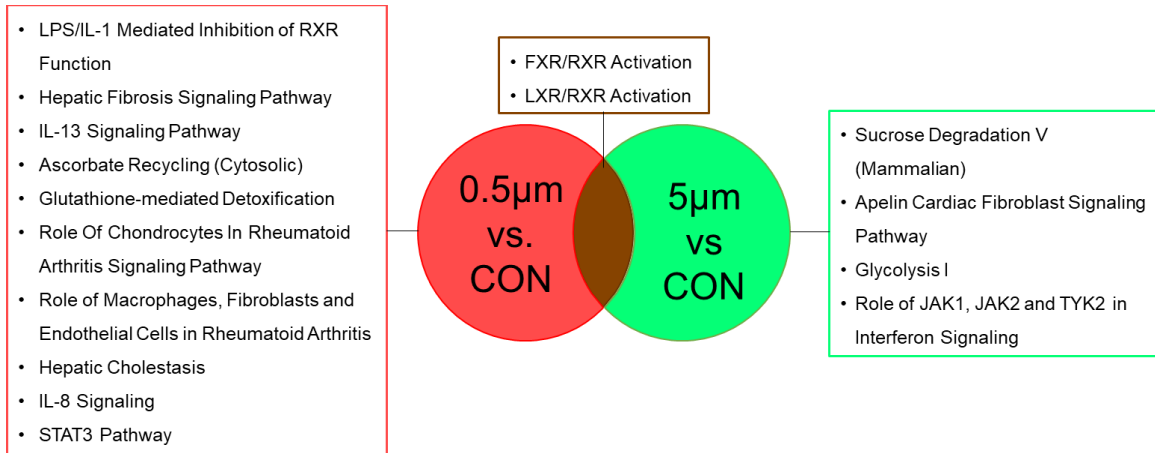


Figure 22: Enrichment analysis of DEGs identified in different sizes of polystyrene exposure.

DEGs (q –value < 0.05) were analyzed by the ingenuity pathway analysis (IPA) software. Pathway identified enriched processes in 0.5 μm vs control and 5 μm vs control comparison groups. Two processes were predicted to be activated in both groups. Venn diagram displays top 10 enriched process by 0.5 μm and 5 μm PS exposure groups. Cut-off values for enriched pathways are \log_2 fold change of 0 and a q -value < 0.05. Additional enriched processes and related genes are in Appendix table 7.

DISCUSSION

In this study, we investigated the effects of microplastics exposure (PS) on the liver based on previous findings showing that PS exposure increased *Firmicutes* to *Bacteroidetes* (F/B) ratio, which was associated with obesity [27]. As obesity is known as a risk factor for NAFLD, we postulated that PS may induce NAFLD. Using 0.5 μm and 5 μm sized PS beads at 1.0 $\mu\text{g}/\text{ml}$ concentration in drinking water, we assessed fatty liver endpoints. In addition, RNA transcriptomics analysis was carried out for hypothesis-generation purposes and to shed further light on our findings. Our data showed that PS exposure did not induce fatty liver disease. However, minor changes in inflammatory and fibrotic gene expression, as well as subtle changes in metabolic gene expression including hepatic cholesterol levels, indicate a size dependent effect from PS exposure. This size-dependent effect was further confirmed by the results obtained from RNA sequencing analysis on liver samples. In addition, enriched pathways such as FXR and LXR signaling enrichment predicted using IPA software indicates signs of hepatic reprogramming from altered gut-microbiome contributing to systematic effects in both PS exposure groups.

A previous study by Zhao et al. [27] demonstrated that PS exposure altered gut microbiome composition and increased *Firmicutes* to *Bacteroidetes* ratio in C57BL/6Jmice. These previous findings provided the rationale for our current study which was to investigate the effects of microplastics on the liver in the context of the gut-liver axis. In this study, we observed an increase in insulin

resistance in the PS exposed mice compared to the unexposed mice, consistent to previous findings [27]. Therefore, we suspect that in the current study, there was a change in the F/B ratio indicating possible alterations to the gut microbiome by both bile acid [102] and PS exposure [27].

The RNA transcriptomic findings in addition to our initial characterization of the liver indicate a size-dependent effect from PS exposure. Our results showed that inflammation, fibrosis, and energy metabolism related genes were altered in either the 0.5-micron, 5 micron or both. The differential alteration of similar genes by each exposure group indicates a size-dependent effect. A possible explanation for this is the ability of smaller-sized beads (0.5 μm) to cross the lipid bilayer easily and exert more molecular effects compared to the larger-sized beads. Similar to particulate matter which ranges in size as some microplastics, it has been previously reported in particulate matter and microplastic studies that smaller-sized particulate matter has more effects on downstream processes compared to larger-sized particulate matter [103, 104]. Alluding to our earlier explanation about a size-dependent effect, more genes were differentially expressed in the 0.5 μm PS exposed mice compared to the 5 μm PS exposed mice. In addition, there were more enriched processes in the 0.5 μm PS exposed mice compared to the 5 μm PS exposed mice.

Furthermore, IPA analysis of RNA sequencing data predicted the enrichment of multiple pathways in the liver, indicating to changes in the gut and its microbiome. Some of the enriched pathways include FXR and LXR enrichment which was observed in both PS exposure groups and LPS/IL-1

mediated inhibition of RXR function, aryl hydrocarbon receptor signaling, toll-like receptor signaling and xenobiotic metabolism AHR signaling pathways, which was observed in the 0.5-micron exposure group. However, among the listed enriched pathways, FXR and LXR pathway enrichment could provide an explanation for our findings in the initial characterization of the liver.

As earlier stated in the introduction, FXR activation mediates bile acid, lipid, and glucose metabolism and can indirectly influence protein metabolism as well [16, 19]. In addition, FXR signaling can regulate hepatic inflammation and fibrosis pathways [19]. Therefore, the predicted enrichment of the FXR signaling pathway could explain the increase in hepatic cholesterol and the decrease plasma cholesterol levels, the lack of effects in hepatic and plasma triglyceride levels and FXR-related glucose metabolism genes, as well as the minor changes in protein metabolism, hepatic inflammation, and fibrosis related genes. Moreover, LXR signaling is also involved in the maintenance and regulation of cholesterol, lipids and glucose metabolism and together with FXR, LXR maintains body lipid and cholesterol homeostasis [105]. These findings suggest a possible LXR and FXR receptor crosstalk which could be contributing to hepatic transcription reprogramming. However, further confirmatory analysis such RT-qPCR and western blot is needed to determine the activation/ inhibition of FXR and LXR receptors.

Furthermore, our findings showing the decrease in liver weight and the decrease in total cholesterol and triglyceride from PS exposure was not uncommon. Deng et al. demonstrated in their PS study that the decrease in liver

weight could be as a result of deficiency in energy metabolism [22]. Energy metabolism deficiency in their studies was correlated with a decrease in ATP concentrations, an increase in lactate dehydrogenase (LDH) activity and the presence of metabolites involved in energy metabolism in the serum. Further, Deng et al. findings showed a decrease in total cholesterol and triglycerides similar to our current study. In addition, Deng et al. observed an increase in lipid metabolism related metabolites such as taurine, and a decrease in the metabolite choline in the serum of PS exposed mice [22]. Their findings suggest that microplastic exposure alters hepatic function and energy metabolism. However, these endpoints were not assessed in this study. In the future, we plan to measure food intake, LDH levels as well as ATP concentrations to assess for energy metabolism changes resulting from PS exposure.

Thus far, our study provides an array of evidence showing that PS exposure is size-dependent and alters various metabolic pathways. However, the major limitation in this study was the lack of fatty liver disease in the exposed mice. Our aim was to investigate the effects of PS on the liver as previous studies showed that PS exposure induced obesity and diabetes in the C57BL/6J [27]. As diabetes and obesity are risk factors for fatty liver disease, our assessment comprised of fatty liver endpoints. In the future, we plan to measure ATP and LDH levels as well as serum metabolite to evaluate the effects of PS on energy metabolism. As earlier listed, some of the predicted pathways from our RNA transcriptomics analysis indicate changes in gut-derived signaling molecules such as lipopolysaccharides (LPS) and bile acids. Therefore, we also

plan to measure plasma, hepatic and intestinal metabolites as well as hepatic and intestinal short-chain fatty acid and bile acid levels. Another limitation in this study was the lack of replicating human microplastics exposure. Humans are exposed to a diverse range of microplastics consisting of different sizes, polymers, and additives. Moreover, these microplastics beads, having been through various degrees of degradation, modifications, and through interaction with the environment, may have bound to environmental pollutants such as persistent organic pollutant and microorganism [84, 87]. However, for this study, we used commercially purchase beads which do not mimic microplastic exposure in humans. Therefore, models that more accurately mimic human exposures are needed to effectively understand the potential effects of microplastics on the body. In addition, humans are not only exposed to the microplastic but other environmental pollutants like PCBs and lifestyle factors could contribute to the effects of microplastics seen in humans. In future studies, the incorporation of multiple exposures will also provide a better understanding of the interactive effects of microplastics in the body.

Considering the limitations of this study, the future direction of this study includes but is not limited to the following: Our findings relied largely on gene expression data and does not reflect actual protein levels. Hence, protein assays such as western blots and proteomic analysis are needed to confirm the changes in mRNA levels observed in these mice. Next, an ongoing metabolomics analysis would show the short chain fatty acids changed due to PS exposure and the metabolites generated due to microplastics exposure. Importantly, the

metabolomics analysis will show the various bile acids present in both the liver and the gut. This information can provide better understanding to our RNA transcriptomics assessment on the enrichment of FXR and LXR receptors as well as the effects observed in the liver.

CHAPTER IV: SUMMARY

There is a worldwide increase in NAFLD, with various factors contributing to this disease such as high caloric diet, sedentary lifestyle, and exposure to environmental pollutants [90]. TAFLD is a subtype of NAFLD that arises from exposure to environmental pollutants. Due to the growing industrialization and plethora of chemicals in our environment today, it is important to study the effects of environmental pollutants on TAFLD development.

The liver is the largest organ in the body, and it is the main organ for metabolism of xenobiotics and endogenous molecules. Therefore, it is prone to various effects from these molecules, especially environmental pollutants. There have been various studies showing the different mechanisms by which environmental pollutants affect the liver [12]. One of these mechanisms is through the gut and its microbiome [12, 15]. One of the ways the gut is connected to the liver is through enterohepatic circulation [20]. Also, there are various receptors whose function is in the regulation and maintenance of the physiological gut and liver homeostasis. These projects showed how the enterohepatic circulation and these receptors contribute to the maintenance of the gut-liver axis.

Aroclor 1260 is a mixture of PCBs known to induce detrimental effects on the gut-liver axis, in part, through the activation of the nuclear receptors CAR and

PXR. However, the full extent of these effects has not been studied in a chronic study. We investigated the chronic effects of Aroclor 1260 exposure on the gut. Our findings showed that Aroclor 1260 did not alter gut microbiome composition as expected but induced minor effects on gut permeability genes, in addition to gut maintenance and repair genes at the end of 34 weeks. We also observed a trend for increase in *Proteobacteria* phyla and a trend for decrease in *Camp* gene expression, which suggest possible increase in microbial activity (Fig 23). Based on our finding, we postulate that a single dose Aroclor 1260 induced toxicity could perhaps reverse with time, especially in the absence of multiple exposures to Aroclor 1260 over time or an initial insult to the gut.

Next, we examined the effect of PS on the liver based on previous findings showing that PS altered gut microbiome composition and induced obesity and insulin resistance in C57BL/6Jmice. This study was a repeat of a previous study using the same parameters and PS bead sizes but only a single effective dose (1 μ g/ml) [27]. The findings from the previous study showed the effects of microplastics on the gut and hinted at the possible effects on the liver. Therefore, we aimed to understand the interactions between the gut and liver. Although we expected to observe fatty liver disease in the exposed mice, our findings suggested that the effects of PS were size-dependent. The size effects observed suggests that the 0.5 μ m PS exposure group could be exerting its effects at the molecular level, while the 5 μ m PS exposure group could be exerting its effects at the cellular level. In addition to our findings based on size, our major finding from the RNA transcriptomic analysis was the enrichment of FXR and LXR

receptors among the enrichment of other hepatic receptors. The enrichment of these receptors implies that PS exposure could impact gut microbiome composition resulting in alteration of gut derived signaling molecules such as bile acids. Importantly, altered bile acids could lead to hepatic reprogramming via FXR activation (Fig 24). However, further analysis is needed to confirm these speculations.

In summary, this project showed the role of environmental pollutants on the gut-liver axis. Although these pollutants act through various mechanisms, they still induce changes in the gut and liver which in turn influence each other. Our findings are unique as it examines organ-organ interactions/ crosstalk and sheds some light on the extrahepatic effects of toxicants, how these effects could lead to liver disease, and potentially other related cardio-metabolic complications such as diabetes, obesity, and cardiovascular disease.

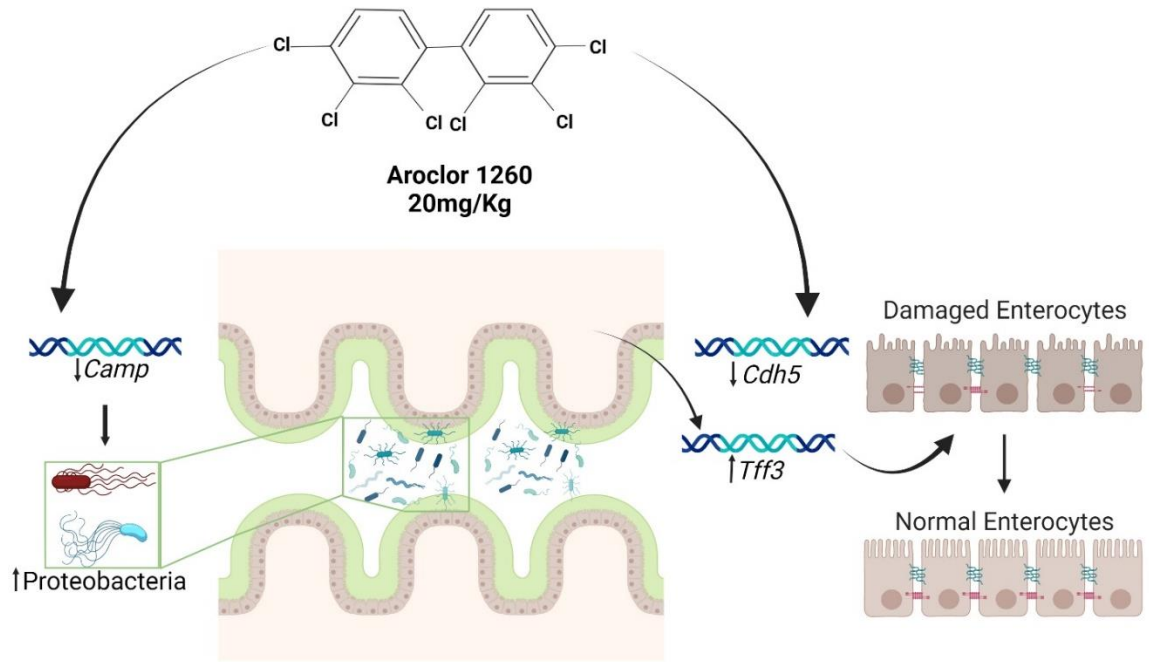


Figure 23: Summary of Aroclor 1260 findings.

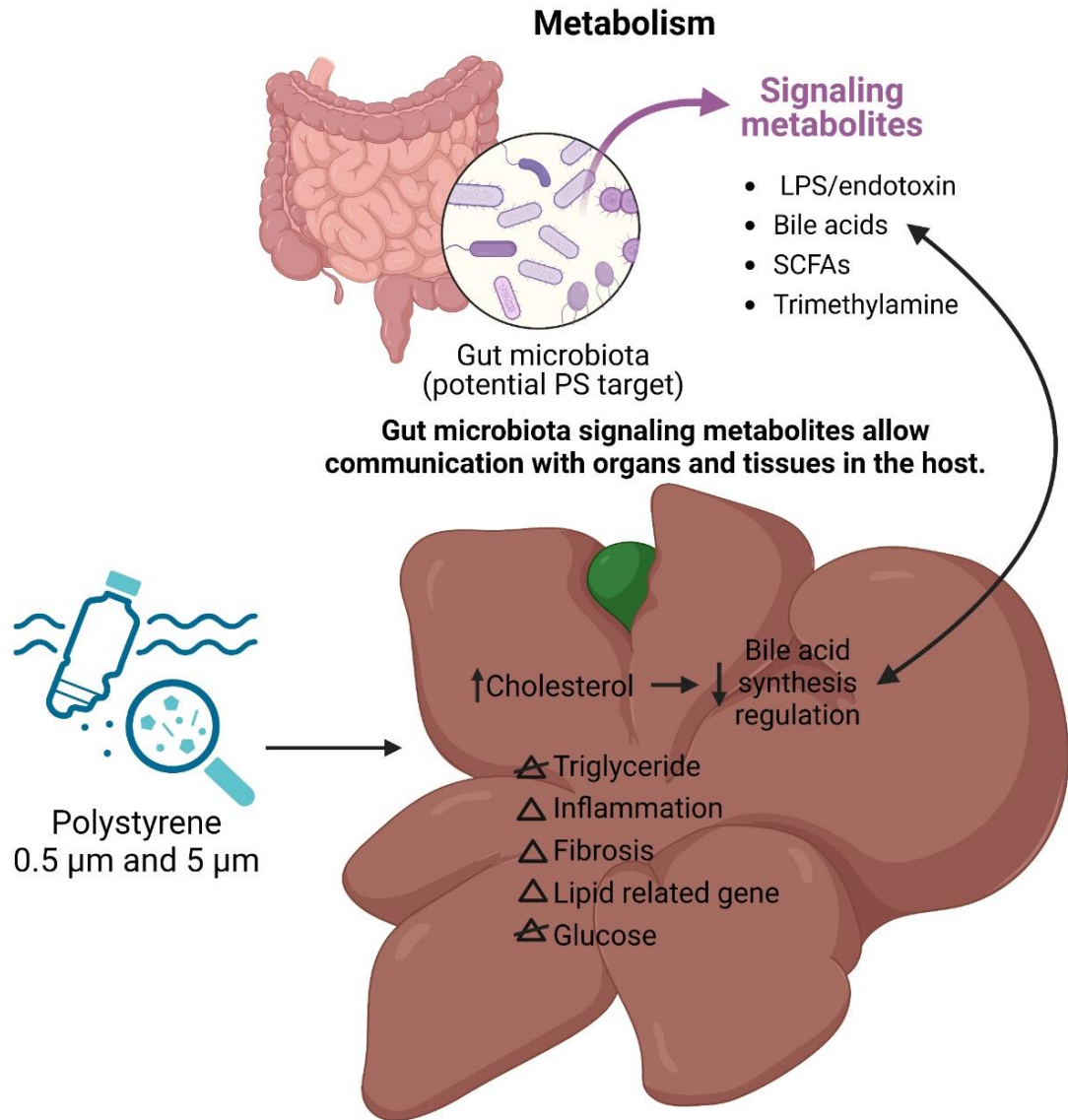


Figure 24: Summary of Polystyrene exposure findings.

REFERENCES

1. Dannaher, C.L., C.H. Tamburro, and L.T. Yam, *Occupational carcinogenesis: the Louisville experience with vinyl chloride-associated hepatic angiosarcoma*. Am J Med, 1981. **70**(2): p. 279-87.
2. Ukaogo, P.O., U. Ewuzie, and C.V. Onwuka, *21 - Environmental pollution: causes, effects, and the remedies*, in *Microorganisms for Sustainable Environment and Health*, P. Chowdhary, et al., Editors. 2020, Elsevier. p. 419-429.
3. Guglielmi, G., *How to destroy 'forever chemicals': cheap method breaks down PFAS*. Nature, 2022.
4. Banerjee, M., D. Robbins, and T. Chen, *Targeting xenobiotic receptors PXR and CAR in human diseases*. Drug Discov Today, 2015. **20**(5): p. 618-28.
5. Cave, M.C., et al., *Nuclear receptors and nonalcoholic fatty liver disease*. Biochim Biophys Acta, 2016. **1859**(9): p. 1083-1099.
6. Cobbina, E. and F. Akhlaghi, *Non-alcoholic fatty liver disease (NAFLD) - pathogenesis, classification, and effect on drug metabolizing enzymes and transporters*. Drug Metab Rev, 2017. **49**(2): p. 197-211.
7. Kim, C.H. and Z.M. Younossi, *Nonalcoholic fatty liver disease: a manifestation of the metabolic syndrome*. Cleve Clin J Med, 2008. **75**(10): p. 721-8.

8. Ludwig, J., et al. *Nonalcoholic steatohepatitis: Mayo Clinic experiences with a hitherto unnamed disease*.
9. Cave, M., et al., *Toxicant-associated steatohepatitis in vinyl chloride workers*. *Hepatology*, 2010. **51**(2): p. 474-481.
10. Wahlang, B., et al., *Toxicant-associated steatohepatitis*. *Toxicol Pathol*, 2013. **41**(2): p. 343-60.
11. Wahlang, B., et al., *Polychlorinated Biphenyls and Nonalcoholic Fatty Liver Disease*. *Curr Opin Toxicol*, 2019. **14**: p. 21-28.
12. Wahlang, B., et al., *Mechanisms of Environmental Contributions to Fatty Liver Disease*. *Curr Environ Health Rep*, 2019. **6**(3): p. 80-94.
13. Casals-Casas, C. and B. Desvergne, *Endocrine Disruptors: From Endocrine to Metabolic Disruption*. *Annual Review of Physiology*, 2011. **73**(1): p. 135-162.
14. Baker, S.S. and R.D. Baker, *Gut Microbiota and Liver Injury (II): Chronic Liver Injury*, in *Gut Microbiota and Pathogenesis of Organ Injury*, P. Chen, Editor. 2020, Springer Singapore: Singapore. p. 39-54.
15. Wahlang, B., et al., *Polychlorinated biphenyls altered gut microbiome in CAR and PXR knockout mice exhibiting toxicant-associated steatohepatitis*. *Toxicol Rep*, 2021. **8**: p. 536-547.
16. Klaassen, C.D. and J.Y. Cui, *Review: Mechanisms of How the Intestinal Microbiota Alters the Effects of Drugs and Bile Acids*. *Drug Metab Dispos*, 2015. **43**(10): p. 1505-21.

17. Albillos, A., A. de Gottardi, and M. Rescigno, *The gut-liver axis in liver disease: Pathophysiological basis for therapy*. J Hepatol, 2020. **72**(3): p. 558-577.
18. Grüner, N. and J. Mattner, *Bile Acids and Microbiota: Multifaceted and Versatile Regulators of the Liver-Gut Axis*. Int J Mol Sci, 2021. **22**(3).
19. Mori, H., et al., *Farnesoid X Receptor, Bile Acid Metabolism, and Gut Microbiota*. Metabolites, 2022. **12**(7).
20. Cao, H., et al., *Effect of Enterohepatic Circulation on the Accumulation of Per- and Polyfluoroalkyl Substances: Evidence from Experimental and Computational Studies*. Environ Sci Technol, 2022. **56**(5): p. 3214-3224.
21. Islam, K.B., et al., *Bile acid is a host factor that regulates the composition of the cecal microbiota in rats*. Gastroenterology, 2011. **141**(5): p. 1773-81.
22. Deng, Y., et al., *Tissue accumulation of microplastics in mice and biomarker responses suggest widespread health risks of exposure*. Sci Rep, 2017. **7**: p. 46687.
23. Al-Eryani, L., et al., *Identification of Environmental Chemicals Associated with the Development of Toxicant-associated Fatty Liver Disease in Rodents*. Toxicol Pathol, 2015. **43**(4): p. 482-97.
24. Basu, R., M. Nouredin, and J.M. Clark, *Nonalcoholic Fatty Liver Disease: Review of Management for Primary Care Providers*. Mayo Clin Proc, 2022. **97**(9): p. 1700-1716.

25. Younossi, Z.M., et al., *Global epidemiology of nonalcoholic fatty liver disease—meta - analytic assessment of prevalence, incidence, and outcomes*. *Hepatology*, 2016. **64**(1): p. 73-84.
26. Estes, C., et al., *Modeling NAFLD disease burden in China, France, Germany, Italy, Japan, Spain, United Kingdom, and United States for the period 2016–2030*. *Journal of Hepatology*, 2018. **69**(4): p. 896-904.
27. Zhao, J., et al., *Polystyrene bead ingestion promotes adiposity and cardiometabolic disease in mice*. *Ecotoxicol Environ Saf*, 2022. **232**: p. 113239.
28. Wahlang, B., et al., *Evaluation of Aroclor 1260 exposure in a mouse model of diet-induced obesity and non-alcoholic fatty liver disease*. *Toxicol Appl Pharmacol*, 2014. **279**(3): p. 380-390.
29. Agency, U.S.E.P. *Table of Aroclors*. [cited 2023 05/08]; Available from: <https://www.epa.gov/pcbs/table-aroclors>.
30. Cusack, C., et al., *The Anniston Community Health Survey*. *J Environ Health*, 2020. **83**(2): p. 38-41.
31. Beyer, A. and M. Biziuk, *Environmental fate and global distribution of polychlorinated biphenyls*. *Rev Environ Contam Toxicol*, 2009. **201**: p. 137-58.
32. Safe, S., et al., *PCBs: structure-function relationships and mechanism of action*. *Environ Health Perspect*, 1985. **60**: p. 47-56.
33. Weitekamp, C.A., et al., *A state-of-the-science review of polychlorinated biphenyl exposures at background levels: Relative contributions of*

- exposure routes*. Science of The Total Environment, 2021. **776**: p. 145912.
34. Faroon, O.M., et al., *Carcinogenic effects of polychlorinated biphenyls*. Toxicology and industrial health, 2001. **17**(2): p. 41-62.
 35. Faroon, O.M., et al., *Effects of polychlorinated biphenyls on development and reproduction*. Toxicology and Industrial Health, 2001. **17**(3): p. 63-93.
 36. Wahlang, B., et al., *Polychlorinated Biphenyl-Xenobiotic Nuclear Receptor Interactions Regulate Energy Metabolism, Behavior, and Inflammation in Non-alcoholic-Steatohepatitis*. Toxicological Sciences, 2015. **149**(2): p. 396-410.
 37. Dempsey, J.L., et al., *Pharmacological Activation of PXR and CAR Downregulates Distinct Bile Acid-Metabolizing Intestinal Bacteria and Alters Bile Acid Homeostasis*. Toxicol Sci, 2019. **168**(1): p. 40-60.
 38. Head, K.Z., et al., *Investigating the effects of long-term Aroclor 1260 exposure on fatty liver disease in a diet-induced obesity mouse model*. Frontiers in Gastroenterology, 2023. **2**.
 39. Cave, M., et al., *Polychlorinated biphenyls, lead, and mercury are associated with liver disease in American adults: NHANES 2003-2004*. Environ Health Perspect, 2010. **118**(12): p. 1735-42.
 40. *Toxicology and carcinogenesis studies of a binary mixture of 3,3',4,4',5-pentachlorobiphenyl (PCB 126) (Cas No. 57465-28-8) and 2,2',4,4',5,5'-hexachlorobiphenyl (PCB 153) (CAS No. 35065-27-1) in female Harlan*

- Sprague-Dawley rats (gavage studies)*. Natl Toxicol Program Tech Rep Ser, 2006(530): p. 1-258.
41. Steele, G., P. Stehr-Green, and E. Welty, *Estimates of the biologic half-life of polychlorinated biphenyls in human serum*. N Engl J Med, 1986. **314**(14): p. 926-7.
 42. Estaki, M., et al., *QIIME 2 Enables Comprehensive End-to-End Analysis of Diverse Microbiome Data and Comparative Studies with Publicly Available Data*. Current Protocols in Bioinformatics, 2020. **70**(1): p. e100.
 43. Fung, C., et al., *Automation of QIIME2 Metagenomic Analysis Platform*. Current Protocols, 2021. **1**(9): p. e254.
 44. Kuczynski, J., et al., *Using QIIME to Analyze 16S rRNA Gene Sequences from Microbial Communities*. Current Protocols in Microbiology, 2012. **27**(1): p. 1E.5.1-1E.5.20.
 45. Kamble, A., S. Sawant, and H. Singh, *16S ribosomal RNA gene-based metagenomics: A review*. Biomedical Research Journal, 2020. **7**(1): p. 5-11.
 46. Callahan, B.J., et al., *DADA2: High-resolution sample inference from Illumina amplicon data*. Nat Methods, 2016. **13**(7): p. 581-3.
 47. Shannon, C.E., *A mathematical theory of communication*. The Bell System Technical Journal, 1948. **27**(3): p. 379-423.
 48. Lemos, L.N., et al., *Rethinking microbial diversity analysis in the high throughput sequencing era*. J Microbiol Methods, 2011. **86**(1): p. 42-51.

49. Callahan, B.J., P.J. McMurdie, and S.P. Holmes, *Exact sequence variants should replace operational taxonomic units in marker-gene data analysis*. *Isme j*, 2017. **11**(12): p. 2639-2643.
50. Faith, D., *The role of the phylogenetic diversity measure*. PD, in *bioinformatics*, 2006.
51. Lozupone, C. and R. Knight, *UniFrac: a new phylogenetic method for comparing microbial communities*. *Appl Environ Microbiol*, 2005. **71**(12): p. 8228-35.
52. Lozupone, C.A., et al., *Quantitative and qualitative beta diversity measures lead to different insights into factors that structure microbial communities*. *Appl Environ Microbiol*, 2007. **73**(5): p. 1576-85.
53. Kers, J.G. and E. Saccenti, *The Power of Microbiome Studies: Some Considerations on Which Alpha and Beta Metrics to Use and How to Report Results*. *Frontiers in Microbiology*, 2022. **12**.
54. Jaccard, P., *The distribution of the flora in the alpine zone. 1*. *New phytologist*, 1912. **11**(2): p. 37-50.
55. DeSantis, T.Z., et al., *Greengenes, a chimera-checked 16S rRNA gene database and workbench compatible with ARB*. *Appl Environ Microbiol*, 2006. **72**(7): p. 5069-72.
56. Goecks, J., A. Nekrutenko, and J. Taylor, *Galaxy: a comprehensive approach for supporting accessible, reproducible, and transparent computational research in the life sciences*. *Genome Biol*, 2010. **11**(8): p. R86.

57. Afdhal, N.H., *Management of Nonalcoholic Fatty Liver Disease: A 60-Year-Old Man With Probable Nonalcoholic Fatty Liver Disease: Weight Reduction, Liver Biopsy, or Both?* JAMA, 2012. **308**(6): p. 608-616.
58. Larsson, E., et al., *Analysis of gut microbial regulation of host gene expression along the length of the gut and regulation of gut microbial ecology through MyD88.* Gut, 2012. **61**(8): p. 1124-31.
59. Vancamelbeke, M., et al., *Genetic and Transcriptomic Bases of Intestinal Epithelial Barrier Dysfunction in Inflammatory Bowel Disease.* Inflamm Bowel Dis, 2017. **23**(10): p. 1718-1729.
60. Vancamelbeke, M. and S. Vermeire, *The intestinal barrier: a fundamental role in health and disease.* Expert Rev Gastroenterol Hepatol, 2017. **11**(9): p. 821-834.
61. Stojanov, S., A. Berlec, and B. Štrukelj, *The Influence of Probiotics on the Firmicutes/Bacteroidetes Ratio in the Treatment of Obesity and Inflammatory Bowel disease.* Microorganisms, 2020. **8**(11).
62. Rizzatti, G., et al., *Proteobacteria: A Common Factor in Human Diseases.* Biomed Res Int, 2017. **2017**: p. 9351507.
63. Xia, Y., et al., *Gut microbiome and microbial metabolites in NAFLD and after bariatric surgery: Correlation and causality.* Front Microbiol, 2022. **13**: p. 1003755.
64. McFarland, V.A. and J.U. Clarke, *Environmental occurrence, abundance, and potential toxicity of polychlorinated biphenyl congeners:*

- considerations for a congener-specific analysis*. Environ Health Perspect, 1989. **81**: p. 225-39.
65. John, G.K. and G.E. Mullin, *The Gut Microbiome and Obesity*. Curr Oncol Rep, 2016. **18**(7): p. 45.
66. Wahlang, B., et al., *Identifying sex differences arising from polychlorinated biphenyl exposures in toxicant-associated liver disease*. Food Chem Toxicol, 2019. **129**: p. 64-76.
67. Rubio, L., R. Marcos, and A. Hernández, *Potential adverse health effects of ingested micro- and nanoplastics on humans. Lessons learned from in vivo and in vitro mammalian models*. Journal of Toxicology and Environmental Health, Part B, 2020. **23**(2): p. 51-68.
68. Thompson, R.C., *Plastic debris in the marine environment: consequences and solutions*. Marine nature conservation in Europe, 2006. **193**: p. 107-115.
69. (PEMRG), P.E. *Annual production of plastics worldwide from 1950 to 2021*. 2022; Available from: <https://www.statista.com/statistics/282732/global-production-of-plastics-since-1950/>; Plastics - the Facts 2022, page 16.
70. Guglielmi, G., *In the next 30 years, we'll make four times more plastic waste than we ever have*. Science, 2017.
71. OECD, *Plastic Pollution is Growing Relentlessly as Waste Management and Recycling Fall Short, Says OECD*. 2022.

72. Pico, Y. and D. Barcelo, *Analysis and Prevention of Microplastics Pollution in Water: Current Perspectives and Future Directions*. ACS Omega, 2019. **4**(4): p. 6709-6719.
73. Thompson, R.C., et al., *Lost at sea: where is all the plastic?* Science, 2004. **304**(5672): p. 838.
74. Duis, K. and A. Coors, *Microplastics in the aquatic and terrestrial environment: sources (with a specific focus on personal care products), fate and effects*. Environ Sci Eur, 2016. **28**(1): p. 2.
75. Silva, A.B., et al., *Microplastics in the environment: Challenges in analytical chemistry - A review*. Analytica Chimica Acta, 2018. **1017**: p. 1-19.
76. Napper, I.E. and R.C. Thompson, *Plastic Debris in the Marine Environment: History and Future Challenges*. Glob Chall, 2020. **4**(6): p. 1900081.
77. Akdogan, Z. and B. Guven, *Microplastics in the environment: A critical review of current understanding and identification of future research needs*. Environmental Pollution, 2019. **254**: p. 113011.
78. Cole, M., et al., *Microplastics as contaminants in the marine environment: A review*. Marine Pollution Bulletin, 2011. **62**(12): p. 2588-2597.
79. Schwabl, P., et al., *Detection of Various Microplastics in Human Stool: A Prospective Case Series*. Ann Intern Med, 2019. **171**(7): p. 453-457.

80. Liu, S., et al., *Detection of various microplastics in placentas, meconium, infant feces, breastmilk and infant formula: A pilot prospective study*. *Sci Total Environ*, 2022. **854**: p. 158699.
81. Leslie, H.A., et al., *Discovery and quantification of plastic particle pollution in human blood*. *Environ Int*, 2022. **163**: p. 107199.
82. Bartsch, N., et al., *Chemical stabilization of polymers: Implications for dermal exposure to additives Part A Toxic/hazardous substances & environmental engineering*. 2018.
83. Hesler, M., et al., *Multi-endpoint toxicological assessment of polystyrene nano- and microparticles in different biological models in vitro*. *Toxicology in Vitro*, 2019. **61**: p. 104610.
84. Crawford, C.B. and B. Quinn, *The interactions of microplastics and chemical pollutants*. *Microplastic pollutants*, 2017: p. 131-157.
85. Kirstein, I.V., et al., *Dangerous hitchhikers? Evidence for potentially pathogenic Vibrio spp. on microplastic particles*. *Marine environmental research*, 2016. **120**: p. 1-8.
86. Xia, B., et al., *Secondary PVC microplastics are more toxic than primary PVC microplastics to Oryzias melastigma embryos*. *Journal of Hazardous Materials*, 2022. **424**: p. 127421.
87. Prata, J.C., et al., *Environmental exposure to microplastics: An overview on possible human health effects*. *Science of The Total Environment*, 2020. **702**: p. 134455.

88. Lu, L., et al., *Polystyrene microplastics induce gut microbiota dysbiosis and hepatic lipid metabolism disorder in mice*. *Science of the Total Environment*, 2018. **631**: p. 449-458.
89. Khan, M.J., et al., *Role of gut microbiota in the aetiology of obesity: proposed mechanisms and review of the literature*. *Journal of obesity*, 2016. **2016**.
90. Juanola, O., et al., *Non-Alcoholic Fatty Liver Disease: Metabolic, Genetic, Epigenetic and Environmental Risk Factors*. *Int J Environ Res Public Health*, 2021. **18**(10).
91. Pai, R.K., et al., *Standardising the interpretation of liver biopsies in non-alcoholic fatty liver disease clinical trials*. *Aliment Pharmacol Ther*, 2019. **50**(10): p. 1100-1111.
92. Bligh, E.G. and W.J. Dyer, *A rapid method of total lipid extraction and purification*. *Can J Biochem Physiol*, 1959. **37**(8): p. 911-7.
93. Folch, J., M. Lees, and G.H. Sloane Stanley, *A simple method for the isolation and purification of total lipids from animal tissues*. *J Biol Chem*, 1957. **226**(1): p. 497-509.
94. Jones, D.P. and Y. Liang, *Measuring the poise of thiol/disulfide couples in vivo*. *Free Radic Biol Med*, 2009. **47**(10): p. 1329-38.
95. Illumina, *BaseSpace User Guide*. 2014.
96. Andrews, S., *FastQC: A Quality Control Tool for High Throughput Sequence Data*.

97. Dobin, A., et al., *STAR: ultrafast universal RNA-seq aligner*. Bioinformatics, 2012. **29**(1): p. 15-21.
98. Anders, S., P.T. Pyl, and W. Huber, *HTSeq—a Python framework to work with high-throughput sequencing data*. Bioinformatics, 2014. **31**(2): p. 166-169.
99. Love, M.I., W. Huber, and S. Anders, *Moderated estimation of fold change and dispersion for RNA-seq data with DESeq2*. Genome Biology, 2014. **15**(12): p. 550.
100. Yu, G., et al., *clusterProfiler: an R package for comparing biological themes among gene clusters*. Omics, 2012. **16**(5): p. 284-7.
101. Huck, I., et al., *Hepatocyte-Specific Hepatocyte Nuclear Factor 4 Alpha (HNF4) Deletion Decreases Resting Energy Expenditure by Disrupting Lipid and Carbohydrate Homeostasis*. Gene Expr, 2021. **20**(3): p. 157-168.
102. Begley, M., C.G. Gahan, and C. Hill, *The interaction between bacteria and bile*. FEMS Microbiol Rev, 2005. **29**(4): p. 625-51.
103. Yang, N.J. and M.J. Hinner, *Getting across the cell membrane: an overview for small molecules, peptides, and proteins*. Methods Mol Biol, 2015. **1266**: p. 29-53.
104. Kim, K.-H., E. Kabir, and S. Kabir, *A review on the human health impact of airborne particulate matter*. Environment International, 2015. **74**: p. 136-143.

105. Kalaany, N.Y. and D.J. Mangelsdorf, *LXRS and FXR: the yin and yang of cholesterol and fat metabolism*. *Annu Rev Physiol*, 2006. **68**: p. 159-91.

APPENDIX

Appendix Table 1: Aroclor 1260 effects on ileal gene expression. * $p \leq 0.05$ between 5 μ m to control and † $p \leq 0.05$ between 0. 5 μ m and 5 μ m.		
	CONTROL	PCB
<i>Tjp1</i>	1.00 ± 0.38	1.03 ± 0.47
<i>Icam</i>	1.00 ± 0.86	0.88 ± 1.00
<i>Il-10</i>	1.00 ± 0.45	1.13 ± 1.14
<i>Cyp1a1</i>	1.00 ± 1.51	0.59 ± 0.66

Appendix Table 2: Polystyrene effects on hepatic gene expression.
* $p \leq 0.05$ between 5 μm to control and † $p \leq 0.05$ between 0.5 μm and 5 μm .

	CONTROL	0.5μm	5μm
<i>Tnfa</i>	1.00 ± 0.38	1.18 ± 0.41	1.04 ± 0.34
<i>Mip-2α</i>	1.00 ± 0.26	3.78 ± 6.83	0.63 ± 0.38 [†]
<i>Timp1</i>	1.00 ± 0.52	1.19 ± 0.52	1.01 ± 0.32
<i>Gclm</i>	1.00 ± 0.08	0.94 ± 0.17	1.00 ± 0.10
<i>Gclc</i>	1.00 ± 0.16	0.95 ± 0.40	0.89 ± 0.25
<i>Cd36</i>	1.00 ± 0.26	0.75 ± 0.22	1.01 ± 0.40
<i>Fasn</i>	1.00 ± 0.34	0.89 ± 0.36	1.17 ± 0.49
<i>Srebf1</i>	1.00 ± 0.18	1.05 ± 0.17	1.16 ± 0.13
<i>Fgf21</i>	1.00 ± 0.82	0.90 ± 1.01	1.53 ± 1.02
<i>Abop</i>	1.00 ± 0.09	1.08 ± 0.13	0.99 ± 0.10
<i>Fxr</i>	1.00 ± 0.18	0.90 ± 0.23	1.07 ± 0.15
<i>Ppara</i>	1.00 ± 0.33	0.87 ± 0.30	1.11 ± 0.18
<i>Pnpla2</i>	1.00 ± 0.15	1.15 ± 0.22	1.37 ± 0.22* [†]

Appendix Table 3: Top 20 induced DEGs for PS_0.5_μm_vs_control ($p \leq 0.05$; $q \leq 0.05$; $\log_2FC \geq 0$; FPKM ≥ 1 in ≥ 3 samples; AVG FPKM ≥ 1 MIN COUNT: 10).				
Gene Symbol	Description	Log ₂ FC	p-value	q-value
Steap4	STEAP family member 4	1.074	1.788e-10	2.381e-06
Yod1	YOD1 deubiquitinase	0.608	2.309e-09	1.537e-05
Tnfaip3	tumor necrosis factor, alpha-induced protein 3	1.012	6.326e-09	2.808e-05
Bach1	BTB and CNC homology 1, basic leucine zipper transcription factor 1	0.805	2.071e-08	6.898e-05
Fgfr1	fibroblast growth factor receptor 1	0.745	4.303e-08	0.000
Cobl	cordon-bleu WH2 repeat	0.643	5.733e-08	0.000
Rrn3	RRN3 RNA polymerase I transcription factor homolog (yeast)	0.710	5.941e-08	0.000
Stat3	signal transducer and activator of transcription 3	0.661	1.367e-07	0.000
Ripk1	receptor (TNFRSF)-interacting serine-threonine kinase 1	0.507	1.629e-07	0.000
Saa2	serum amyloid A 2	0.769	3.216e-07	0.000
Ccl2	chemokine (C-C motif) ligand 2	0.870	7.982e-07	0.000
Sdad1	SDA1 domain containing 1	0.423	1.585e-06	0.001
Il17ra	interleukin 17 receptor A	0.553	1.650e-06	0.001
Baz1a	bromodomain adjacent to zinc finger domain 1A	0.702	1.676e-06	0.001
Lrig1	leucine-rich repeats and immunoglobulin-like domains 1	0.533	2.760e-06	0.001
Grem2	gremlin 2, DAN family BMP antagonist	0.853	2.901e-06	0.001
Arid5b	AT rich interactive domain 5B (MRF1-like)	0.826	2.945e-06	0.001
Il1r1	interleukin 1 receptor, type I	0.737	3.673e-06	0.002
Tirap	toll-interleukin 1 receptor (TIR) domain-containing adaptor protein	0.472	5.470e-06	0.002
Mdn1	midasin AAA ATPase 1	0.605	6.146e-06	0.002

Appendix Table 4: Top 20 suppressed DEGs for PS_0.5 μm _vs_control ($p \leq 0.05$; $q \leq 0.05$; $|\log_2\text{FC}| \geq 0$; $\text{FPKM} \geq 1$ in ≥ 3 samples; $\text{AVG FPKM} \geq 1$ MIN COUNT: 10).

Gene Symbol	Description	Log ₂ FC	p-value	q-value
Cyp2c37	Cytochrome P450, family 2, subfamily c, polypeptide 37	-0.644	1.349e-07	0.000
Pcp411	Purkinje cell protein 4-like 1	-0.718	7.446e-07	0.000
Plin5	Perilipin 5	-0.421	5.705e-06	0.002
Ptp4a3	Protein tyrosine phosphatase 4a3	-0.623	7.491e-06	0.003
Retsat	retinol saturase (all trans retinol 13,14 reductase)	-0.501	1.088e-05	0.003
Gm11837	Predicted gene 11837	-0.608	1.699e-05	0.004
Tpm2	Tropomyosin 2, beta	-0.769	1.839e-05	0.004
Tor3a	Torsin family 3, member A	-0.597	2.043e-05	0.005
Ly6a	Lymphocyte antigen 6 complex, locus A	-0.650	2.415e-05	0.005
Dhrs7	Dehydrogenase/reductase (SDR family) member 7	-0.323	3.161e-05	0.006
Trib3	Tribbles pseudokinase 3	-0.749	3.864e-05	0.007
Septin4	Septin 4	-0.466	5.530e-05	0.009
Slc25a4	Solute carrier family 25 (mitochondrial carrier, adenine nucleotide translocator), member 4	-0.451	6.287e-05	0.010
Gsto1	Glutathione S-transferase omega 1	-0.349	6.830e-05	0.010
Mgst3	Miicrosomal glutathione S-transferase 3	-0.595	0.000	0.013
Cavin2	Caveolae associated 2	-0.428	0.000	0.014
Gm20319	Predicted gene, 20319	-0.287	0.000	0.015
Cyp2c38	Cytochrome P450, family 2, subfamily c, polypeptide 38	-0.540	0.000	0.016
Abhd6	Abhydrolase domain containing 6	-0.348	0.000	0.016

G0s2	G0/G1 switch gene 2	-0.701	0.000	0.017
------	---------------------	--------	-------	-------

Appendix Table 5: Top 20 induced DEGs for PS_5 μm _vs_control ($p \leq 0.05$; $q \leq 0.05$; $|\log_2\text{FC}| \geq 0$; $\text{FPKM} \geq 1$ in ≥ 3 samples; $\text{AVG FPKM} \geq 1$ MIN COUNT: 10).

Gene Symbol	Description	Log_2FC	p -value	q -value
Ccnt2	Cyclin T2	0.585	1.339e-07	0.001
Tmf1	TATA element modulatory factor 1	0.627	1.599e-07	0.001
Firre	Functional intergenic repeating RNA element	0.954	2.612e-07	0.001
C730036E19Rik	RIKEN cDNA C730036E19 gene	0.866	2.879e-07	0.001
Fam193b	Family with sequence similarity 193, member B	0.846	1.260e-06	0.003
Rrnad1	Ribosomal RNA adenine dimethylase domain containing 1	0.506	1.326e-06	0.003
Pnlsr	PNN interacting serine/arginine-rich	0.653	1.842e-06	0.003
Srsf11	Serine and arginine-rich splicing factor 11	0.370	2.284e-06	0.003
Leng8	Leukocyte receptor cluster (LRC) member 8	0.714	2.375e-06	0.003
Fnbp4	Formin binding protein 4	0.553	3.532e-06	0.005
Fbxl12	F-box and leucine-rich repeat protein 12	0.682	8.956e-06	0.008
Zkscan7	Zinc finger with KRAB and SCAN domains 7	0.479	1.036e-05	0.009
Mug-ps1	Murinoglobulin, pseudogene 1	0.782	1.271e-05	0.010
Trmt13	tRNA methyltransferase 13	0.571	1.566e-05	0.012
Zc3h7a	Zinc finger CCCH type containing 7 A	0.353	1.741e-05	0.012
Hnrnpdl	Heterogeneous nuclear ribonucleoprotein D-like	0.293	1.802e-05	0.012
C4a	Complement component 4A (Rodgers blood group)	0.753	1.848e-05	0.012
Rev1	REV1, DNA directed polymerase	0.647	1.886e-05	0.012
Cyp2d37-ps	Cytochrome P450, family 2, subfamily d, polypeptide 37, pseudogene	0.696	2.045e-05	0.012
Ccnl1	Cyclin L1	0.603	2.238e-05	0.013

Appendix Table 6: Top 20 suppressed DEGs for PS_5 μm _vs_control ($p \leq 0.05$; $q \leq 0.05$; $\log_2\text{FC} \geq 0$; $\text{FPKM} \geq 1$ in ≥ 3 samples; $\text{AVG FPKM} \geq 1$ MIN COUNT: 10).				
Gene Symbol	Description	Log_2FC	p -value	q -value
Slpi	Secretory leukocyte peptidase inhibitor	-0.931	3.649e-07	0.001
Pea15a	Proliferation and apoptosis adaptor protein 15A	-0.342	8.750e-06	0.008
Ccn2	Cellular communication network factor 2	-0.712	2.637e-05	0.013
Ccdc80	Coiled-coil domain containing 80	-0.407	2.774e-05	0.013
Hsd17b13	Hydroxysteroid (17-beta) dehydrogenase 13	-0.320	4.165e-05	0.019
Tpi1	Triosephosphate isomerase 1	-0.260	0.000	0.041
Cavin2	Caveolae associated 2	-0.411	0.000	0.049
Sgk1	Serum/glucocorticoid regulated kinase 1	-0.565	0.000	0.049

Appendix Table 7: Enriched processes in 0.5 μ m vs control differential expressed genes (DEGs) analyzed by IPA software. ($p \leq 0.05$; $q \leq 0.05$; $|\log_2FC| \geq 0$).

Ingenuity Canonical Pathways	$-\log(p\text{-value})$	Predicted Genes
LPS/IL-1 Mediated Inhibition of RXR Function	3.77	ABCG5, ABCG8, ACSL4, Cyp2c54 (includes others), CYP2C8, GSTA5, GSTO1, HS3ST3B1, IL1R1, MGST3, TRAF6
IL-13 Signaling Pathway	3.44	AKT1, IL13RA1, IL17RA, POSTN, ROCK2, STAT3, TRAF6
Hepatic Fibrosis Signaling Pathway	3.44	AKT1, CCND1, FGFR1, ICAM1, IL17RA, IL1R1, PTCH1, RIPK1, RND3, ROCK2, STAT3, TGFBR1, TIRAP, TRAF6
Ascorbate Recycling (Cytosolic)	3.42	GLRX, GSTO1
FXR/RXR Activation	3.23	ABCG5, ABCG8, AKT1, FOXA3, PON1, SAA1, SLC10A2
Glutathione-mediated Detoxification	3.1	Gsta4, GSTA5, GSTO1, MGST3
Role Of Chondrocytes in Rheumatoid Arthritis Signaling Pathway	2.94	CEBPG, IL17RA, IL1R1, RIPK1, STAT3, TLR2, TRAF6
Role of Macrophages, Fibroblasts and Endothelial Cells in Rheumatoid Arthritis	2.82	AKT1, CCND1, CEBPG, ICAM1, IL17RA, IL1R1, RIPK1, ROCK2, STAT3, TLR2, TRAF6
Hepatic Cholestasis	2.81	ABCG5, ABCG8, ATP8B1, IL1R1, PPRC1, SLC10A2, TIRAP, TRAF6
IL-8 Signaling	2.55	AKT1, CCND1, GNAT1, GNG11, ICAM1, RND3, ROCK2, TRAF6
STAT3 Pathway	2.35	FGFR1, IL13RA1, IL17RA, IL1R1, STAT3, TGFBR1
NRF2-mediated Oxidative Stress Response	2.24	AKT1, BACH1, Cyp2c54 (includes others), CYP2C8, FKBP5, GSTA5, GSTO1, MGST3
Xenobiotic Metabolism PXR Signaling Pathway	2.18	CYP2C8, GSTA5, GSTO1, HS3ST3B1, MGST3, PPP1R10, PPP1R3C
CD40 Signaling	2.15	ICAM1, STAT3, TNFAIP3, TRAF6
IL-17A Signaling in Airway Cells	2.15	AKT1, IL17RA, STAT3, TRAF6
ID1 Signaling Pathway	2.09	AKT1, CCND1, FGFR1, PLXNB1, STAT3, TGFBR1, WDR48
IL-10 Signaling	2.08	AKT1, CCND1, ICAM1, IL1R1, STAT3, TRAF6
IL-17A Signaling in Fibroblasts	2.04	IL17RA, LCN2, TRAF6
Aryl Hydrocarbon Receptor Signaling	2.01	CCND1, Cyp2c54 (includes others), CYP2C8, GSTA5, GSTO1, MGST3
Neuroinflammation Signaling Pathway	1.98	AKT1, ICAM1, IL1R1, MFGE8, RIPK1, TGFBR1, TIRAP, TLR2, TRAF6
TREM1 Signaling	1.94	AKT1, ICAM1, STAT3, TLR2

Acetone Degradation I (to Methylglyoxal)	1.92	CYP2C8, DHRS7, POR
Toll-like Receptor Signaling	1.92	TIRAP, TLR2, TNFAIP3, TRAF6
Colorectal Cancer Metastasis Signaling	1.9	AKT1, CCND1, GNAT1, GNG11, RND3, STAT3, TGFBR1, TLR2
Role of JAK family kinases in IL-6-type Cytokine Signaling	1.9	CCND1, CTF1, MCL1, STAT3
LXR/RXR Activation	1.88	ABCG5,ABCG8,IL1R1,PON1,SA A1
IL-6 Signaling	1.8	AKT1,IL1R1,MCL1,STAT3,TRAF6
Apelin Muscle Signaling Pathway	1.77	AKT1, GNAT1, GNG11
Xenobiotic Metabolism AHR Signaling Pathway	1.76	GSTA5, GSTO1, MGST3, PON1
Spliceosomal Cycle	1.74	BUD13, PRPF18, SF3B1
FAT10 Cancer Signaling Pathway	1.72	AKT1, STAT3, TGFBR1
Acute Phase Response Signaling	1.72	AKT1,IL1R1,RIPK1,SA A1,STAT3,TRAF6
γ -linolenate Biosynthesis II (Animals)	1.72	ACSL4, FADS2
Cardiac Hypertrophy Signaling (Enhanced)	1.67	AKAP13,AKT1,CTF1,FGFR1,GNG11,IL13RA1,IL17RA,IL1R1,RCAN1,ROCK2,STAT3,TGFBR1
Production of Nitric Oxide and Reactive Oxygen Species in Macrophages	1.66	AKT1,PON1,PPP1R10,PPP1R3C,RND3,TLR2
IL-1 Signaling	1.62	GNAT1, GNG11, IL1R1, TRAF6
PI3K/AKT Signaling	1.57	AKT1,CCND1,IL13RA1,IL17RA,IL1R1,MCL1
The Visual Cycle	1.56	DHRS7, RDH13
Vitamin-C Transport	1.56	GLRX, GSTO1
PTEN Signaling	1.54	AKT1, CCND1, FGFR1, MAGI3, TGFBR1
IL-22 Signaling	1.52	AKT1, STAT3
Semaphorin Signaling in Neurons	1.5	PLXNB1, RND3, ROCK2
Bupropion Degradation	1.49	CYP2C8, POR
Pulmonary Fibrosis Idiopathic Signaling Pathway	1.48	AKT1,CCND1,FGFR1,IL13RA1,IL17RA,ROCK2,STAT3,TGFBR1
Role of JAK2 in Hormone-like Cytokine Signaling	1.48	CCND1, PTPN1, STAT3
1,25-dihydroxyvitamin D3 Biosynthesis	1.47	POR
Glucocorticoid Receptor Signaling	1.46	AKT1,FKBP5,ICAM1,IL13RA1,IL17RA,IL1R1,MT-ND6,STAT3,TAF2,TGFBR1,TLR2,TRAF6
ERB2-ERBB3 Signaling	1.43	AKT1, CCND1, STAT3
Transcriptional Regulatory Network in Embryonic Stem Cells	1.41	AKT1, FGFR1, ONECUT1, STAT3, TGFBR1

Chronic Myeloid Leukemia Signaling	1.4	AKT1,CCND1,MCL1,PTCH1,SPRED1,STAT3,TGFBR1
Glutathione Redox Reactions I	1.4	GSTA5, MGST3
CXCR4 Signaling	1.37	AKT1, GNAT1, GNG11, RND3, ROCK2
Thrombin Signaling	1.36	AKT1, ARHGEF26, GNAT1, GNG11, RND3, ROCK2
SPINK1 General Cancer Pathway	1.36	AKT1, Mt2, STAT3
Glutathione Redox Reactions II	1.35	GLRX
Gαq Signaling	1.35	AKT1, GNAT1, GNG11, RND3, ROCK2
HER-2 Signaling in Breast Cancer	1.35	AKT1, CCND1, DDX19B, NUP160, NUP58, STAT3
GM-CSF Signaling	1.34	AKT1, CCND1, STAT3
Protein Kinase a Signaling	1.34	AKAP13, GNG11, PPP1R10, PPP1R3C, PTCH1, PTPN1, PTPN3, ROCK2, TGFBR1
p38 MAPK Signaling	1.32	IL1R1, TGFBR1, TIFA, TRAF6
Ephrin B Signaling	1.31	GNAT1, GNG11, ROCK2

CURRICULUM VITAE

Ngozi Adiele

678.799.6115 • Louisville, Ky. 40206 • nvadie01@louisville.edu •

www.linkedin.com/in/ngozi-adiele-6941ba165

EDUCATION

University of Louisville, School of Medicine - Louisville, KY

Master's – Pharmacology and Toxicology, expected May 2023

University of Toledo – Toledo, OH

Bachelor of Science – Pharmacology and Toxicology, Minor: Chemistry, May 2020

WORK EXPERIENCE

University of Louisville - Louisville, KY

August 2021 – Present

Student research assistant

Worked on two projects titled: Impact of chronic Aroclor 1260 exposure on gut microbiome and intestinal toxicity and investigating the effects of Polystyrene microplastics on hepatic function.

- Used histological staining to observe liver morphology.
- Used RT-qPCR to quantify mRNA level in various murine organs.
- Used the concept of normal distribution and homogeneity of variance to determine the appropriate statistical test to analyze my data.

- Assisted in the writing of a mini voucher.
- Assisted on projects with lab members and my member of collaborating laboratories.

University of Toledo - Toledo, OH

January 2020 -June 2020

Undergraduate Researcher in Dr. Amanda Bryant-Friedrich's Lab

Contributed to ongoing experiments (Thymine Synthesis) while carrying out the listed responsibility:

- Synthesized and purified nucleotides.
- Protected and Deprotected nucleotides.
- Purified compounds using chromatography (HPLC or Column).
- Observed the progress of reaction using Thin-Layer Chromatography.
- Used NMR and Mass spectrometers to analyze products obtained.
- Kept a regulatory checked Lab Note.
- Worked on a pseudo-uridine annotated bibliography.

University of Toledo - Toledo, OH

August 2019 – November 2019

Intern in Dr. Ming Lui's Lab

Completed an assisted project titled: The sulfating activity of SULT1A3 on the drug Pentazocine.

- Understood the purpose of SULT1A3 enzyme does in the body.
- Understood the various allozymes of SULT1A3 enzymes.
- Used radiolabeling to understand the effect of Pentazocine on SULT1A3.
- Extracted result using TLC and X-ray films.

- Presented a poster the University of Toledo Scholars event.

PUBLICATIONS AND CONFERENCES

Publications

- Bolatimi, O. E., Head, K. Z., Luo, J., Gripshover, T. C., Lin, Q., **Adiele, N. V.**, Watson, W. H., Wilkerson, C., Cai, L., Cave, M. C., & Young, J. L. (2023). Can Zinc Supplementation Attenuate High Fat Diet-Induced Non-Alcoholic Fatty Liver Disease? *International journal of molecular sciences*, 24(2), 1763. <https://doi.org/10.3390/ijms24021763>

Conferences

- **N.V. Adiele**, R. Singhal, K.Z. Head, B.J. Petri, K.M. Piell, J. Luo, T.C. Gripshover, E.C. Rouchka M.C. Cave, C.M. Klinge, and B. Wahlang. Impact of Long-term Aroclor 1260 exposure on gut microbiome and intestinal toxicity. In: *The Toxicologist*. Supplement to *Toxicological Sciences*, 192 (1096-6080), Society of Toxicology, 2023. Abstract no. (4354).
- J. Luo, B. Wahlang, W. H. Watson, C. M. White, S. Singh, O. E. Bolatimi, **N. V. Adiele**, L. L. Jophlin, J. L. Marshall, R. J. Sullivan, and M. C. Cave. The effects of fluorene exposure in conjunction with high-fat diet on toxicant-associated fatty liver disease. In: *The Toxicologist*. Supplement to *Toxicological Sciences*, 192 (1096-6080), Society of Toxicology, 2023. Abstract no. (4683).
- J. Zhao, D. Gomes, **A. Ngozi**, D. Conklin, M. Cave, and T. O'Toole. Delphinidin alleviates the adverse metabolic effects of polystyrene

exposure in mice. In: *The Toxicologist*. Supplement to *Toxicological Sciences*, 192 (1096-6080), Society of Toxicology, 2023. Abstract no. (4721).

- **N.V. Adiele**, K.Z. Head, B.J. Petri, K.M. Piell, J. Luo, T.C. Gripshover, M.C. Cave, C. Klinge, and B. Wahlang. Effects of long-term exposure to polychlorinated biphenyls on ileal gene expression. In proceeding from American Association for the study of liver diseases; November 7, 2022; Washington, DC. #4320.
- C.M. White, J. Luo, W. Watson, **N. Adiele**, O.E. Bolatimi, C.J. McClain, M.C. Cave and L.L. Jophlin. Effects of zinc supplementation on high fat diet-induced non-alcoholic fatty liver disease. In proceeding from American Association for the study of liver diseases; November 5, 2022; Washington, DC. #2662.
- O.E. Bolatimi, J. Young, B. Wahlang J. Luo, K.Z. Head, T.C. Gripshover, Q. Lin, C.M. White, **N. Adiele**, W. Watson, C. Wilkerson, L. Cai, and M.C. Cave. Effects of zinc supplementation on high fat diet-induced non-alcoholic fatty liver disease. In proceeding from American Association for the study of liver diseases; November 5, 2022; Washington, DC. #2621.
- Z. Qaissi, R. Singhal, **N.V. Adiele**, O.E. Bolatimi, E.C. Rouchka, M.C. Cave and B. Wahlang. Evaluating sex-dependent changes in the gut microbiome caused by polychlorinated biphenyl (PCB) exposures. In

proceeding from American Association for the study of liver diseases;
November 7, 2022; Washington, DC. #4322.

- **N.V. Adiele**, K.Z. Head, B.J. Petri, K.M. Piell, J. Luo, T.C. Gripshover, M.C. Cave, C. Klinge, and B. Wahlang. Effects of long-term exposure to polychlorinated biphenyls on ileal gene expression. Poster presented at: 2022 Ohio Valley Society of Toxicology Annual Meeting; October 14, 2022; Louisville, Kentucky.
- O.E. Bolatimi, J. Young, B. Wahlang, J. Luo, K. Head, T. Gripshover, Q. Lin, C. White, **N. Adiele**, W. Watson, C. Wilkerson, L. Cai, and M. Cave. Effects of subchronic dietary zinc supplementation on high fat diet-induced nonalcoholic fatty liver disease. Poster presented at: 2022 Ohio Valley Society of Toxicology Annual Meeting; October 14, 2022; Louisville, Kentucky.
- **N.V. Adiele**, K.Z. Head, B.J. Petri, K.M. Piell, J. Luo, T.C. Gripshover, M.C. Cave, C. Klinge, and B. Wahlang. Effects of long-term exposure to polychlorinated biphenyls on ileal gene expression. Poster presented at: 2022 Research! Louisville Annual Meeting; September 20, 2022; Louisville, Kentucky.
- C. White, J. Luo, W. Watson, **N. Adiele**, E. Bolatimi, C. McClain, M. Cave, and L. Jophlin. Chronic sodium benzoate ingestion approximating typical human exposure increases body fat and exacerbates fatty liver disease in mice. Poster presented at: 2022 Research! Louisville Annual Meeting; September 21, 2022; Louisville, Kentucky.

- O.E. Bolatimi, J.L. Young, B. Wahlang, J. Luo, K.Z. Head, T.C. Gripshover, Q. Lin, C. White, **N.V. Adiele**, W.H. Watson, C. Wilkerson, L. Cai, and M.C. Cave. Effects of zinc supplementation on high fat diet-induced non-alcoholic fatty liver disease. Poster presented at: 2022 Research! Louisville Annual Meeting; September 20, 2022; Louisville, Kentucky.
- J. Luo, B. Wahlang, W. Watson, M. Cave, C. White, S. Singh, Oluwanifemi Bolatimi, **N. Adiele**, Loretta Jophlin, J. Marshall, and R. Sullivan. The effects of fluorene exposure in conjunction with high-fat diet on toxicant-associated fatty liver disease. Poster presented at: 2022 Research! Louisville Annual Meeting; September 21, 2022; Louisville, Kentucky.
- **N.V. Adiele**, K.Z. Head, B.J. Petri, K.M. Piell, J. Luo, T.C. Gripshover, M.C. Cave, C. Klinge, and B. Wahlang. Effects of long-term exposure to polychlorinated biphenyls on ileal gene expression. Platform presentation presented at: 2022 Ohio Valley Society of Toxicology Virtual Trainee Summer Meeting; July 29, 2022; Louisville, Kentucky.
- O.E. Bolatimi, J. Young, B. Wahlang, J. Luo, K. Head, T. Gripshover, Q. Lin, C. White, **N. Adiele**, W. Watson, C. Wilkerson, L. Cai, and M. Cave. Effects of subchronic dietary zinc supplementation on high fat diet-induced nonalcoholic fatty liver disease. 3 minutes presentation presented at: 2022 Ohio Valley Society of Toxicology Virtual Trainee Summer Meeting; July 29, 2022; Louisville, Kentucky.

AWARDS AND HONORS

Undergraduate Fall Research grant - Toledo, OH May 2019

Summa Cum laude - Toledo, OH May 2020

- Grade with As and a B

Departmental Honors - Toledo, OH May 2020

- Honors Thesis in Medicinal Biological Chemistry
- Honors Seminar in Medicinal and Biological Chemistry

Travel Awards - Washington, DC November 2022

- Graduate studies counsel award and CIEHS award for AASLD conference

PROFESSIONAL MEMBERSHIPS

- Society of Toxicology Member in 2023
- American Association for the Study of Liver Diseases (AASLD) Member in 2022
- Superfund Research Program (SRP) Trainee in 2022
- Sigma Phi Sigma, Department of Pharmacy and Pharmaceutical Sciences, University of Toledo Member in 2019

OTHER WORK EXPERIENCE

Faster – Holland, OH January 2021 – May 2021

Quality Control technician

Inspect incoming products as well as outgoing products, to ensure they meet the company's specifications. Record daily inspections and bookkeep the bad products.

University of Toledo – Toledo, OH

Mailroom Student Worker

November 2018-March 2020

Carry out daily activities at the university surplus and sort and deliver mails at the university's mailroom.

New Student Orientation Leader

May 2016 – June 2018

Providing incoming students with hospitality and information they needed to thrive at the University of Toledo.

Chemistry Peer Leader

August 2017 – April 2018

Teach and assist student with chemistry problems.

Upward Bound Resident Assistant

June 2018 – July 2018

Supervise and assist Upward bound student with their summer studies.

Pharmacy Camp Counselor

July 2017

Supervise and assisted pharmacy camp high schooler with their daily activities.

Residence Life Student Desk Worker

July 2017

Helped guests, answered questions on resident life.

Youth Nations Counselor

July 2017

Assisted a group of high school juniors and seniors in creating a presentation on a given topic related to a country.

VOLUNTEER EXPERIENCE

University of Louisville- *Louisville, KY*

September 2022

Department of Communications

- Assisted in teaching an undergraduate communication class, by sitting in on a panel.

University of Toledo - Toledo, OH

August 2016

Student Ambassador

- Provided directions to first-year students and Visitors at the start of the school year.

University of Toledo - Toledo, OH

August 2015

Clean the stream.

- Cleaned the Ottawa river.